High Pressure Die Casting of Aluminium and Magnesium Alloys
- Grain Structure and Segregation Characteristics

Hans Ivar Laukli

A thesis submitted to the
Norwegian University of Science and Technology (NTNU)
in partial fulfilment of the requirements for the degree of

Doktor Ingeniør

Trondheim, April 2004

ISBN 82-471-6324-1 (printed)
ISBN 82-471-6323-3 (electronic)
ISSN 1503-8181

PREFACE

The thesis is submitted in partial fulfilment of the requirements for the degree of doktor ingeniør at the Norwegian University of Science and Technology (NTNU). The work, including the compulsory courses corresponding to full-time studies in two semesters, has taken place in the period from May 2001 to April 2004. The research was done at the Department of Materials Technology at NTNU, and at the University of Queensland for 6 months in 2003.

The work was funded through the NorLight Shaped Castings project. The main contributors have been the Research Council of Norway, Alcoa Automotive Castings, Scandinavian Casting Centre ANS, Elkem Aluminium ANS, Fundamus AS, Hydro Aluminium Metal Products and Norsk Hydro ASA. Additional financial support has been given by the Australian Government's CRC for Cast Metals Manufacturing (CAST) and the Dr.Ing. Håkon Styri fellowship administered by Polyteknisk Forening.

Compared to wrought products the mechanical properties of high pressure die castings (HPDC) have a reputation of being inconsistent. Whilst this has typically been attributed to variations in process parameters, such documentation is often unsatisfactory. At the initiation of the project Norsk Hydro installed a state of the art, well equipped HPDC machine. More systematic investigations of the HPDC process and the effect of different parameters on different products and alloys were therefore possible. In the project committee it was decided to start a doctorate work on the shot sleeve conditions and analysis of the effects on the microstructure in the castings caused by the metal fed into the die.

Professor Otto Lohne has been the principal supervisor and Professor Lars Arnberg has been the co-supervisor.

The results have mainly been reported and published throughout the period. The articles included in the thesis are presented in the form they were submitted for publication or printed. Deviations from the original text, such as typing errors etc, are marked with a footnote.

ACKNOWLEDGEMENTS

My acknowledgements go to: Professor Otto Lohne for his numerous suggestions, for having unwavering confidence in me and for giving opportunities to fulfil my goals; Professor Lars Arnberg for scientific advice, encouragement and for keeping me in his group; Professor Erik Nes for motivating me during my undergraduate studies, to continue with a doctorate work.

Of invaluable importance: - the HPDC experiments were done with unlimited support from Hydro Aluminium at the Magnesium Competence Centre in Porsgrunn. Dr. Stian Sannes and Haavard Gjestland are acknowledged for constructive criticism and advice. The opportunity to occasionally discuss matters is appreciated. Sten Bjørneboe provided skilful, practical in-situ advice during the production of hundreds of castings.

Assoc. Prof. Arne Kristian Dahle at the University of Queensland (UQ) gave me the opportunity to stay in his group at UQ for 6 memorable months. His enthusiastic and uninhibited support has been very important for large parts of this work. Christopher Gourlay (UQ) was an excellent research companion through stimulating and challenging discussions, competent advice and friendly, fruitful cooperation.

My acknowledgements also to Jorunn Snøan Mæland and Petter Åsholt, both at Hydro Al RDM whom, typically on short notice, supplied metal for casting experiments and performed chemical analysis. Dr. Anne-Lise Dons provided the Alstruc calculations presented in the articles and Dr. Harald Laux gave advice on two-phase flow. Cato Dørum was helpful in giving information on the global deformation behavior of HPDC components, whilst proof-reading was kindly carried out by Raimo Helenius.

The friendly surroundings provided for by my previous room-mates, Marisa Di Sabatino and Dr. Emmanuelle Ott, and my fellow colleagues at NTNU and SINTEF is appreciated.

Finally, my gratitude to my parents for their genuine interest in my work, and to my wife, Ingerid for helpful advice in the writing of the thesis. Additionally, Ingerid and my two sons, Sivert and Henrik, for giving the appropriate perspective.

ABSTRACT

Cold chamber high pressure die casting, (HPDC), is an important commercial process for the production of complex near net shape aluminium and magnesium alloy castings. The work presented in the thesis was aimed at investigating the microstructure formation in this type of casting. The solidification characteristics related to the process and the alloys control the formation of grains and defects. This again has a significant impact on the mechanical properties of the castings.

The investigations were carried out mainly using the AM60 magnesium alloy and the A356 aluminium alloy. Two different casting arrangements were used: the cold chamber HPDC and the gravity die casting methods, which allowed for different flow and solidification conditions. The microstructures in the castings were investigated using optical microscopy, image analysis, scanning electron microscopy, electron back scatter diffraction measurements and electron probe microanalysis.

In the HPDC experiments, the shot sleeve solidification conditions were investigated primarily by changing the melt superheat on pouring. This significantly affected the microstructures in the castings. The fraction of externally solidified crystals (ESCs) was consistently found to be largest near the gate in both the AM60 and the A356 die castings. This was attributed to the inherent shot sleeve solidification conditions and the flow set up by the plunger movement. When the superheat was increased, a lower fraction of ESCs was found in the castings. Furthermore, a high superheat gave ESCs with branched dendritic/elongated trunk morphology whilst a low superheat generated coarser and more globular ESCs, both in the AM60 and the A356 castings. The ESCs typically segregated towards the central region of the cross sections at further distances from the gate in the die castings.

When a thin layer of thermal insulating coating was applied on the shot sleeve wall in the production of AM60 die castings, it nearly removed all ESCs in the castings. Using an A356 alloy, (and no shot sleeve coating), with no Ti in solution gave a significantly lower fraction of ESCs, whereas AlTi5B1 grain refiner additions induced an increase in the fraction of ESCs and a significantly finer grain size in the castings. The formation of globular ESCs was enhanced when AlTi5B1 grain refiner was added to the A356 alloy.

In controlled laboratory gravity die casting experiments, typical HPDC microstructures were created by pouring semi-solid metal into a steel die: The ESCs were found to segregate/migrate to the central region during flow, until a maximum packing, (fraction of ESCs of ~35-40%), was reached. The extent of segregation is determined by the fraction of ESCs, and the die temperature affects the position of the ESCs. The segregation of ESCs was explained to occur during flow as a result of lift forces.

The formation of banded defects has also been studied: the position of the bands was affected by the die temperature and the fraction of ESCs. Based on the nature of the bands and their occurrence, a new theory on the formation of defect bands was proposed: During flow the solid distribution from the die wall consists of three regions: 1) a solid fraction gradient at the wall; 2) a low solid fraction region which carries (3) a network of ESCs. A critical fraction solid exists where the deformation rate exceeds the interdendritic flow rate. When the induced stress exceeds the network strength, deformation can occur by slip, followed by liquid flow. The liquid flow is caused by solidification shrinkage, hydrostatic pressure on the interior ESC network, and gaps forming which draw in liquid.

CONTENTS

Guide to the Reader

The thesis consists of two parts:

PART 1 is intended to give the reader sufficient background for the basic principles of the die casting process, its inherent challenges and the physical fundamentals that have been used in the interpretation of the results in the appended articles.

PART 2 consists of the following articles in the doctorate work:

ARTICLE 1, pp.45-54.
The Effect of Solidification of Metal Prior to Injection in HPDC on the Grain Size Distribution in a Complex Die Casting. *NADCA Transactions 2002*, vol.21, T02-035, pp.1-4.

ARTICLE 2, pp.55-69.
Grain Size Distribution in a Complex AM60 Magnesium Alloy Die Casting. *International Journal of Cast Metals Research*, 2003, vol.16, no.6, pp.515-521.

ARTICLE 3, pp.71-83.
The Effect of Variations in Melt Temperature on the Grain Structures in an AM60 Die Casting. *Proceedings of the 6th International Conference on Magnesium Alloys and their Applications*, 2003, vol.6, pp.182-189.

ARTICLE 4, pp.85-104.
Effects of Grain Refiner Additions on the Grain Structures in HPDC A356 Castings. Submitted for publication in: *Metallurgical and Materials Transactions A*, 2004.

ARTICLE 5, pp.105-127.
Migration of Crystals During the Filling of Semi-Solid Castings. Submitted for publication in: *Metallurgical and Materials Transactions A*, 2004.

ARTICLE 6, pp.129-152.
Segregation Band Formation in Al-Si Die Castings. *Metallurgical and Materials Transactions A*, 2004. Accepted.

In addition to the articles included in the thesis, parts have been presented in the following publications:

O. Lohne, H.I. Laukli: HPDC U-profil of aluminium. Summary of the work of Paolo Lucarelli in autumn 2002. *SINTEF Report STF24 F02535*, March, 2002.

H.I. Laukli: Tensile Testing of AM60 U-profile. *NTNU Report*, May, 2002.

H.I. Laukli, O. Lohne, L. Arnberg: Effect of Premature Solidification on the Grain Structure in Light Metal Die Castings. *NorLight-konferansen 2003*, Trondheim.

S. Sannes, H. Gjestland, H. Westengen, H.I. Laukli, O. Lohne: Die Casting of Magnesium Alloys – The importance of Controlling Die Filling and Solidification. *SAE conference*. Detroit, 2003, 03M-192.

H.I. Laukli, O. Lohne, L. Arnberg: Grain Structure Characterization of AM60 Die Castings by Electron Backscatter Diffraction Measurements (EBSD) in SEM. *6th Int. Conf. Mg Alloys Applic*. Wolfsburg, 2003, pp.232-35.

S. Sannes, H. Gjestland, H. Westengen, H.I. Laukli, O. Lohne: Die Casting for High Performance. *6th Int. Conf. Mg Alloys Applic*. Wolfsburg, 2003, pp.725-31.

S. Barbagallo, H.I. Laukli, O. Lohne, E. Cerri: Divorced Eutectic in a HPDC Magnesium-Aluminium Alloy. *Journal of Alloys and Compounds*. 2004. In press.

C.M. Gourlay, H.I. Laukli, A.K. Dahle: An Investigation into Banded Defects in Die Castings. *CAST seminar*, Lorne, Australia, December, 2003.

C.M. Gourlay, H.I. Laukli, A.K. Dahle: The Formation of Segregation Bands in Al-Si Castings. *9th Int. Conf. Al Alloys*. (ICAA9). Brisbane, Australia, 2004. Accepted for publication.

Nomenclature

A_i	$[m^2]$	Interface area between alloy and system component i
ζ# #	$[m^2s^{-1}]$	Thermal diffusivity#
η		Fill fraction of shot sleeve cross section behind wave front
c_0	[wt%]	Nominal bulk composition
c_l	[wt%]	Solid/liquid interface composition
C_p	$[kJkg^{-1}K^{-1}]$	Specific heat
D	[m]	Grain size
D_l	$[m^2s^{-1}]$	Compositional diffusivity
D_{pl}	[m]	Plunger diameter
ι_s	[m]	Solutal boundary layer
ι_T	[m]	Thermal boundary layer
$\div G$	[J]	Total free energy change
$\div G_v$	$[Jm^{-3}]$	Volumetric free energy
$\div H_f$	$[kJkg^{-1}]$	Latent heat of fusion
$\div H_f^v$	$[Jm^{-3}]$	Volumetric latent heat of fusion
$\div T_{remelt}$	[K]	Amount of melt cooling due to crystal remelting
$\div T_i$	[K]	Temperature difference between alloy and component i#
$\div T_n$	[K]	Nucleation undercooling #
$\div T_{ts}$	[K]	Melt superheat above thermosolutal transition temperature
$\div T_t$	[K]	Thermal undercooling
f_{fill}		Initial shot sleeve fill fraction
f_s		Fraction solid
f_s^{ch}		Coherency fraction solid
$f(\chi)$		Shape factor function#
λ		Initial fill fraction of shot sleeve cross section
g	$[ms^{-2}]$	Acceleration of gravity
G	$[Km^{-1}]$	Thermal gradient (=dT/dx)
G_a	$[m^2]$	Gate area
ν_{sl}	$[Jm^{-2}]$	Interfacial energy
h	[m]	Upstream depth
h_i	$[Wm^{-2}K^{-1}]$	Heat transfer coefficient for interface A_i
k		Distribution coefficient (c_s/c_l)
k_{die}		Die constant
k_{H-P}		Hall-Petch parameter
ρ	$[Wm^{-1}K^{-1}]$	Thermal conductivity
m_l	$[Kwt\%^{-1}]$	Liquidus slope
n	$[m^{-3}]$	Number of particles pr.unit volume
Q	$[m^3s^{-1}]$	Volumetric metal flow rate
r	[m]	Radius of nucleus/crystal
r_{tube}	[m]	Tube radius
ψ	$[kgm^{-3}]$	Density

t	[s]	Time
t_s	[s]	Solidification time
T	[K]	Temperature of the alloy
T_{die}	[K]	Die temperature
T_{eut}	[K]	Eutectic temperature
T_{liq}	[K]	Liquidus temperature
T_m	[K]	Melt temperature
T_M	[K]	Equilibrium melting temperature of pure solvent
T_{trans}	[K]	Thermosolutal transition temperature
ϑ##	# # # #	Lewis number#
χ	^{o}	Wetting angle
v	[ms^{-1}]	Upstream velocity
V	[m^3]	Volume of the alloy
v_{crit}	[ms^{-1}]	Critical plunger velocity
v_p	[ms^{-1}]	Plunger velocity
v_s	[ms^{-1}]	Solute diffusion controlled melting rate
v_T	[ms^{-1}]	Thermally controlled melting rate
v_w	[ms^{-1}]	Wave velocity
v_x	[ms^{-1}]	Velocity of growth front
y_1	[m]	Depth of fluid in front of wave
y_2	[m]	Depth of fluid behind wave front
x		Growth direction

PART 1

INTRODUCTION

1 INTRODUCTION

High Pressure Die Casting – Present Requirements and Future Perspectives

The transportation industry, and in particular the automotive industry, is imposed to seek light materials in the development of robust parts. The global production of aluminium and magnesium alloys has therefore increased, and the consumption of aluminium concurrently exceeds the existing production capacity of primary metal. It is therefore necessary to exploit, or invent, economically sustainable processes that can give light weight products with integrated functions that fulfill the requirements for recycling and fuel consumption regulations. High pressure die casting (HPDC) is a method well suited for those demands.

HPDC is a fully automatic, large volume, high productivity process for the production of complex, thin walled near net shape castings, with part weights ranging from a few grams to more than 15kg. It has traditionally been utilised in the production of housings etc, but this has changed. Presently, feasible products are automotive front end structures and instrument panels in magnesium alloys and B-pillars in aluminium alloys. However, for HPDC to be competitive for extended automotive applications and attractive for new market segments, the crash worthiness and fatigue properties must be improved and a scientific comprehension of the process and metal behavior is required.

The Cold Chamber HPDC Process

The text in the following chapter is principally extracted from the major textbooks on the subject [1-4]. H.H. Doehler was among the first to patent die casting-related technology in 1910. The initial machines produced aluminium castings in reusable metal moulds, where a manually powered pull bar transmitted the force required to fill the mould. In 1927, the horizontal cold chamber die casting machine was developed, which represents the basis of today's technology.

The four principal metals, with different alloy compositions, that are commonly hot- or cold chamber die cast are aluminium, zinc, magnesium and copper-base alloys. The injection system in the hot chamber machines is immersed into the melt and the pressure is therefore limited. The system also degrades quickly if exposed to aluminium. In the cold chamber process, the metal reservoir is separated from the injection system. The metal is filled into a steel shot sleeve, as shown in Figure 1, (magnesium is automatically metered [5]). The shot sleeve is typically 200-300^{o}C.

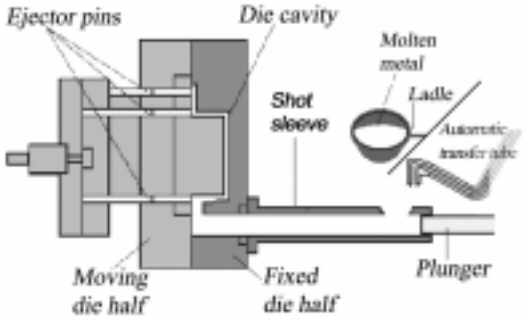

Figure 1: Illustration of cold chamber high pressure die casting. Reproduced from [6, 7].

A production cycle in HPDC consists of: 1) metering of metal into the shot sleeve; 2) plunger movement; 3) rapid die filling. The steel die, typically 200-300^{o}C, dissipates the latent heat, and during solidification the casting is 4) pressurized hydraulically by the plunger to feed the solidification shrinkage. Locking forces up to 4000 tons are commercially available to withstand the large pressures. Eventually, 5) the die is opened and 6) the casting is ejected. The hydraulic energy is provided by a computerized system that permits control of metal position, velocity and plunger acceleration to optimize the flow and the pressure during filling and solidification.

The die cavity may be evacuated to reduce air entrapment during die filling, and high integrity die castings can therefore be produced by utilizing vacuum systems [1]. Alternatively semi-solid metalworking (SSM) [8] can be used to reduce turbulence.

A short die filling time and thin walls results in high cooling rates, (typically 100-1000Ks^{-1}) [3]. This promotes a fine grain size which provides decent mechanical properties. However, the properties can be improved by intimate interrelationship between product and process design through amended metal handling, accurate process control, and optimized runner and die design. The capacity of the injection system is described by the so called P-Q^2 diagram which is supplied with the HPDC machine. It has been deduced that the pressure, P, is proportional to the square of the flow rate, Q. The die characteristics can be described by the equation $P=(k_{die}/G_a)Q^2$. The working conditions are determined from the intersection of the die line with the machine line in the P-Q^2 diagram [9]. Furthermore, suitable timing, good dimensional stability and correct assessment of the fluid and heat flow are prerequisites for better castings. Apparently minor factors such as amount of lubrication, its composition and application procedures can turn out to be of utmost importance for the final casting characteristics.

Whilst several process parameters can affect the properties of the castings, the alloy itself is similarly important. The alloy characteristics must fulfill the necessary requirements in castability which involve i.a. higher fluidity, good feeding and low hot tearing tendency. Initially, the doctorate work was aimed at investigating an Al-Mg and an Mg-Al alloy. Casting experiments with Al-Mg proved to be difficult. The most common HPDC aluminium alloy is the A380 (AlSi9Cu3) alloy, but a generally more utilized foundry alloy is the A356 Al-Si alloy which possesses good fluidity. Due to its availability, versatility and being well documented it has been used in the doctorate work. The common AM60B Mg-Al alloy has been used in this work as well.

The standard composition ranges and the major effects of the elements in the A356 and AM60B alloys are shown in Table 1. The magnesium alloys are designated by an alphanumerical code; the first letter of the two major alloy constituents and their respective amounts describes the alloys: **A**luminium**M**anganese**6**%**0**.5%. The character B, (as in AM60B), refers to the composition ranges, and unless otherwise stated, AM60=AM60B in the thesis.

Table 1. Effects of elements in the A356 and the AM60B alloys.

	[wt%]	A356* (AlSi7Mg0.35)	[wt%]	AM60B (MgAl6Mn0.5)
Si	6.5-7.5	Increased fluidity	< 0.1	Improved creep strength, fluidity
Al	Balance	Primary element	5.5-6.5	Increased strength, hardness, fluidity
Mg	0.25-0.45	Increased strength	Balance	Primary element
Fe**	< 0.2	Brittle Al_5FeSi particles	< 0.005	Impurity, reduced corrosion resistance
Mn***	0.3	$Al_{15}(Mn,Fe)_3Si_2$ particles [10]	0.25-0.6	Removes iron: Increased ductility, corrosion resistance
Ti, B	Ti < 0.2	Grain refinement	-	-
Sr	0.01	Modified Al-Si eutectic	-	-
Zn	< 0.1	Affects corrosion type	< 0.22	Increased strength, fluidity
Be	-	-	0.0005-0.0015	Minimize oxidation
Cu	< 0.03	Impurity	< 0.01	Reduced corrosion resist.

*The A356 alloy composition depends on the batch; **Fe content is typically higher in HPDC to reduce die soldering. It is necessary to keep the sludge factor (SF) low, i.e. SF = wt%Fe + 2wt%Mn + 3wt%Cr < 1.75 [11]), to avoid large intermetallic inclusions; ***Mn is added to improve the ductility.

2 THEORETICAL BACKGROUND

2.1 Solidification of Alloys

In casting of metals, the nucleation events occur by heterogeneous nucleation on substrates that provide an appropriate interface. The classical theory on heterogeneous nucleation is given in textbooks on solidification [12, 13], and is commonly assessed in grain refinement theory [14]. In the forthcoming section, the physical fundamentals for nucleation are outlined.

2.1.1 Nucleation of Crystals on a Substrate

At a specific temperature, the thermodynamically stable state has the lowest free energy (G). For a given undercooling, ÷T, there is a driving force for solidification ÷G=G_s-G_l. The undercooling has to be sufficiently large to provide the energy required for forming new interfaces. For a sphere with radius r, ÷G consists of two competing terms; the interfacial energy, (proportional to r^2), and the free energy per volume, (proportional to r^3):

$$\div G = 4\phi r^2 \nu_{sl} - \frac{4}{3}\phi r^3 \div G_v \left(\frac{2 - 3\cos\chi + \cos^3\chi}{4} \right) \qquad (1)$$

The last term in equation 1 is the shape factor function, f(χ), where χ is the wetting angle between the nucleus and the substrate. Good wetting occurs when χ is small, and f(χ) becomes 0 when χ=0. Thus, when the wetting between the crystal and substrate improves, the nucleation barrier decreases. This is taken advantage of in the casting process, where inoculants are added to the melt. It is required that they are thermodynamically stable over a sufficient time period, possess low lattice disregistry, good wetting, are sufficiently large to overcome the surface energy barrier, possess suitable density, are adequately small and evenly distributed to be accepted in the casting.

Nucleation Mechanisms

As outlined in the previous section, the solidification of alloys begins when crystals are nucleated on suitable substrates at a sufficient undercooling of the melt. In the dynamic nature of the casting process, the nucleation events can occur by several mechanisms in the absence of chemical additions of inoculants. Textbooks on casting and

solidification only provide brief explanations of the nucleation mechanisms [12, 15, 16], and in the following, the principal mechanisms are summarized in the context of HPDC.

Filling the shot sleeve in HPDC is similar to pouring of melt into a permanent mould. The liquid in contact with the cold mould wall is rapidly cooled below the liquidus temperature, T_{liq}. The classical theories then predict three different scenarios:

1) The melt becomes thermally undercooled adjacent to the mould wall, as schematically illustrated in Figure 2. The thermal undercooling, $\div T_t$, can be sufficient to overcome the required nucleation undercooling, $\div T_n$, which depends on the substrates that are present. Furthermore, the thermal gradient, G, (which depends on the melt superheat and the mould wall temperature), can alter the amount of thermal undercooling. This is the principal requirement for the *separation theory* presented by Ohno [17] as well as the theory on *free chill crystals* by Chalmers [18]. Additionally, the *showering theory* by Southin [19], presumes that the heat loss by means of radiation at the melt surface generates a thermal undercooling which is sufficiently large for nucleation of crystals.

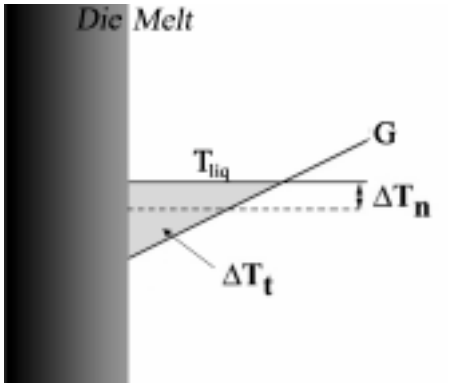

Figure 2: Nucleation is feasible in the thermally undercooled region adjacent to the die wall when the melt undercooling, $\div T_t$, exceeds the required nucleation undercooling $\div T_n$.

2) A solid layer eventually grows from the mould wall. In alloys with eutectic phase diagrams, such as Al-Si and Mg-Al, solute is then rejected at the growing interface creating a solute enriched zone. This is shown in Figure 3 for a planar growth front: In the diffusion boundary layer, the amount of solute, (c_l), decreases with distance and the local melting point ahead of the growth front therefore varies as shown by the solid

curve, (T_{liq}), in the lower left-hand illustration. The actual temperature, imposed by the simultaneous solute diffusion and extraction of latent heat of fusion, is T_m. A constitutionally undercooled zone is therefore present in which suitable substrates can nucleate crystals, as represented by the *supercooling theory* by Winegard et al [20]. In unconstrained growth, the latent heat is conducted into the surrounding melt which generates the thermal gradient required for constitutional undercooling.

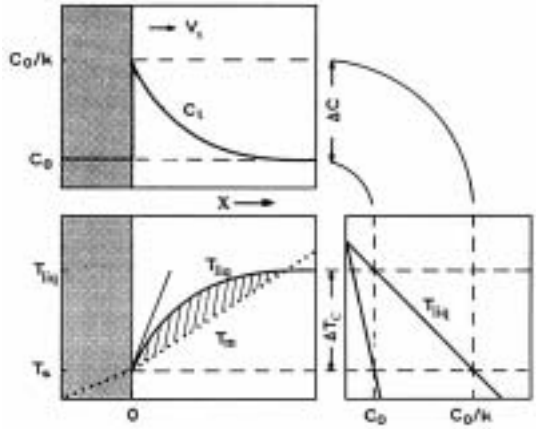

Figure 3: Illustration of the principles for constitutional undercooling [13] in constrained growth. Solute rejection at the crystal interface and simultaneous release of latent heat of fusion generates a constitutionally undercooled zone.

For an equiaxed dendrite the principal difference between alloy systems is the growth restriction factor (GRF): $GRF=m_l c_0(k-1)$ [21]. Furthermore, the solute undercooling is typically larger than the thermal undercooling by a factor of 100-1000 [14].

3) Furthermore, dendrite fragmentation processes, as represented by Jackson et al. *remelting theory* [22], involves the complexity of: micro-segregation, thermal and solutal convection, solid/liquid diffusion and ripening. Nevertheless, it is important to be aware that the fragmentation of dendrites in general represents a significant source of equiaxed dendrites in the casting process.

Aluminium foundry alloys are usually grain refined by chemical additions of Al-Ti and Al-Ti-B master alloys. The exact nucleation mechanisms are debated, but it is a common perception that when the alloy is grain refined, nucleation occurs more effectively because a lower undercooling is required. Grain refinement of magnesium-aluminium alloys is not as well established. However, some methods have been developed [23], and are briefly listed by topic here: 1) superheating followed by rapid

cooling of the metal to the casting temperature; 2) the "Elfinal" process that involves the addition of ferric chloride to the melt, (which is not attractive due to the detrimental effect of Fe on the corrosion resistance); 3) carbon inoculation. Magnesium alloys, that do not contain aluminium, can be grain refined by zirconium master alloy additions. Zirconium is the most strongly segregating element in Mg.

2.1.2 Remelting/Dissolution of Crystals

Because the major physical process of interest in solid-liquid state phase transformations is solidification, remelting of crystals is seldom treated in the literature. However, the assessment of the remelting of crystals is practically relevant as shown in the appended articles, where crystals are formed and transported into hotter regions. A brief introduction to the problem is therefore provided in the following:

When solid remelts, the rate of phase change is determined by the melt thermal diffusivity, ζ, and when it dissolves, it is controlled by the compositional diffusivity, D_l [24]. This can be expressed implicitly by the Lewis number [25], ϑ, which is typically more than 10^4 for aluminium and magnesium alloys:

$$\vartheta \equiv \frac{\zeta}{D_l} \tag{2}$$

For the purpose of providing the reader with an intuition of the A356 and the AM60B alloys, the physical properties [13, 26, 27] are shown in Table 2.

Table 2. Physical properties of the A356 alloy [13, 27], and the AM60B alloy[26].

Alloy	ψ [kg/m^3]	T_{liq} [^{o}C]	T_{eut} [^{o}C]	$\div H_f$ [kJ/kg]	$\div H_f^v$ [J/m^3]	C_p [kJ/kg·K]	ρ [W/m·K]
A356	2700	615	565	389	10.5 x10^8	1.11	210
AM60	1800	619*	435	370	6.6 x10^8	1.02	61

*T_{liq} is reported in the literature as either 615^{o}C or 619^{o}C, the latter used in this work.

Heat Required to Melt Solid

The heat required to melt a dilute dispersion of solid in liquid in an adiabatic system corresponds to (heat supplied to solid = heat extracted from liquid):

$$n\frac{4}{3}\phi\,\rho r^3 \div H_f \equiv C_p \div T_{remelt} \tag{3}$$

The remelting of solid can cause a significant temperature decrease compared to the fractions of a degree required of thermal undercooling for nucleation and dendrite growth in commercial alloys. The volumetric latent heat of fusion in magnesium is half of that of aluminium, cf. Table 2, which generate lower liquid cooling. This is further exaggerated when reducing the particle size. In a casting operation, the major heat extraction is by conduction through the mould wall.

Thermosolutal Transition Temperature

A sharp transition in the melting rate of primary crystals occurs with increased melt superheat [24, 25], and it is necessary to assess the dissolution and remelting of crystals, similar to the theories presented in [25, 28, 29]. The temperature where solid melts without composition change is termed the thermosolutal transition temperature, (T_{trans}) [25], and is expressed as:

$$T_{trans} = T_M - m_l (k - 1) c_0 \quad (4)$$

Estimated values of T_{trans} for the A356 and AM60B alloys are shown in the low-solute parts of the Al-Si and Mg-Al binary phase diagrams in Figure 4. It varies with composition and depends on the alloy system; in Mg-6%Al T_{trans} is 19K above T_{liq}, whereas in Al-7%Si it is 37K above T_{liq}.

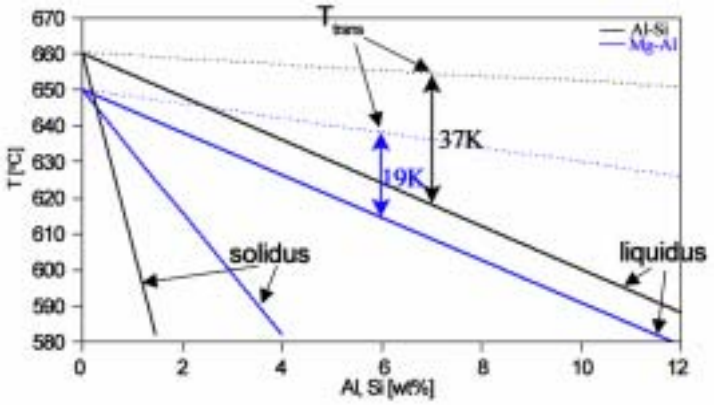

Figure 4: The low-solute parts of the Al-Si, (black lines), and Mg-Al, (blue lines), binary phase diagrams. Liquidus-lines assumed linear. Thermosolutal transition temperatures indicated with T_{trans}.

For a further introductory treatment, it is assumed that: 1) the melt is superheated, ($T_m > T_{liq}$), and isothermal; 2) a dilute dispersion of spherical crystals is present; 3) the distribution coefficient, (k), is constant and $k<1$; 4) the diffusion layers are limited due

to convection and steady state liquid diffusion pertains in the solvent boundary layers; 5) there is no barrier for atom detachment and 6) undercoolings are neglected.

Thermally Controlled Melting Rate

When the melt temperature is above T_{trans}, the solid remelts by supply of heat through a thermal boundary layer, (ι_T), at a thermally controlled melting rate, v_T [29]:

$$v_T = \frac{\rho \Delta T_{ts}}{\iota_T \Delta H_f \psi_s} \tag{5}$$

Solute Diffusion Controlled Melting Rate

When a particle, (of uniform composition $c_s < c_0$), is carried into a slightly superheated liquid, ($T_{liq} < T_m < T_{trans}$), of composition c_0, it will start to dissolve. The mass balance is[29]:

$$v_s / c_0 - k c_0 = -D_l \left(\frac{dc}{dx}\right)_l + D_s \left(\frac{dc}{dx}\right)_s \tag{6}$$

The solid diffusion rate is generally orders of magnitude lower than diffusion in the liquid, and the last term on the right-hand side of equation 6 can therefore be neglected. Furthermore, $(dc/dx)_l$ can be expressed as the variation in solute concentration through the solute diffusion boundary layer, ι_s, i.e. $(c_l - c_0)/\iota_s$. Hence:

$$v_s = -\frac{D_l / c_l - c_0}{c_0 / 1 - k \iota_s} \tag{7}$$

Despite the relatively extensive list of simplifications, the theory presented above gives a first order understanding of remelting of crystals. It is important to note the existence of a variation in the melting/dissolving rate of crystals with melt temperature.

Further Solidification

When the melt cools, crystals survive and solidification eventually proceeds. Further growth involves solute segregation which can generally be described by the *Gulliver-Scheil equation*. In the case of no solid diffusion and complete mixing in the liquid, the expression takes the form [13]:

$$c_l = c_0 / 1 - f_s)^{k-1} \tag{8}$$

This equation overestimates the amount of eutectic but is relatively representative at low solid fractions, and has been suitable in most applications in the doctorate work. Crystals that grow evolve into dendrites and develop different order branches which depend on the dendrite tip radius (r), the local thermal gradient (G), solute diffusion (D) and the constitutional conditions that are present. When the diffusion fields encapsulating the crystals impinge on each other, peripheral growth is substituted by coarsening [13]. Eventually, the crystals are no longer free to move. The consequence of this on the solidifying structure is explained in the following paragraph.

2.1.3 Dendrite Coherency and Mechanical Strength

Dendrite coherency is described here because of its importance in the interpretation of the mechanisms that control the extent of segregation of ESCs and the formation of banded defects in HPDC.

During stirring of a melt which is cooled, the shear strength can be measured as a function of the fraction solid. Measurements obtained with this method are shown in Figure 5. The shear strength of the material pass through several stages, and the coherency point is identified by changes in the shear strength of the mushy material, i.e. when the material starts to build up strength. The fraction solid at which this occurs depends on the crystal morphology. The coherency point, (f_s^{ch}), is displaced to larger fraction solid when the crystals change from large dendritic to small globular. With increasing fraction solid, a maximum packing fraction is reached where the shear strength of the dendrite network is further increased.

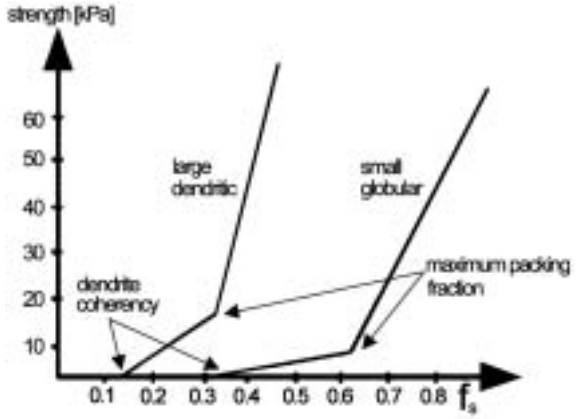

Figure 5: Measurements of the shear strength of the material as a function of fraction solid, (f_s), for the two extremes in crystal morphology; large dendritic crystals and small globular crystals [30].

The coherency fraction solid is considered to mark the transition from mass to interdendritic feeding [31]. Beyond coherency, the restrictions imposed on the liquid flow, and the development of contraction stresses in the continuous solid network, can result in common casting defects such as macrosegregation, hot tearing, shrinkage and gas porosity. The rigidity of the developing dendritic network may also have a significant impact on the formation of defects.

2.2 Shot Sleeve Principles

The pouring of molten metal into the shot sleeve of a die casting machine resembles gravity pour die casting, and in the preceding chapter the fundamental solidification theory was briefly outlined in the context of such applications. This chapter concerns the filling and solidification in the shot sleeve, and the implications that are important for the doctorate work, as presented in the appended articles.

2.2.1 Filling of the Shot Sleeve (1-8s) and Solidification

There have been many investigations on the metal behavior during shot sleeve filling and a relatively large amount of literature is therefore available on the subject. Numerical modeling and experimental work generally reveal a similar constitutive metal behavior. Shot sleeve filling simulations are shown in Figure 6 [32, 33], and the major flow characteristics are: 1) the metal impinges on the shot sleeve bottom, near the plunger; 2) it flows to the end of the shot sleeve, and then backwards; 3) a surge wave moves backwards towards the pouring hole; 4) additionally, metal continuously washes upon the plunger and partly accumulates there, (note the velocity scale bar at the top of figure 6a). The surge wave is similar to a hydraulic jump [34], where the metal flow is characterized by the Froude number [35], $Fr = v/(gh)^{1/2}$. It is important to consider where the metal becomes positioned during filling, as shown in Figure 6b [33]: the green particles are immersed in the melt early, and primarily become located near the die. The "older" red and yellow particles remain near the plunger.

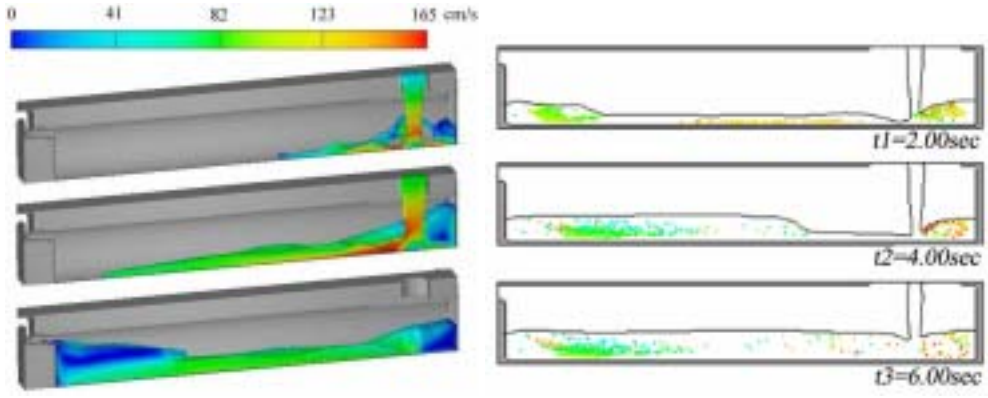

Figure 6: a) Simulation of the filling of an A380 aluminium alloy [32]. The scale bar indicates metal velocity; b) Simulation of particle position during filling. Reproduced with data from [33].

The shot sleeve filling time depends on the amount of metal being poured, (volume of shot sleeve), and is in the range of ~1-8s, (a fill fraction of 0.5 is usually employed). Furthermore, a common foundry practice in aluminium HPDC is to let the metal settle for a few seconds, to allow for any air bubbles to escape from the melt.

When aluminium melt is transferred from the casting furnace to the shot sleeve, it could be anticipated that there is a continuous dissipation of the superheat, (which is typically 60K [36]). However, it has been found that a negligible heat loss is experienced in the ladle [32, 37]. The magnesium melt resides in a heated steel tube adjacent to the pouring hole, and therefore possesses the required melt temperature when the shot sleeve filling starts. The principal heat extraction therefore occurs when the melt is poured into the shot sleeve, which eventually induces formation of solid.

An analytical model for the solidification in the shot sleeve has been developed [38]. The removal of melt superheat through the different shot sleeve interfaces, *i*, is given by the heat balance:

$$\rho V C_p \frac{dT}{dt} = -\sum_i A_i h_i (T - T_i) \tag{9}$$

The thickness solid formed, ι_i, at the different interfaces can be calculated:

$$\iota_i = \frac{h_i (T_{liq} - T_i)\theta}{\rho L H_f} \tag{10}$$

The total fraction solid, f_s, is then:

$$f_s = \frac{\sum_i A_i \iota_i}{V} \tag{11}$$

A rigorous treatment by numerical simulations has shown how the fraction solid varies with different heat transfer coefficients, *h* [39], determined from experimental measurements [40]. Furthermore, the alloy, amount of superheat, fill- and residence time, shot sleeve volume, fill fraction and melt-wall contact conditions are parameters that control the amount of heat dissipation, as outlined by e.g. *Campbell* [16]. Significant amounts of the metal, (20%)[1] [41, 42], can be solidified when the die filling starts in magnesium HPDC. An example of the simulation of temperature evolution in the melt

[1] With a fill fraction of 0.35 and 50mm inner diameter shot sleeve

during shot sleeve filling of an A356 aluminium alloy is shown in Figure 7. It is important to note the non-isothermal conditions that are present.

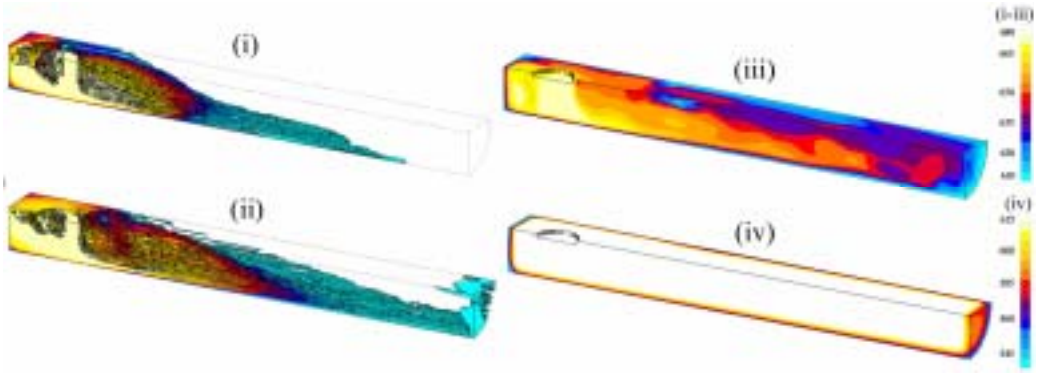

Figure 7: Simulation of the melt temperature evolution in the shot sleeve, (longitudinal cross section), for an A356 aluminium alloy, (details in APPENDIX B). Total f_s when injection starts is ~10%. The heat transfer coefficient was determined from experimental measurements.

It is important to determine the shot sleeve thermal conditions to improve the modeling of the HPDC filling/solidification. The current models neglect the non-isothermal melt conditions in the shot sleeve and its influence on the metal behavior during die filling and solidification. The metal is typically assumed isothermal and fully liquid. This can affect the prediction of defects. Additionally, the pre-solidification imparts significant effects on the microstructure and the mechanical properties in the castings.

Cold Flakes

When the plunger moves it can force the solid layer on the shot sleeve wall to collapse and mix with the melt. This is conceptually illustrated in Figure 8a. The interfaces between the surface layer, which is formed early, and the residual melt is indicated with arrows. Furthermore, the metal adjacent to the plunger possesses large, columnar dendrites, as shown in Figure 8b.

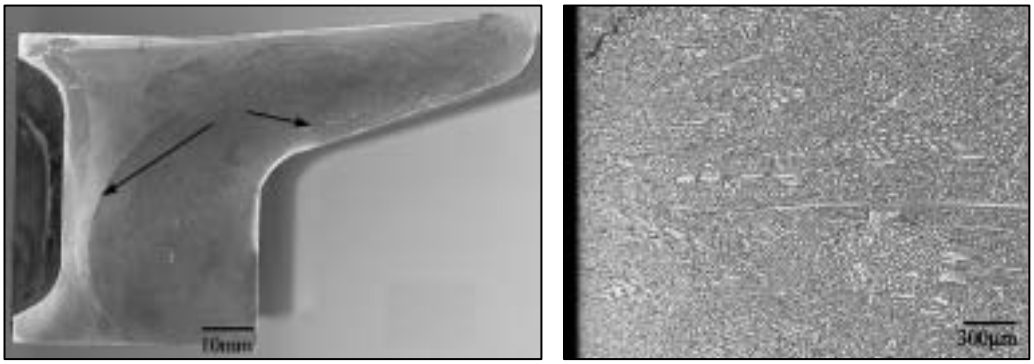

a) b)

Figure 8: a) Cross sectional micrograph from the biscuit. Interfaces between solid surface layers and melt solidified later indicated with arrows; b) Magnification of the microstructure near the plunger. AM60B alloy.

The debris, (i.e. chill layers [43], externally solidified product (ESP) [44]), or cold flakes [11], is commonly observed in aluminium HPDC. The cold flakes possess one interface, (exposed to the shot sleeve wall), which does not weld to the residual melt during solidification in the die cavity. They can be relatively large, as shown in Figure 9 [44], and are deteriorating for the ductility in the casting [45].

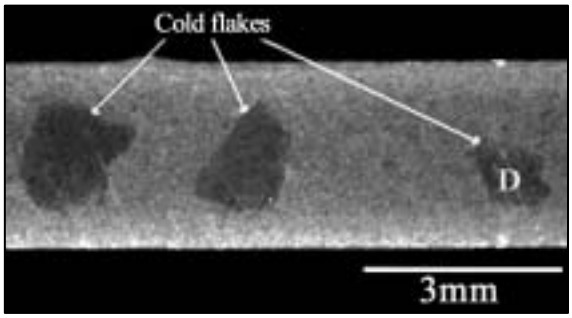

Figure 9: Cross sectional micrograph from an A380 aluminium alloy die casting [44] which shows large cold flakes embedded in the microstructure.

2.2.2 Externally Solidified Crystals (ESCs)

A subject that has until recently received less attention than cold flakes, is the pre-solidification that results in equiaxed single crystals in the liquid. Despite that these crystals are generally not mentioned in the traditional literature, they are proven by their existence in aluminium and magnesium die castings. The terminology describing the crystals is somewhat inconsistent: floating crystals, externally solidified dendrites

[46] or externally solidified grains (ESG) [47]. ESCs, (externally solidified crystals), are interpreted in the following.

The ESCs are a striking feature in the microstructure, because they are significantly larger than the grains formed from the metal that solidified in-situ in the die cavity. The ESCs are more frequently observed in the central regions of cross sections in the castings and a traditional misconception has therefore been that these coarser crystals are a result of the slower solidification encountered here. At different locations in a casting, the ESCs are observed to occupy up to 40% of the volume in magnesium alloy die castings and up to 20% in aluminium alloy die castings. An example of ESCs in an industrially produced AM60 instrument panel is shown in Figure 10.

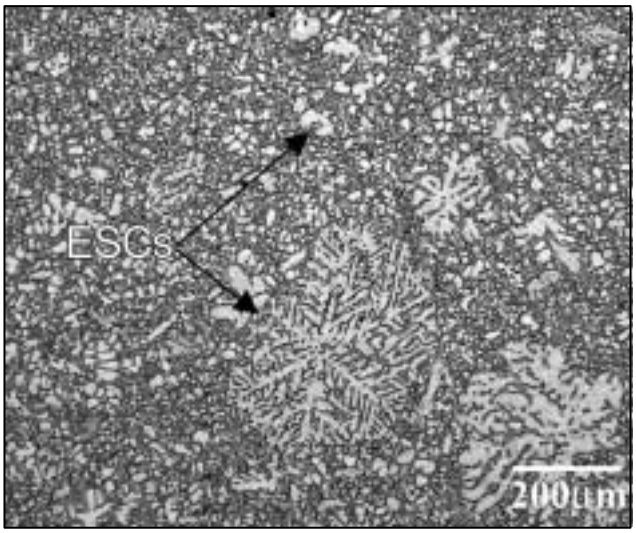

Figure 10: Optical micrograph from an industrially produced HPDC AM60 instrument panel. Etched microstructure: The large white particles are ESCs, whilst the gray structure is the fine grained matrix.

2.3 Plunger Movement

A comprehension of each HPDC casting can be achieved by inspection of the shot diagram, as shown in Figure 11. The diagram provides a connection between the plunger movement and the pressure build-up as a function of time. Significant discrepancies between the measured and the programmed values can give indications of the quality of the casting. The plunger movement is usually separated into three different phases: I) the slow shot phase (1-7s); II) the die filling phase (0.01-0.3s), and; III) the pressurization phase (400-1200bar for 5-20s) [9, 48].

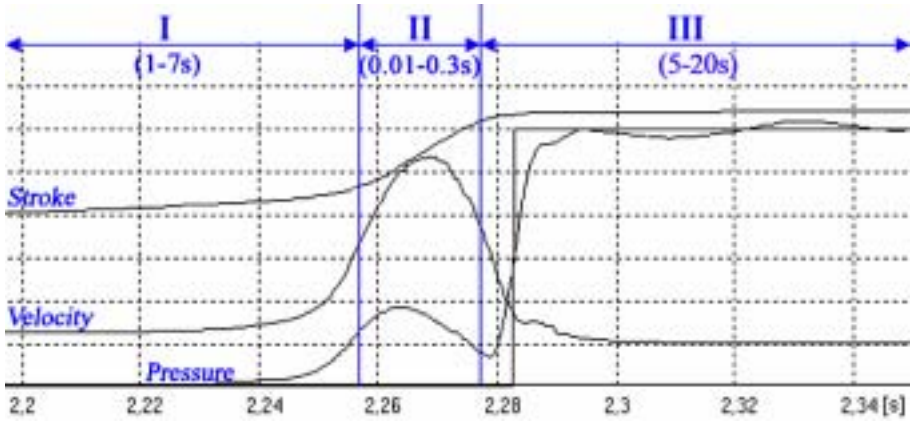

Figure 11: Shot profile from an AM60 magnesium alloy die casting. The diagram shows plunger stroke, velocity and pressure as a function of time. I): slow shot phase (1-7s); II) die filling phase (0.01-0.3s); III): pressurization phase (5-20s).

It is a common conception that an optimal movement of the plunger is a prerequisite to obtain high quality die castings. Formerly, the plunger movement was instantaneously brought to die filling speed when the shot sleeve pouring was completed. This typically resulted in the entrapment of air, and it was therefore necessary to improve the plunger movement [49].

2.3.1 The Slow Shot Phase (1-7s)

The purpose of the slow shot phase, (I), is to build up a wave that forces the air in front. An optimal plunger movement, which requires a specific plunger acceleration, thus forces the exposed metal surface into the runner system, through the die and into the overflows. Contrarily, if the slow shot velocity exceeds a critical value, a breaking wave that encapsulates air forms. The oxidized melt surface can mix with the melt and

affect the ductility in the casting when brought into the die cavity. Similarly, a wave traveling faster than the plunger can impinge on the die, and travel backwards towards the oncoming plunger and entrap air.

The first analytical model on plunger movement was based on the Bernoulli equation[2], and was developed by *Garber* [50]. This model does not include surface tension, viscosity variations and is only applicable in cases where the shot sleeve fill ratio is ~0.5. Figure 12 shows how the surge wave appears, and provides the basis for *Garber's* model.

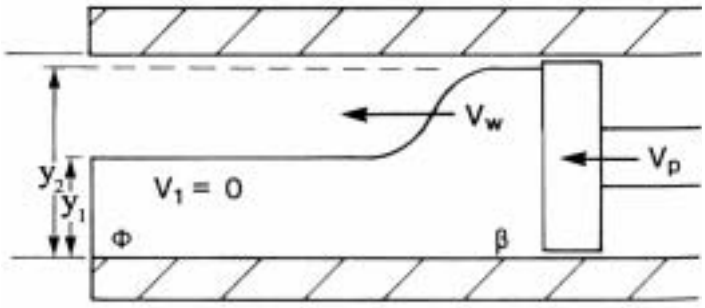

Figure 12: Surge wave, with velocity v_w, ahead of plunger tip, with velocity v_p.

The critical plunger velocity, where an optimal wave is formed, can be estimated. The requirement is that the plunger velocity, v_p, does not exceed the wave velocity, v_w. For a given plunger velocity, the wave velocity is:

$$v_w = \frac{\eta}{\eta - \lambda} v_p \tag{12}$$

and;

$$v_p = \left\{ 2g \frac{(y_2 - y_1)(\eta - \lambda)}{\eta - 2\lambda} \right\}^{1/2} \tag{13}$$

Additionally, empirical equations are used to calculate the critical plunger velocity, v_{crit}, for an optimal plunger movement. An example is [11]:

$$v_{crit} = 22.8 \cdot f_{fill} \cdot \sqrt{D_{pl}} \tag{14}$$

[2] Deduction of the Bernoulli equation is provided in e.g. [35].

Although the mathematical description of the optimal plunger movement is debated, the existence and the importance of a critical wave velocity is undisputable and has been experimentally validated in i.a. [51]. More refined models have been developed, and when suitable numerical models are used, variable shot sleeve lengths, diameters and fill ratios, as well as surface tension and free surfaces can be included in the calculations of the plunger movement. However, the common prerequisite for these modeling environments is that a similar optimal constitutive metal flow behavior pertains when the plunger moves.

For the purpose of visualization, an example from the simulation of plunger movement is shown in Figure 13 [52]. When the plunger moves, the metal near the plunger is lifted up, and fills the cross section. With further plunger movement, a wave is formed ahead of the plunger. The metal adjacent to the die in the shot sleeve remains quiescent at this stage. Eventually, the quiescent metal is forced upwards, filling the residual empty part of the shot sleeve and, furthermore, flows into the runner system. Note that the hottest part of the melt enters the runner first, cf. the scale bar.

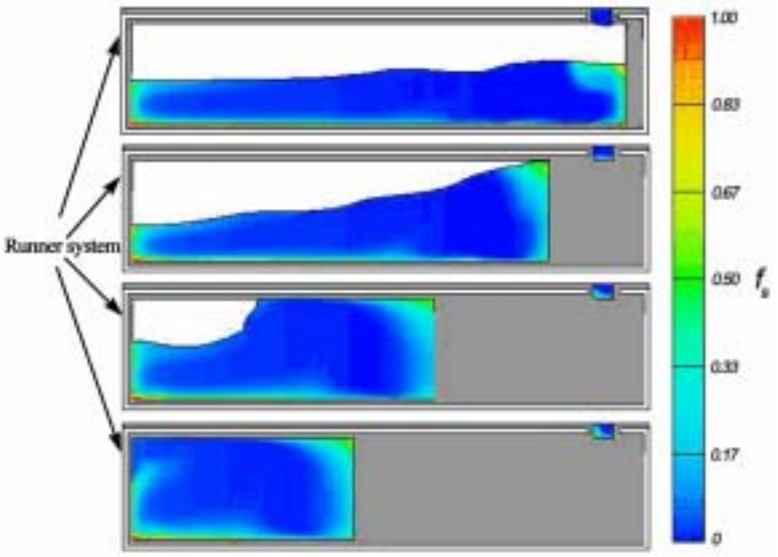

Figure 13: Simulation of slow shot plunger movement and simultaneous metal flow and fraction solid distribution, indicated by the color scale bar [52]. The hottest melt, (blue colour), enters runner first.

2.3.2 The Die Filling Phase (0.01-0.3s)

The transition from the slow shot (I) to the die filling phase (II), typically occurs when the metal is at the gate [3]. Due to the narrower cross section of the gate, the counter-pressure increases, as shown implicitly in the shot diagram in Figure 11. A high plunger velocity is then applied to accommodate for a rapid filling of the die cavity.

There are different interpretations to the metal flow mode in the die, i.a. atomized and turbulent flow. However, it is widely accepted that the die filling becomes complicated by rib structures, bends and variable metal velocities. It may therefore be inappropriate to generalize the flow mode. The apparently simple filling of a box-shaped die cavity can be difficult to predict and analyze. In an interrupted plunger movement, the plunger can be stopped during the die filling stage. The metal freezes quickly, approximately in-situ, providing an understanding of the metal flow pattern in the die cavity. Some features are shown in Figure 14, (from the HPDC castings in the doctorate work). The photograph in Figure 14a, indicates the extent of fragmentation at the flow front, and the arrow in Figure 14b shows a location where two metal flows met and the metal froze through the thickness during die filling.

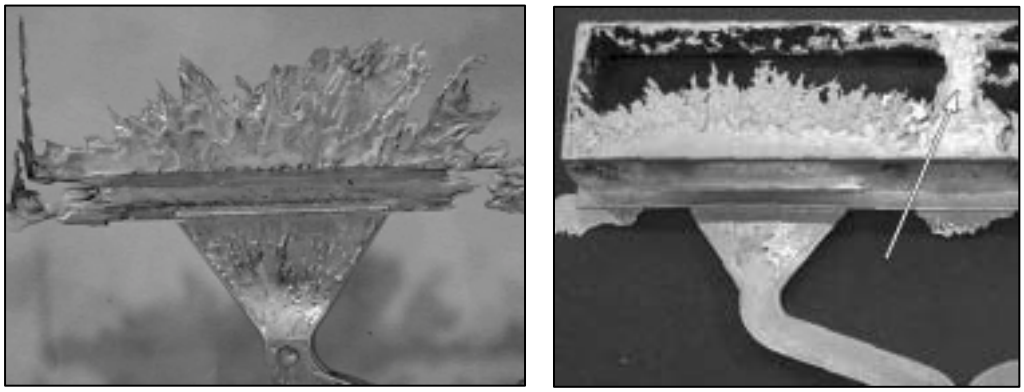

a) b)

Figure 14: At approximately 70% plunger movement photographs of: a) The fragmented flow front; b) A location where the metal has frozen through the thickness during die filling, (marked with arrow). Principal die filling direction is vertical, parallel with acceleration of gravity.

[3] Occasionally a pre-filling method is utilized: the rapid plunger movement is not initiated until some of the metal has entered the die cavity.

2.3.3 The Pressurization Phase (5-20s)

When the die is filled with metal, the after-pressure is applied to feed the shrinkage of the casting during solidification. This pressure is typically 400-1200bar, and is applied for 5-20 seconds till solidification is completed. The small gate area that separates the biscuit and runner system from the casting may freeze early and the entire pressure is thus prevented from being successfully transmitted to the entire casting. Squeeze pins in the die cavity are therefore occasionally used in locations where additional pressure is required.

In the doctorate work, the pressure has been applied according to the size of the castings, the feasibility of the HPDC machine and common HPDC practices. Furthermore, the process parameters used for producing the HPDC castings in the doctorate work are provided in APPENDIX C.

2.4 Microstructure Phenomena in HPDC

The filling of the metal into the relatively cold die dissipates the residual heat contained in the metal. A simplified analytical approach to assess the heat loss during die filling is outlined in [53]. It follows the logics briefly presented by *Flemings* [12], and is analogous to the heat balance in the shot sleeve represented by equation 9. In the present context, the heat transferred from a unit of the alloy to the die during flow is:

$$\psi V C_p \frac{dT}{dt} = 4 h_i A / T_m 4 T_{die} 0 \tag{15}$$

For a cylinder, the temperature change in the unit of metal is then:

$$\frac{dT}{dt} = 4 \frac{2 h_i / T_m 4 T_{die} 0}{\psi r_{tube} C_p} \tag{16}$$

Because this unit dissipates heat into the die, it affects the heat transfer conditions for the next unit of metal. It is therefore possible to simultaneously calculate the metal heat dissipation and conduction into the die, and obtain an approximation of the metal temperature when the die filling is completed. However, more refined models with finer resolution are required for a better assessment of the die filling and concurrent solidification.

2.4.1 Surface Layer

The formation of a solid surface layer in the die is important in the understanding of how it affects the distribution of ESCs and the formation of banded defects treated in the doctorate work. The surface layer consists of very fine grains, and is typically referred to as the skin [54]. The terminology “skin” can be misconceiving because it is commonly several hundred microns thick.

One attempt on explaining the formation of a surface layer in aluminium HPDC has been presented by *Chen* [55]: the amount of melt impingement affects the formation of a surface layer under applied pressure in the die. Furthermore, it is proposed that the surface layer forms during the pressure intensification and obtains a thickness, S, as approximated by the expression: $S=h_i t_s((T_m-T_{die})/(\psi - H_f)$, where h depends on the pressure. This theory does not present any detailed mechanism on the formation of the surface layer and it assumes that the layer forms after the die filling is completed.

The heat dissipation during die filling depends on the contact between the melt and the die wall, the melt velocity, and the melt and die temperatures [40]. The local heat extraction can be sufficient to induce an outer layer during flow, adjacent to the die wall, which possesses a fraction solid gradient. When the surface layer reaches a critical fraction solid, it can be capable of resisting further movement [42], whereas the interior still flows. Then the conditions may be suitable for the formation of banded defects, which is explained in the next section.

2.4.2 Banded Defects

Many defects that occur in HPDC are related to the craftsmanship in the casting process, as described in [11]. Not all defects, however, are included in the HPDC textbooks. Striking features commonly observed in HPDC microstructures are the defect bands. The bands typically follow the contour of the casting and consist of segregated eutectic and/or porosity. An example of a segregation band is shown in Figure 15a, whilst a porosity band is shown in Figure 15b.

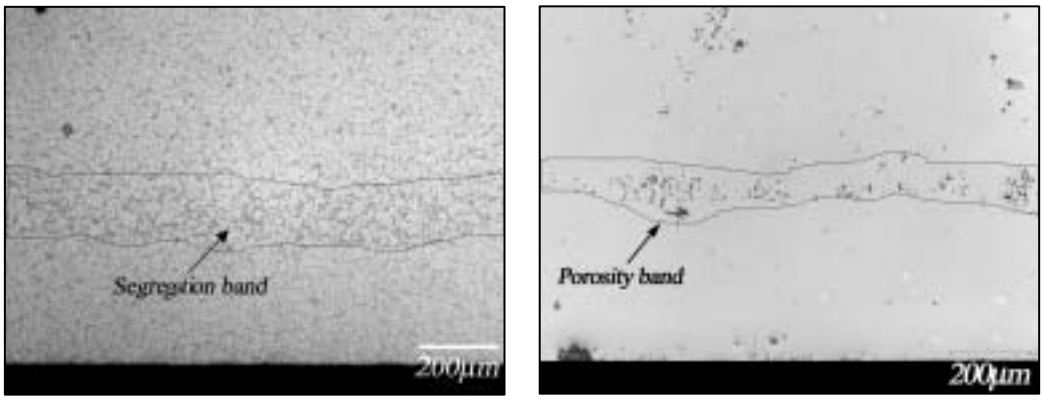

a) b)

Figure 15: a) Segregation band in an A356 die casting; b) A porosity band in an AM60 die casting. Bands delineated with black lines and marked with arrows.

Banded defects have often been associated with magnesium die castings and the formation of the bands has not been sufficiently understood. Among the first to address this phenomenon in HPDC, was *Hill* [56], who termed the microstructure that consisted of porosity bands as a *sandwich structure*. It was suggested that the banded defects results from local die-filling conditions, where local successive metal streams, or possibly local directionalities of heat extraction, generated the porosity bands.

Two decades later, a theoretical framework was put forward by *Dahle et al*. [30] to explain the banded defects: The defect bands form by a combination of a fraction solid gradient away from the die walls, (because of heat transfer into the relatively cold die), and the migration of ESCs to the centre as a result of lift forces acting on the solid. The solute enriched liquid concentrates next to the die walls resulting in the formation of the casting skin, leaving a region of solute enriched liquid between the semi-solid inner core and the outer skin. Deformation therefore concentrates in the lower fraction solid region, which then forms a shear plane. The nature of the defect bands can depend on the local f_s in the shear plane during flow, it is argued, and if $f_s < f_s^{ch}$ for much of the filling, bands of segregation appears. Contrarily, if larger f_s is present in the plane, the band can be made up of pores or tears. The relationship between the strength, fraction solid, and the developing microstructure is shown in Figure 16. The central region moves in plug-type flow, whilst the liquid segregates to the low f_s regions forming a band.

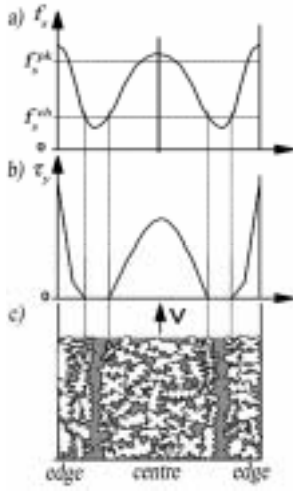

Figure 16: Illustration of: a) The fraction solid profile; b) The corresponding strength profile; c) The resulting microstructure where the central region facilitates deformation by slip along the segregated shear plane [30].

Changes in casting parameters in industrial die castings, have been shown to affect the bands, e.g. [57-59], and recently, an additional explanation on the formation of defect bands was presented [60]: 1) agglomeration of ESCs in the central region of cross sections is a prerequisite for bands to form; 2) the bands mainly form after the casting contracts away from the die wall; 3) the tensile stresses that build up in the residual liquid causes a pressure drop and viscous flow in the mushy zone, forming a segregation band.

Figure 17a is an example of an A356 aluminium alloy die casting where distinct segregation bands are aligned parallel with the surface of the casting, and few ESCs are present.

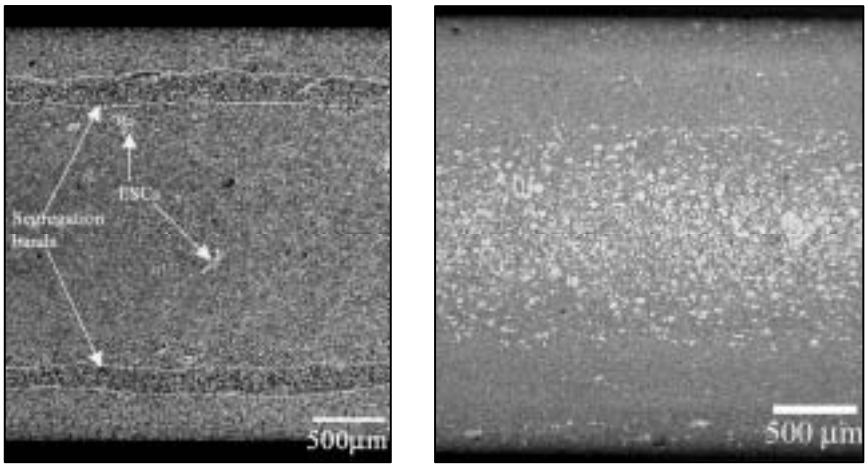

a) b)

Figure 17: a) Segregation bands in an A356 aluminium alloy die casting. Few ESCs are present; b) Typical HPDC microstructure: The ESCs are located in the central region of the cross section. Flow direction to the right and parallel to the page.

2.4.3 Segregation of ESCs

When a mixture of crystals and liquid flows into the die cavity, it resembles two-phase flow common in industrial and environmental processes [61]. A characteristic observation then is the migration of particles towards the central regions during flow. As pointed out in paragraph 2.2.2, this is also a typical observation in HPDC where the ESCs are segregated to the central region, as shown in Figure 17b. Despite the similarity with two-phase flow in industrial applications, the mechanisms that control the migration of particles are not possible to directly interpret in the context of HPDC.

There have been some brief attempts to explain the segregation of ESCs in HPDC. One of those theories was mentioned in paragraph 2.4.2, above. Another theory explains the segregation of ESCs as follows: an inhomogeneous temperature distribution is inherently present in the shot sleeve which results in non-uniform solidification conditions. A higher fraction of ESCs is present near the gate and lower fractions are present farther from the gate in the castings. Additionally, a surface layer forms during flow, which constricts the metal to flow in the centre.

2.5 Mechanical Properties

The thickness of the surface layer/skin in the casting is often regarded as a controlling parameter for the mechanical properties because it consists of a sound and fine-grained microstructure. There have been several attempts to obtain a correlation between skin thickness and the mechanical properties [41, 54]. The grain size affects the yield stress as expressed by the Hall-Petch equation [62]: $\sigma=\sigma_0+k_{H-P}D^{-1/2}$. It is widely accepted that the effect of grain size on the strength is greater in magnesium than in aluminium, and $k_{H-P}(Mg) > k_{H-P}(Al)$.

Measurements of the hardness are occasionally used for characterization of the variation in strength. In Figure 18, the measurements of the microhardness, (VHN), in two AM60 magnesium alloy castings are shown. The microstructure consists of a large fraction of ESCs distributed over the cross section in Figure 18a. In Figure 18b the ESCs are only present in the central region, and the hardness is observed to decrease significantly towards the centre.

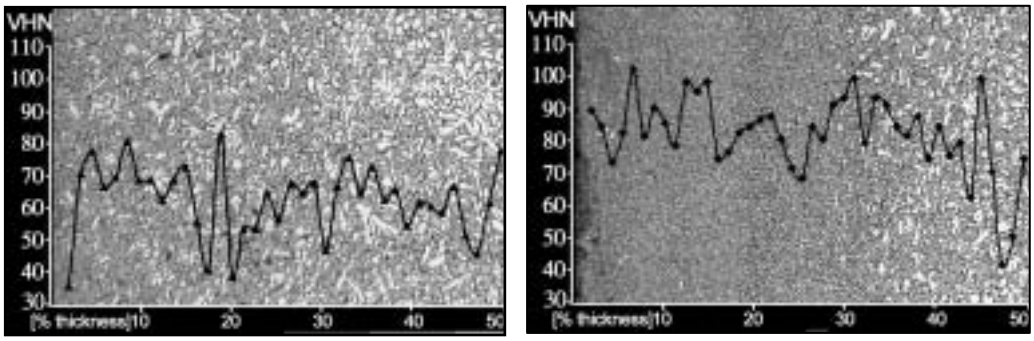

a) b)

Figure 18: Measurements of microhardness (VHN), (10g indentation load), from the surface to the centre in half of the cross sections of thin walled, (2.5mm), AM60 magnesium alloy die castings: a) Large fraction of ESCs ~evenly distributed, with an average VHN 63; b) The ESCs are only located in the central region. Average VHN: 79.

Examples on how the amount and distribution of ESCs can affect the fracture surfaces of tensile specimens are shown in Figure 19. Figure 19a is from a location near the gate in the die casting and a large fraction of ESCs are distributed quite evenly. The fracture surface appears rugged. In Figure 19b the ESCs are centred and the fracture surface appears twofold: shear fracture from the surfaces, and a rugged surface in the central region.

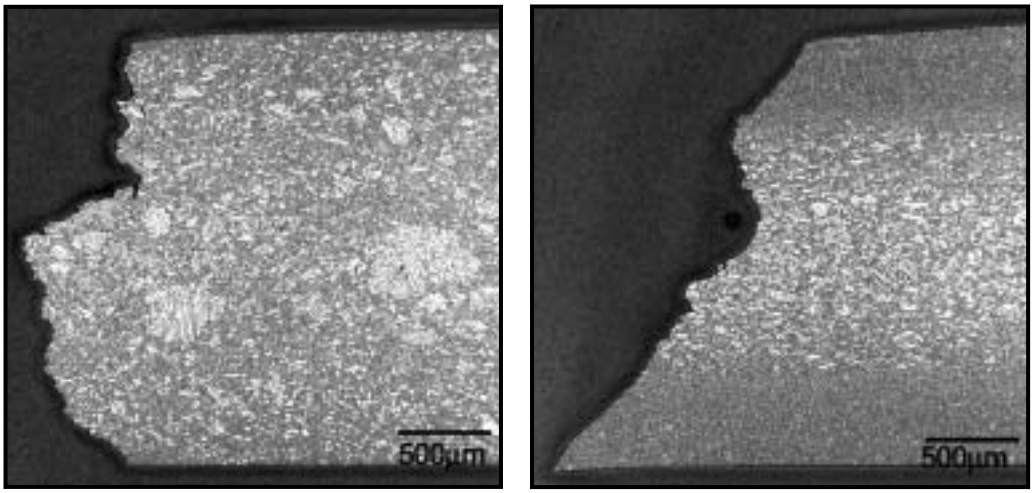

a) b)

Figure 19: Cross sectional micrographs from tensile tested specimens taken from AM60 magnesium alloy die castings: a) Near the gate, typical elongation: 3-10%; b) Farther from the gate, typical elongation: 15-25%.

Whilst the effect of ESCs on the hardness and fracture surfaces are shown above, the ESCs can also affect defect formation during the casting operation as e.g. presented in paragraph 2.4.2. Additionally, if the ESCs are large and branched and occupy a large volume fraction, the permeability, which controls feeding during solidification and thus formation of porosity, is affected. Furthermore, a large amount of ESCs near the gate can reduce the efficiency of the after-pressure through gate blockage. In [63] it was concluded that among variations in several different HPDC process parameters, the metal temperature had the strongest influence on the properties in magnesium die castings: increased metal temperature generated a reduction in the area fraction of ESCs which was the major cause of improved tensile strengths, increased yield stress and elongation to fracture.

The mechanical properties of the finished die castings can be difficult to predict. A key parameter, however, is the ductility in the casting which is critical for the automotive industry, and is what the suppliers seek to improve. As mentioned earlier, there is a broad range of defects that affects the mechanical properties, and testing of HPDC properties is typically done on die cast tensile specimens where the encapsulating skin is intact. When taking out specimens from a casting, parts of the exterior will have a machined surface. Thus, the properties are generally better when specimens cast to

shape are compared with specimens taken out of larger castings. It is therefore important to consider the initial specimen condition before the test results are assessed.

Additionally, to be able to measure the effects of a variable microstructure, the selection of testing method is important. One example is three-point bending, which is typically the deformation mode that a B-pillar (u-shape) in a car is exposed to during a side impact: For castings loaded in u-mode, the first part of the force-deformation characteristics, i.e. before any fracture takes place, is limited by local buckling. The buckling phenomenon is controlled by the material hardening, slenderness and initial imperfections in the casting. When the buckling load has been reached, the local plastic deformation in the buckles increases rapidly with further global deformation and fracture eventually occurs. Thus, relative to the global force-deformation behaviour, the variations in local tensile ductility are of little importance. For castings tested in n-mode buckling does not occur, and the local plastic deformation increases gradually with global deformation. Then variations in local ductility can significantly affect the component behaviour [64, 65].

Final Introductory Remarks

In the preceding sections the reader has been provided with background on: 1) the shot sleeve solidification conditions; 2) how the metal is injected into the die, and; 3) how it affects the microstructure in the HPDC castings. Additionally, some paragraphs on the mechanical properties of die castings have been presented. In the forthcoming chapter, the major results from this doctorate work are summarized.

3 SUMMARY OF RESULTS - FURTHER DEVELOPMENTS

The summary presents the major results achieved in the doctorate work. It is presented in a similar chronological order as the appended articles, and therefore simultaneously provides the logics in the progress of the work. Articles #1 and #2 present investigations of the grain distributions in A356 and AM60 box shaped cold chamber high pressure die castings, (see e.g. Figure 1a in article #1). The ESC morphologies, in particular, are dealt with in articles #3 and #4, whilst article #5 presents investigations of the segregation/migration of crystals during flow. In article #6 a new mechanism for the formation of defect bands is presented.

Grain Distributions

The major results in article #1 are related to the distribution of ESCs [4] in A356 box shaped die castings: The ESCs occupy significantly larger fractions of the volume near the gate in the casting, whilst farther away from the gate the ESCs are more dilute and less evenly distributed. Occasionally they are entirely absent. Investigations of the microstructure in many positions in the castings, revealed three different locations with distinctly different microstructures. Similar consistent observations were done in the AM60 castings. These three locations were therefore emphasized in articles #1-4, and are referred to as position A, B and C.

The inhomogeneous distribution of ESCs is attributed to the shot sleeve filling, solidification conditions and the plunger movement. The convection and flow near the plunger in the shot sleeve generates a large amount of ESCs, whereas near the die the melt is more quiescent and fewer ESCs are formed. When the plunger moves, the metal that possesses few ESCs, flows into the runner system. The metal that consists of a larger fraction of ESCs, (originates from near the plunger) thereafter follows.

Furthermore, the bimodal distribution of grain size in the castings is taken as a proof that the ESCs are formed in the shot sleeve. This is shown by means of: 1) EBSD grain maps, which differentiate the grain size that results from the different cooling rates in the shot sleeve and the die; 2) chemical EPMA analysis indicates that the ESCs possess a lower Si-content than the grains formed in the die cavity, which implies they have been formed in different solidification conditions.

[4] Floating crystals is termed externally solidified crystals (ESCs) here.

The results in article #1 therefore provided motivation for investigations of similar effects in AM60 castings. It was, furthermore, expected that the thermal condition was important for the solidification in the shot sleeve. To test this hypothesis, additional castings were produced with variations in the melt superheat. These results are presented in article #2:

The observations in the AM60 castings, (article #2), were analogous to the results on the A356 alloy, (article #1): The HPDC microstructures were generally observed to consist of 1) a fine grained microstructure, or 2) a mixture of fine grains and coarse grains, (ESCs), which was either centered or dispersed in the cross section. These grain structures were observed to vary with position in the casting. Near the gate a coarse grained microstructure dominated, whereas the fine grains were mainly present farther from the gate. The amount of ESCs in the casting was shown to depend on the initial superheat of the melt.

Interrupted die filling tests revealed that the microstructure in the runners consisted of increasing amounts of ESCs with increased plunger movement. It was therefore concluded that the plunger movement and the variable melt temperature in the shot sleeve contribute to the solid redistribution which resulted in the inhomogeneous grain distributions in the die castings. Additionally, the local melt flow characteristics significantly affect the formation of the grain structure.

The results can therefore provide a conceptual understanding of the filling and solidification behaviour in the A356 and AM60 die castings. This is schematically illustrated in Figure 20. The isotherms are for visualization only, and do not necessarily represent the exact locations. An increasing amount of pre-solidified material, cf. locations designated I-III and the scale, enters the runner system with further plunger movement.

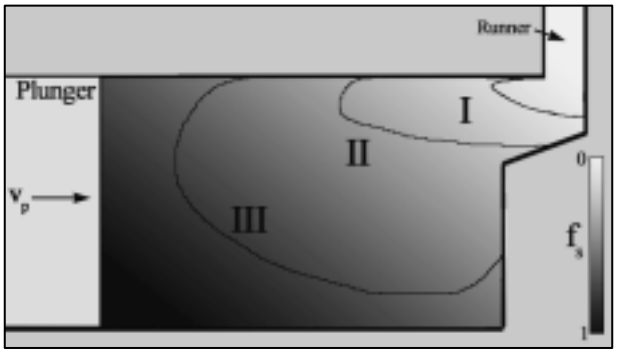

Figure 20: Schematic illustration of the plunger movement and corresponding qualitative description of fraction solid distribution. Metal with increasing f_s, (ESCs), corresponding to locations I-III, enters the runner with further plunger movement.

This results in different fractions of ESCs in different locations in the castings. Figure 21 shows the microstructures in the box shaped die castings that result from metal with thermal histories approximately corresponding to the different isotherms in Figure 20. The distance between the locations in the casting is indicated, (position III is 25mm from the gate in the casting). The fraction of ESCs decreases with distance from the gate.

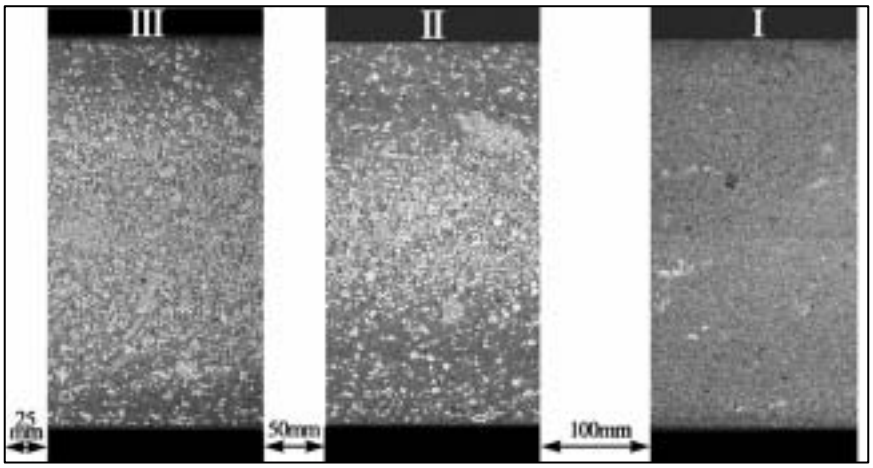

Figure 21: The solidification and metal flow in the shot sleeve results in microstructures with different thermal histories in the casting. The microstructures correspondingly possess different fractions of ESCs. The locations marked III, II and I, correspond to position A, B and C, respectively, in the box shaped die castings in article #1-4. Thickness of the casting: 2.5mm.

It was found that the variations in the melt superheat significantly affect the resulting microstructures, and it was therefore necessary to conduct more profound investigations of the shot sleeve thermal conditions. Experiments dedicated at looking into the prevailing mechanisms were therefore carried out, and the principal results from article #3 and #4 are presented in the following:

Formation of ESCs in the Shot Sleeve and Resulting Morphologies

In article # 3, the results from producing AM60 die castings with variations in the melt superheat are presented. The results were principally threefold:

1) The initial amount of superheat and the thermal conditions in the shot sleeve affect the distribution of ESCs: A larger area fraction of ESCs is obtained in the castings with a low superheat and colder shot sleeve. This is attributed to the large number of ESCs formed and the increased survival rate. A lower area fraction of ESCs results when a larger melt superheat, or altered heat transfer conditions in the shot sleeve is used. This is proposed to result from the fewer floating crystals that are formed and that fewer of them survive.

2) The grain structures were found to be affected by the melt superheat and result from three different phenomena: a) Melt solidified in the die, b) fragments of dendrites formed at the shot sleeve wall and c) crystals formed near the shot sleeve wall during pouring and subsequent settling. The ESC morphologies were affected by the melt superheat: With a low melt temperature, wall mechanisms were proposed to dominate. This result in ESCs with a coarse dendritic, (rosette like), and globular morphology. Branched and elongated dendrites were obtained with larger melt superheat, which was caused by fragmentation of columnar dendrites in the shot sleeve.

3) The shot sleeve thermal conditions can significantly affect the fraction of ESCs in the castings as well as the morphology of the ESCs. Using a very large superheat did not, however, remelt and remove all ESCs in the castings. Additional castings were produced with a thermal insulating coating applied to the shot sleeve wall. This resulted in castings where the ESCs were absent. It has been found that this significantly improves the mechanical properties of the castings and particularly the ductility [66].

The significant alterations of the microstructure with different shot sleeve thermal conditions in the AM60 die castings provided motivation for similar casting experiments with the A356 alloy. Additionally, it was expected that the familiar grain refinement behavior in the A356 alloy could affect the formation of ESCs because of the observed variations in the fraction and morphology of the ESCs with variations in the shot sleeve thermal conditions. A356 castings were therefore produced with different melt superheats and grain refiner additions to study the nucleation mechanisms in detail. These investigations are presented in article #4, and the major results are as follows:

The area fraction of ESCs increases with a decrease in the melt superheat and decreases with an increase in the melt superheat, (analogous to the results on the AM60 castings). Furthermore, a low superheat generates coarser, more globular ESCs, whilst a larger superheat results in branched, dendritic crystals.

The castings produced with additions of Ti in solution possessed a greater fraction of ESCs, whereas AlTi5B1 grain refiner additions in the A356 alloy (without Ti in solution), were found to enhance the formation of globular, coarse ESCs. Additionally, the AlTi5B1 grain refiner additions generated a finer grain size in the castings.

The results on the formation of ESCs in the A356 and AM60 HPDC castings can then be summarized as shown in Table 3.

Table 3. Summary of the effects of variations in the shot sleeve thermal and constitutional conditions on the ESC formation mechanisms and the grain structures in the die castings.

Increased distance from the gate in the casting	
Large fraction of ESCs →	Small fraction of ESCs
Coarse dendritic ESCs →	Finer ESCs
Increased melt superheat on pouring	
Wall mechanisms →	Dendrite fragmentation
Coarse dendritic/globular ESCs →	Elongated/branched dendritic ESCs
Colder shot sleeve	
Generally increased fraction of ESCs in the castings	
Coating the shot sleeve wall (AM60)	
Removing ESCs in the casting	
Grain refinement in A356	
Small fraction of ESCs →	Large fraction of ESCs
Elongated/branched dendritic ESCs →	Coarse dendritic/globular ESCs

Segregation/Migration of ESCs

A deeper understanding of the shot sleeve thermal conditions and how it affects the microstructure formation was thus established for the AM60 and A356 alloys. However, the HPDC microstructure commonly consists of ESCs that are positioned in the central region of the cross sections. Hence, the local distribution of ESCs in the castings required further investigations, and controlled laboratory scale casting experiments were therefore conducted, with particular emphasis on the flow and solidification conditions. An A356 aluminium alloy was used to produce castings by pouring semi-solid metal into a steel die, and microstructures similar to those encountered in HPDC were produced. The castings were produced with variations in the die temperature and fraction solid. The results from these experiments are presented in article #5, and summarized here:

The ESCs were observed to segregate/migrate towards the central region, and the distribution of the ESCs was affected by the die temperature and by the initial f_s. The ESCs were observed to reach a maximum packing in the centre. When further packing was not possible, the ESCs occupied a larger area of the cross section. Thus, at higher f_s, the distribution of ESCs generally became wider and was spread towards the surface. This is schematically illustrated in Figure 22. The central ESC-rich region becomes larger by an amount $\phi \div r(2r+\div r)$, when the fraction solid, (f_s^{ESC}), is increased.

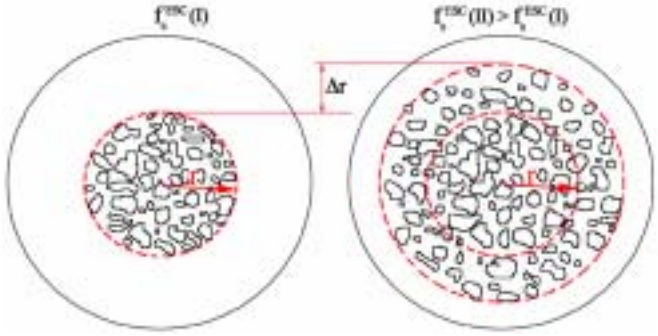

Figure 22: Schematic illustration of the packing of ESCs in the central region. At a specific fraction solid, further packing is restricted and the central region with ESCs becomes larger by an amount $\phi \div r(2r+\div r)$.

It was, furthermore, found that the segregation/migration of ESCs requires a flow which is constrained at all melt/die interfaces which is affected by the die temperature. Potential lift mechanisms were assessed: an assessment of the Saffman lift force on individual particles shows it has no significant effect on the ESC migration. However, it was proposed that other shear gradient-induced lift mechanisms may control the migration.

Formation of Banded Defects

Due to the complex, dynamic nature of the HPDC process, it is difficult to study the effect of individual parameters on band formation. A novel approach to investigate this in detail was therefore developed. The motivation beyond creating microstructures similar to those observed in HPDC was two-fold: 1) to investigate the segregation of ESCs (article #5) as summarized above, and; 2) to investigate the formation of banded defects which is presented in article #6 and summarized as follows:

A356 castings typically generated segregation bands, whilst MgAl6 castings induced porosity bands. Thus, bands similar to those found in cold chamber high pressure die cast alloys were observed in gravity pour die castings.

The effect of die temperature and fraction solid on the segregation bands were investigated in the castings. The band, (in the A356 aluminium alloy), was found to be a region of higher fraction Al-Si eutectic than the surroundings and consisted of a number of interconnected eutectic pathways. The position of the bands was found to be affected by the die temperature and the fraction of ESCs. The nature of the bands developed from poorly defined multiple bands to a well-defined single band and to no band at all with increasing fraction of ESCs. These results were considered with reference to the rheological properties of the filling of semisolid metal and a new formation mechanism for defect bands was proposed, where the principal points are:

1) The solid distribution during flow comprises three regions: a) a plug of coherent ESCs flowing in the centre; b) a low solid fraction region carrying the plug; c) a largely immobile solid fraction gradient at the wall. Thus, the response of the immobile f_s gradient to stresses induced by the fluid flow is important.

2) A critical fraction solid exists where the volumetric flow rate of the liquid through the dendrite network is unable to accommodate the deformation rate caused by the flowing material. If the applied stress exceeds the network strength, the deformation can occur by local slip of the network, at the weakest local spot. Once slip occurs in the dendrite network, it is followed by some liquid flow, if interdendritic flow paths exist.

3) The eutectic in the band originates from the solute enriched liquid between dendrites where slip occurs. This liquid segregates up the solid fraction gradient towards the die wall caused by three mechanisms: a) solidification shrinkage in the wall layer that draws liquid towards the wall; b) the hydrostatic pressure squeezes the viscoelastic

ESC plug which forces liquid laterally; c) gaps forming between slipping dendrites that draw in liquid.

Furthermore, the formation of the band is probably determined in the final stages of solidification when less liquid is available to be drawn into the gaps between slipping dendrites. If there is insufficient interdendritic fluid flow to the band and if the applied stress is sufficiently large, the pressure drop can generate pores and possibly tearing.

Applications

The new knowledge gained in the doctorate work has subsequently culminated in:

1) Industrial investments in new shot sleeve technology emphasizing reduction in the amount of pre-solidification.
2) Work on developing a new simulation tool for the prediction of solidification and wave dynamics in the shot sleeve.
3) A basis for new practices in grain refinement of aluminium high pressure die castings.

4 DIRECTIONS FOR FURTHER WORK

In the doctorate work an AM60 Mg-Al alloy and an A356 Al-Si-Mg alloy have been studied. Other alloys should be investigated for different reasons:

1) Additions of grain refiners in the A356 alloy gave significant effects on the resulting microstructure. The coarser grain size obtained without grain refinement may improve the hardenability.

2) The nucleation of ESCs, and in particular the formation of globular crystals, deserve further work. The branched dendritic crystals can remain branched because solute diffusion away from the crystals is more difficult than for globular crystals. Thus, the globular crystals possibly remelt at larger superheats. Hence, a comprehensive treatment of crystal remelting/dissolution is required.

3) Experiments where the temperature evolution is measured in the shot sleeve wall during pouring and die filling should be carried out. This would provide measurements of the temperature distribution with time and may further improve the understanding of the nucleation of ESCs.

4) In the formation of banded defects, changing the alloy should cause changes in band position and in the nature of the band. The degree of interdendritic fluid flow to the band in the final stages of solidification is strongly dependent on the network structure and permeability, the solidification range and the contraction of the alloy. As these parameters vary widely between alloys, the make-up of the bands (whether segregated, porous or torn) is also highly alloy dependent. Using different die geometries and flow rates can additionally change the defect bands according to the proposed theory. A research program on this subject is currently in progress at the University of Queensland.

5) Experiments should be modelled to study the parameters in detail. Advanced computer models, such as Fluent, which can incorporate two-phase flow, heat transfer, exposed free surfaces and different flow modes, is capable of treating the flow-solidification problems. Additionally, the evolution in crystal morphology in different flow arrangements should be investigated.

5 REFERENCES

[1] E.J. Vinarcik, High Integrity Die Casting Processes, *John Wiley & Sons, Inc.*, 2003.
[2] L.J.D. Sully, Metals Handbook, **15**, 286-295.
[3] M. M. Avedesian, H. Baker, Magnesium and Magnesium Alloys, *ASM International*, 1999.
[4] A. Kaye, A. Street, Die Casting Metallurgy, *Butterworth scientific*, 1982.
[5] N. Fantetti, O. Holta, J.B. Rønhaug, D. Albright, *NADCA Trans.*, 1997, **19**, T97-054.
[6] Melting and handling magnesium for die casting, *Hydro Magnesium Data Sheet*, 2002.
[7] Introduction to Die Casting, *NADCA*, 1997.
[8] A.D. Figueredo, Science and Technology of Semi-Solid Metal Processing, *NADCA*, 2001.
[9] Die Casting - Process Optimization, *Bühler Druckguss*, 2001.
[10] L. Bäckerud, C. Chai, J. Tamminen, Solidification Characteristics of Aluminium Alloys, *AFS/Skanaluminium*, **2**, 1990.
[11] W.G. Walkington, Die Casting Defects - Causes and Solutions, *NADCA*, 1997.
[12] M.C. Flemings, Solidification Processing, *McGraw-Hill*, 1974.
[13] W. Kurz, D.J. Fisher, Fundamentals of Solidification, *Trans Tech Publications*, 1998.
[14] P.A. Tøndel, PhD thesis, Norwegian Institute of Technology (Trondheim), 1994.
[15] D.A. Porter, K.E. Easterling, Phase Transformations in Metals and Alloys, *Chapman & Hall*, 1997.
[16] J. Campbell, Castings, *Butterworth-Heinemann*, 1997.
[17] A. Ohno, Solidification - The Separation Theory and its Practical Applications, *Springer Verlag*, 1987.
[18] B. Chalmers, J. Aust. Inst. of Metals, 1963, **8**, 255-263.
[19] R.T. Southin, Trans. AIME, 1966, **239**, 220-225.
[20] W.C. Winegard, B. Chalmers, Trans. ASM, 1954, **46**, 1214-1224.
[21] I. Maxwell, A. Hellawell, Acta Met., 1975, **23**, 229-237.
[22] K.A. Jackson, J.D. Hunt, D.R. Uhlmann, T.P. Seward, Trans. AIME, 1966, **236**, 149-158.
[23] E.F. Emley, Principles of Magnesium Technology, *Pergamon Press Ltd.*, 1966.
[24] A.W. Woods, J. Fluid Mech., 1992, **239**, 429-448.
[25] G. Hansen, A. Hellawell, S.Z. Lu, R.S. Steube, Met. Mat. Trans. A, 1996, **27A**, 569-581.
[26] Die Cast Magnesium Alloys, *Hydro Magnesium Data Sheet*, 2001.
[27] J.R. Davis, Aluminum and Aluminum Alloys, *ASM International*, 1993.
[28] A. Hellawell, *4th Int. Conf. on Semi-Solid Proc. Alloys Comp.*, 1996, 60-65.
[29] Q. Han, A. Hellawell, Met. Mat. Trans. B, 1997, **28B**, 169-173.
[30] A.K. Dahle, D.H. StJohn, Acta Mat., 1998, **47**, 31-41.
[31] A.K. Dahle, L. Arnberg, J. of Met., 1996, **48**, 34-37.
[32] L. Wang, T. Nguyen, G. Savage, C.J. Davidson, Int. J. C.Met.R., 2003, **16**, 409-417.
[33] L. Wang, T. Nguyen, M. Murray, *NADCA Trans.*, 2001, **21**, T01-014.
[34] H.T. Haaland, PhD thesis, Norwegian University of Science and Technology (Trondheim), 2000.
[35] F.M. White, Fluidmechanics, *McGraw-Hill*, 1999.
[36] S. Sannes, 2003. *Personal communication*.
[37] H. Iwahori, M. Nakamura, K. Tozawa, Y. Yamamoto, *NADCA Trans.*, 1985, **13**, 1-9.

[38] P. Paliani, L. Zalewski, J. Barreto, N. Tsumagari, J. Brevick, C. Mobley, *NADCA Trans.*, 1995, **18**, 149-155.
[39] S. Sannes, Fill Tests - Simulations and Microstructures in U-profile Castings, Hydro Aluminium, Porsgrunn, 2003, 03P_BN2.doc.
[40] P. Schmidt, PhD thesis, Royal Institute of Technology (Stockholm), 1994.
[41] W. Sequeira, PhD thesis, The University of Queensland (Brisbane), 2000.
[42] S. Sannes, H. Gjestland, H. Westengen, H.I. Laukli, *Proc. Int. Conf. Mg. Alloys & Appl.*, 2003, **6**, 725-731.
[43] R. Chatfield, P.W. Rohan, *ADCA Die Casting Conf.*, 2000, paper15; 11-15.
[44] N. Tsumagari, T. Liang, J. Brevick, C. Mobley, *NADCA Trans.*, 2001, **21**, 251-256.
[45] M. Gershenzon, P.W. Rohan, M.T. Murray, *NADCA Trans.*, 1999, **20**, 305-315.
[46] T. Abbott, M. Easton, Mat. Forum, 2001, **25**, 181-201.
[47] D. StJohn, A.K. Dahle, T. Abbott, M.D. Nave, M. Qian, *Proc. Magnesium Techn.*, 2003, 95-100.
[48] S. Sannes, H. Gjestland, 2004. *Personal communication*.
[49] P. Koch, Die Casting Eng., 1974, **18**, 44-46.
[50] L.W. Garber, Die Casting Eng., 1982, **26**, 14-22.
[51] J. Brevick, M. Duran, Y. Karni, *NADCA Trans.*, 1991, **15**, 399-404.
[52] OSU Center for Die Casting, Effects of ESP on wave celerity and die cast products - 2D athermal model, 2002, http://www.mse.eng.ohio-state.edu/~mobley/diecasting/.
[53] E.A. Herman, Heat Flow in the Die Casting Industry, *NADCA*, 1997.
[54] A. Bowles, PhD thesis, The University of Queensland (Brisbane), 2002.
[55] Z.W. Chen, Mat. Sci. Eng. A, 2003, **348**, 145-153.
[56] T.B. Hill, BNF Guide to Better Magnesium Die Casting, *BNF Metals Technology Centre*, 1976.
[57] S. Sannes, H. Westengen, *Proc. Int. Conf. Mg. Alloys & Appl.*, 1998, **4**, 223-228.
[58] P.D.D. Rodrigo, V. Ahuja, *Proc. Int. Conf. Mag. Sci. Techn.*, 2000, 97-104.
[59] C. Pitsaris, T. Abbott, C.J. Davidson, *Light Met. Techn.*, 2003, 223-226.
[60] H. Cao, M. Wessen, *11th Mg Autom.End User Sem.*, 2003, 1-22.
[61] G.K. Batchelor, Theoretical and Applied Mechanics, *Elsevier Science publishers*, 1989, 27-40.
[62] G.E. Dieter, Mechanical Metallurgy, *McGraw-Hill*, 1988.
[63] C. Pitsaris, T. Abbott, C.H.J. Davies, G. Savage, *Proc. Int. Conf. Mg. Alloys & Appl.*, 2003, **6**, 694-699.
[64] C. Dørum, O.S. Hopperstad, O.-G. Lademo, M. Langseth, Int. J. Sol. Struct., 2004, submitted.
[65] C. Dørum, 2004. *Personal communication*.
[66] H. Gjestland, 2004. *Personal communication*.

PART 2

ARTICLES

ARTICLE 1

The Effect of Solidification of Metal Prior to Injection in HPDC on the Grain Size Distribution in a Complex Die Casting

H.I. Laukli[1], A. Graciotti[1], O. Lohne[1], H. Gjestland[2], S. Sannes[2]

[1]Department of Materials Technology
Norwegian University of Science and Technology
N-7491 Trondheim
NORWAY

[2]Magnesium Competence Centre
Hydro Aluminium
N-3907 Porsgrunn
NORWAY

NADCA Transactions 2002, vol.21, T02-035, pp.1-4.

Abstract
Solidification prior to metal injection in cold chamber die casting is frequently observed to occur. Depending on different variables, the initially fully liquid metal solidifies before and during the early stages of the casting process. This results in floating crystals in the casting, which may influence its grain size distribution and properties. The fraction of floating crystals in an AlSi7Mg casting has been found to depend on the position in the casting. The grain structure characterized by means of the EBSD technique have been used to differentiate between floating crystals and the amount of residual melt during solidification in the die cavity.

Introduction

In the process of cold chamber die casting, the metal is injected with high velocities into the runner system and mold cavity and experiences rapid directional changes and large temperature gradients. Depending on the temperature of the melt, local flow and solidification conditions, the final casting possesses an inhomogeneous distribution of microstructures and casting defects resulting in variable mechanical properties. Linkages between prematurely solidified metal and casting defects have been thoroughly presented, e.g. Gershenzon, Rohan and Murray [1] and Tsumagari, Liang, Brevick and Mobley.[2]

In cold chamber die casting molten metal is transferred from a furnace to the shot sleeve by means of ladling or automatic transfer equipment.[3] In order to obtain a quiescent liquid in the chamber, a short delay time, i.e. in the order of a few seconds, for the metal to settle is occasionally applied before the plunger starts.[4] During transport of the metal from the casting furnace to the shot sleeve and during pouring, the melt experiences surroundings with lower temperatures and cools. The amount of cooling depends on e.g. transport method and shot sleeve temperature.[1]

As the melt temperature reaches the liquidus temperature, solidification initiates. Due to a relatively cold cylinder wall and a highly convective filling, crystals may be found both at the chamber wall and in the melt as a result of dendrite fragmentation. The fragmented dendrites can remelt or grow depending on the temperature and composition of the melt.[5] Finally, the mixture of pre-solidified crystals and liquid is forced into the runner system and the die cavity by the aid of an accelerating plunger.

At Hydro's research center in Porsgrunn, Norway, a Bühler SC42D 420-ton cold chamber die casting machine has been installed. For R&D purposes, a die for casting boxes of magnesium and aluminium alloys with a wall thickness of 2.5mm has been made. In figure 1a a complete aluminium casting with runner, gating and overflow system is displayed. Figure 1b shows an example of an interrupted filling of the die at 80 percent plunger stroke. Note the bridge of solid material midway between the gates.

In this paper the main focus has been on the grain structures detected in the die cast box.

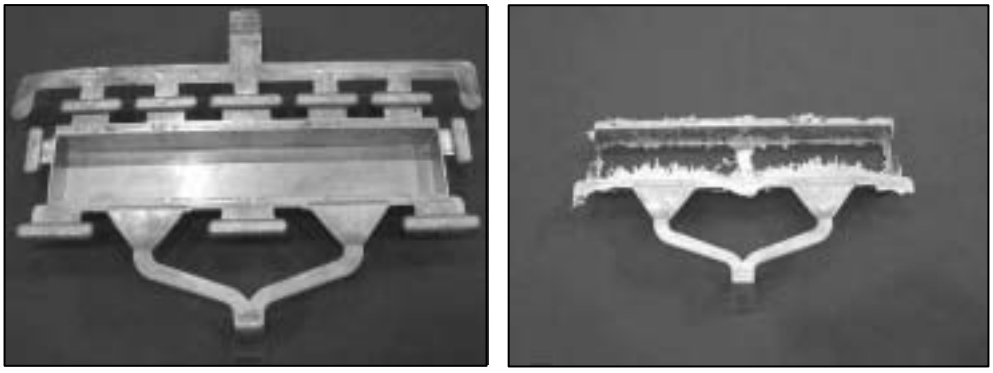

a) b)

Figure 1 - a) The box shaped casting (Length: 400mm, height: 40mm, width: 75mm) with runner and gating system and overflows; b) Interrupted filling of the die at 80% plunger stroke. Note the bridge of solid material midway between the gates.

Experimental

In the present work an AlSi7Mg alloy, with chemical composition as listed in table 1, has been cast. This alloy has a liquidus temperature of approximately 615^{o}C as determined by calculations with Alstruc,[6] a computer program which estimates the fraction solidified and particle formation following the solidification path in the phase diagram.

Table 1. The main alloying elements in the AlSi7Mg alloy [wt%].

Alloy	Mg	Si	Fe	Mn	Ti
AlSi7Mg	0.25	6.95	0.45	0.55	0.12

The boxes investigated were at a production stage of steady state with the following process parameters:

Melt temperature in crucible:	680^{o}C
Shot sleeve volume (ID: 60, L: 340)mm:	0.961 l
Amount of melt poured:	0.480 l
Pouring time:	2-3s
Delay time before plunger start:	1-2s
Filling phase plunger velocity:	4ms^{-1}
Intensification pressure:	600bar

The plunger was accelerated slowly in the first phase and a rapid acceleration was applied in the second phase, i.e. at the start of die filling. When the die was filled, a slight retardation of the velocity was used before an instantaneous intensification pressure was applied.

The shot sleeve was not preheated but reached a quasi-steady state temperature after approximately 25 shots. From infrared thermographic measurements, the temperature at steady state was estimated to be approximately 300^{o}C at the shot sleeve end. Directly under the pouring hole the temperature was measured by means of a surface thermocouple to be approximately 250^{o}C.

The through thickness microstructures of various boxes have been investigated a) at two positions in front of one of the gates and b) at an area midway between the gates in the bottom of the box, (see figure 2). The preparation of the specimens for optical microscopy comprised mechanical grinding, polishing and anodizing in a 5%HBF_4 solution.

In the cross sections of the die cast box, a bimodal distribution of grain sizes was found. As the small grains were difficult to reveal with optical microscopy a far better method was to use the EBSD technique in SEM [7] where grains with different crystal orientations may be mapped with different colors.

To obtain grain maps in the SEM in the present work, mechanical polishing of the samples was followed by a two-hour ion milling process. A JEOL 830 SEM equipped with an EBSD* detector was used for detecting EBSPs of the investigated samples. The samples were tilted 70^{o} and an acceleration voltage of 20kV was used at a working distance of 25mm. For instantaneous processing of the diffraction data as well as analyzing the orientation imaging maps HKL Channel software was used.

Results

The optical micrographs A and B in figure 2 are taken from different positions along cross sections in front of one of the gates. Micrograph C is taken from a position in the bottom midway between the gates.

* Corrected from printed version.

In positions A and B, the grain structure in the center consists of coarse grains surrounded by small grains. Close to the surface fewer coarse grains are observed. The thickness of the layer of coarse grains is largest near the gate and covers nearly the entire cross section. Farther from the gate, i.e. position B, the layer thickness is approximately half the section thickness. In position C few coarse grains are found.

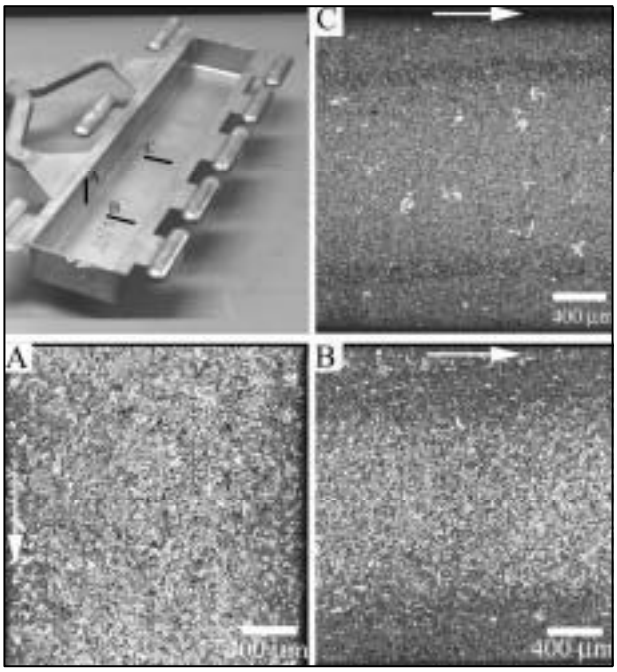

Figure 2 - Upper left: AlSi7Mg die casting with investigated positions indicated, A, B and C. Lower left: Optical micrograph taken from position A. Melt flow vertically. Floating crystals all over the cross section. Lower right: Optical micrograph taken from position B. Melt flow horizontally. Floating crystals mainly in the interior. Upper right: Optical micrograph taken from position C. Melt flow horizontally. Few floating crystals.

The grain maps in figure 3 are taken from the center and subsurface (i.e. approximately 100σm beneath the surface) areas in positions B and C. A fine grained structure with some few coarse grains is seen in the sub-surface map of position B, upper left image of figure 2. In the center of position B, lower left map, many coarse grains are present surrounded by very fine grains.

In the subsurface map of position C, upper right image in figure 2, few coarse grains are present. The grains are slightly coarser than the fine grains observed in the subsurface area of B. The same structure with respect to grain size is present in the center of position C, lower right map of figure 2.

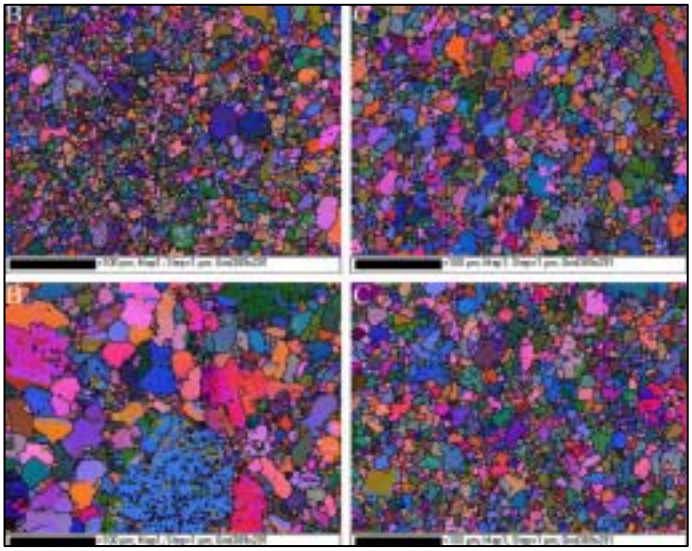

Figure 3 - Upper left: Subsurface area grain map, position B. Lower left: Center area grain map, position B. Upper right: Subsurface area grain map, position C. Lower right: Center area grain map, position C.

Generally the coarse grain size ranges from approximately 50-100σm and the fine grain size is in the range 5-20σm.

The variation in chemical composition along a line crossing fine and coarse grains as measured by EPMA, i.e. electron probe microanalysis, is depicted in figure 4. The specimen was analyzed in as polished condition and the image was obtained after lightly etching the specimen. With a 10 σm spot size and 20σm step size, each point on the micrograph corresponds to the volume analyzed. A significantly lower Si concentration is found in the coarse grain compared with the small grains.

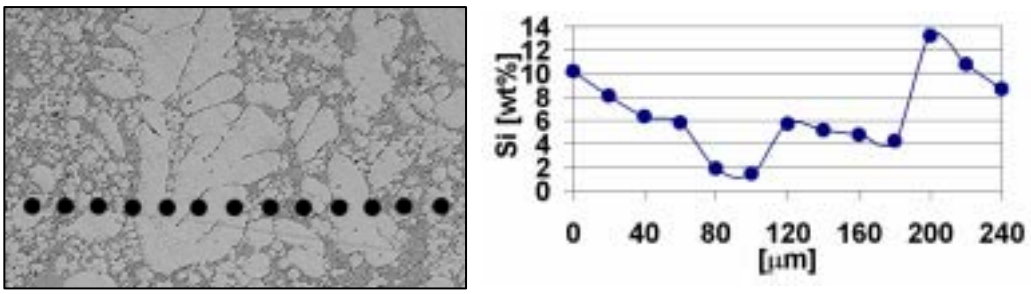

Figure 4 - EPMA-detected variation in Si concentration crossing coarse and fine grains. Microprobe analysis performed in as polished condition. Optical micrograph in lightly etched condition.

Discussion

The variation in grain size distribution which is observed in the die cast box, may be explained by the non-isothermal and turbulent conditions encountered in the shot sleeve. Generally, the pouring and shot delay time is significantly larger than the die filling time and as detected by infrared thermographic measurements the die surface temperature is approximately uniform. It is therefore reasonable to assume that the different grain structures originate from metal coming from different positions in the shot sleeve.

Below the pouring hole turbulent conditions prevail and floating crystals are presumably formed by the fragmentation of dendrites. The metal experiences the water-cooled plunger and a relatively cold chamber wall, thus the melt cools and the temperature obtained is too low to have fully remelting of the fragmented dendrites.

Close to the runner end of the shot cylinder a quiescent melt is rapidly obtained and the last metal poured into the sleeve is accumulated close to the plunger as water model experiments show. The solidification initiates at the cylinder and die walls as proposed in a work on soldering in die casting of aluminium by Chen and Jahedi,[8] which contributes to a more directional solidification and less turbulence. Hence, few floating crystals are formed in the front end of the shot sleeve.

If an idealized plunger movement was applied, as in a work on optimal plunger velocity by Garber,[9] the first metal to enter the runner system would be the melt in the die end of the cylinder. Parts of this volume of metal, solidified in the metal bridge as seen in figure 1b, and possess few floating crystals as shown in figure 2C. The last metal to enter the cavity would origin from close to the pouring hole, and end up in the casting close to the inlet possessing a large fraction of floating crystals, as demonstrated in figure 2A. As the alloying content of the floating crystals is significantly less than the fine grained structures in the surrounding matrix, these grains have been the first to solidify. Therefore the coarse grains possess a Si-content of less than* 2 wt%, corresponding to the intercept between the solidus line and the solidification path in the equilibrium phase diagram.

* Corrected from print in the transactions.

The variation in the amount of floating crystals in the cross sections as displayed in figure 2A and B may simply be a result of the variations in the floating crystal distribution in the shot sleeve. This implies that the floating crystals in figure 2B originate from a volume with a lower fraction of floating crystals in the shot sleeve, i.e. closer to the runner if idealized filling pertains, compared with the amount of floating crystals in figure 2A. However, it should be noted that an approach of fluid mechanics states that particles will be forced to the center of the cross section. A better control of the filling, temperature and distribution of floating crystals in the shot sleeve will therefore be important to obtain a more even grain size distribution in a complex die casting.

Conclusions

The primary objective of this work has been to characterize the grain structure in an aluminium die casting and discuss the origin of the pre-solidified grains found in the castings. From the experimental findings it can be concluded that:

1. Large differences in grain sizes are present in the investigated aluminium box-shaped die casting.
2. EBSD has been found to be an appropriate method for characterizing the grain structure in die castings.
3. The large grains have a low alloying content compared with the fine grains.
4. The large grains have most likely their origin in pre-solidified crystals formed in the shot sleeve.

Acknowledgements

The present work was funded by the project NorLight Shaped Castings, with the following partners: the Norwegian Research Council, Alcoa Automotive Castings, Scandinavian Casting Center ANS, Elkem Aluminium ANS, Fundamus AS, Hydro Aluminium Metal Products, Hydro ASA, NIMR, NTNU, and SINTEF (project responsible). The authors acknowledge the partners for financial support.

References

1. Gershenzon, M, Rohan, P.W, Murray, M.T. (1999). “Formation of cold flakes in Aluminium High Pressure Die Casting”. NADCA Transactions 99-085.
2. Tsumagari, N, Liang, T, Brevick, J, Mobley, C. (2001). “Microstructural features in aluminum alloy die castings”. NADCA Transactions 251-256.
3. “Magnesium die casting”. (1999). Hydro Magnesium. 4-5.
4. Wang, L., Nguyen, T., Murray, M. (2001). “Simulation of flow pattern and temperature profile in the shot sleeve of a high pressure die casting process”. NADCA Transactions 01-014.
5. Ohno, A. (1987). “Solidification - The separation theory and its applications”. Springer Verlag. 51-60, 78.
6. Dons, A.L, Jensen, E. K, Langsrud, Y, Trømborg, E, Brusethaug, S. (1999). “ The Alstruc Microstructure solidification model for industrial aluminium alloys”. Metallurgical and Materials Transactions A. 30A. 2135-2146.
7. Humphreys, F.J. (2001). “Review: Grain and subgrain characterization by electron backscatter diffraction”. Journal of Materials Science. 36. 3833-3854.
8. Chen, Z.W, Jahedi M.Z. (1999). “Metallurgical Phenomena in Die/Casting Interfacial Regions During High Pressure Die Casting of Aluminium Alloys”. NADCA Transactions 99-084.
9. Garber, L.W. (1982). “Theoretical analysis and experimental observation of air entrapment during cold chamber filling”. Die Casting Engineer. May-June. 14-22.

ARTICLE 2

Grain Size Distribution in a Complex AM60 Magnesium Alloy Die Casting

H.I. Laukli, O. Lohne, S. Sannes*, H. Gjestland*, L. Arnberg

Department of Materials Technology
Norwegian University of Science and Technology
N-7491 Trondheim
NORWAY

*Magnesium Competence Centre
Hydro Aluminium
N-3907 Porsgrunn
NORWAY

International Journal of Cast Metals Research, 2003, vol.16, no.6, pp.515-521.

Abstract
Presolidified equiaxed dendritic crystals are observed in magnesium cold chamber high pressure die castings. Depending on the rate at which new crystals are formed and to what extent they survive in the shot sleeve, a mixture of liquid and crystals is injected into the die cavity resulting in floating crystals in the casting. Box shaped die castings of the AM60 magnesium alloy have been made with a cold chamber high pressure die casting machine. The resulting microstructure is generally observed to consist of (a) a fine grained structure or (b) a mixture of fine grains and coarse grains which is either centred or dispersed in the through thickness cross section. The prevalence of structures is observed to vary with position in the casting. Close to the gate a coarse grained microstructure dominates, while fine grains dominate further from the gate. The volume fraction of floating crystals in the casting is shown to depend on the initial superheat of the melt.

Keywords: Die cast Mg alloy, grain size distribution, superheat, cold flakes.

Introduction

Cold chamber high pressure die casting is a convenient method for large scale production of thin walled castings with a complex geometry. Die castings are used extensively in the automotive industry having rapidly evolved from products such as laptop housings and cell phone covers. However, increasing demands on part quality, especially from the automotive industry, force development of new technology and improved understanding of the fundamentals of die casting. Further understanding of solidification and defect formation characteristics to enable correct application of simulation tools is a major challenge.

Conventional cold chamber die casting involves dosing and subsequent pouring of molten metal into a relatively cold shot sleeve. Thus, the metal instantly cools when introduced in the shot sleeve. As the metal is poured from a specific height turbulent filling usually occurs. Alternatives to the conventional cold chamber technique can be used in order to reduce heat loss and air entrapment during pouring. Closed process routes are available where metal is sucked directly from the casting furnace to the shot sleeve by means of vacuum, e.g. the Vacural process.[1] Semiclosed methods, e.g. automatic transfer equipment,[2] are also used, in contrast to entirely open techniques such as ladling from the melt crucible to the shot sleeve.

When liquid metal enters the shot sleeve it starts to solidify in a manner resembling gravity pour permanent mould casting. Work has been presented that focuses on the solidified skin which forms immediately at the wall of the shot sleeve as a result of rapid heat extraction through the sleeve interface.[3,4] When the plunger movement is initiated it causes parts of this skin to collapse. These skin fragments, often termed cold flakes,[5] can be detrimental to the final ductility of the casting if they enter the cavity during filling.

Fractured pieces of skin formed in the shot sleeve are not the only solid material occasionally transported into the runner system during injection. Equiaxed crystals also find their way from the shot sleeve into the die aided by the plunger movement, as observed in die castings of magnesium[4,6,7] and aluminium alloys.[8] The mechanisms which prevail in the shot sleeve and result in the formation of floating crystals are discussed in detail in Ref. 9. The formation of crystals can be represented by wall mechanisms.[10,11] Combination with other mechanisms can also occur, e.g. dendrite arm remelting[12] or nucleation in a constitutionally undercooled zone. During growth of solid at the wall, solute is rejected at the crystal interface creating a solute enriched

zone. This results in a region with a lower liquidus temperature than the bulk of the liquid. Simultaneously, heat is extracted from the growing solid and a thermal gradient is established adjacent to the growing interface. A constitutionally undercooled zone is therefore formed in which suitable substrates can nucleate a crystal.[13] As turbulence and convective currents are present in the shot sleeve, the generated equiaxed crystals can easily be transported from the sleeve wall into the bulk of the liquid. However, a critical criterion for the survival of the presolidified crystals is the amount of superheat present. Generally the crystals survive and grow if the melt is sufficiently cold, i.e. $T_m<T_l$, where T_m is the melt temperature* and T_l is the liquidus temperature. A hotter melt can cause the crystals to shrink and remelt.

This paper presents an investigation of the influence of melt superheat on the presence of floating crystals in box shaped AM60 die castings.

Experimental Procedure

Casting Experiment

The die castings, with 2.5 mm wall thickness, were produced in a Bühler SC42D 420 ton cold chamber die casting machine. The AM60B magnesium alloy was cast with the nominal composition Mg–6Al–0.4Mn(<0.2%Zn,<0.05%Si,<0.008%Cu,<0.001%Ni, <0.004%Fe). This alloy has a liquidus temperature of 619°C as determined by the equilibrium binary Mg–Al phase diagram.[14] Table 1 lists the process parameters used for this work. A typical shot profile can be seen in Fig. 1.

Table 1 Process parameters.

Parameter	Value
T_m (in casting crucible), °C	640, 680, 710
T_{die}, °C	200
Shot sleeve volume+, l	0.961
Fill fraction	0.5
Filling phase plunger velocity, ms^{-1}	5.5, 6.5
Intensification pressure, bar	600

+Inside diameter 60 mm, length 340 mm.

* Corrected from print in the journal.

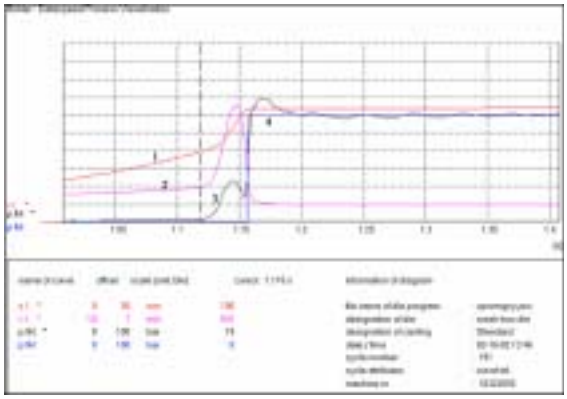

1 measured plunger stroke; 2 measured plunger velocity; 3 measured pressure; 4 programmed pressure

1 Typical shot profile with filling phase plunger velocity of 5.5 ms^{-1} and pressure 600bar.

The liquid metal was transferred from the casting furnace to the shot sleeve in a siphon tube aided by a gas displacement pump.[2] The metal was released in a sprue approximately 20 cm directly above the pouring hole, filling the shot sleeve horizontally. The shot sleeve was not preheated but reached a quasi-steady state temperature after approximately 25 shots, thus the first 25 castings were scrapped. Investigations of the shot sleeve temperature by means of infrared thermographic measurements estimated the temperature directly below the pouring hole to be 250^{o}C while the shot sleeve end was approximately 300^{o}C.[15]

Sample Preparation for Microstructural Investigations

Examination of the microstructure in several positions within the die casting revealed three distinct grain structures. The through thickness microstructures of various boxes were investigated at two positions, A and B, in front of one of the gates and in an area, C, midway between the gates in the bottom of the box (*see* Fig. 2). For investigations in the optical microscope the samples were ground, mechanically polished and finally etched in an acetic acid glycol solution.[16]

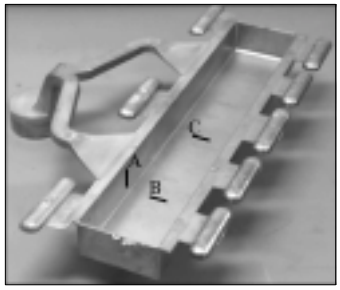

2 AM60 die casting with investigated through thickness cross-sections designated A, B and C.

Grain Size Measurements using EBSD

To reveal the fine grained structure in AM60 die castings, grain orientation mapping was carried out using electron backscattering diffraction (EBSD) analysis in an SEM. At optimal settings a high resolution can be obtained.[17] This technique allows the crystallographic orientation of points in the structure to be determined by scanning the sample surface with the electron beam. With a rapid data acquisition system and post processing hardware grain maps can be constructed. In the present work a Jeol 840 SEM was used, equipped with an EBSD detector. The operating parameters were: acceleration voltage 20 kV, tilt 70^{o} and working distance ~23 mm. For instantaneous post-processing of the data HKL Channel software[18] was used.

The most common method for preparing samples for EBSD is electrolytic polishing. However, AM60 die castings possess a highly inhomogeneous microstructure that consists of ζ-Mg grains, some Al segregated at the boundaries and intergranular divorced eutectic. A chemical etching treatment therefore discriminates phases present in the structure and generates topographical effects. A more suitable preparation method for AM60 die castings is ion milling in which argon ions are accelerated in a low pressure atmosphere bombarding the specimen surface. This was performed on mechanically polished samples in an Ion Tech FAB 306 atom mill. The operating parameters were: current 5 mA, acceleration voltage 5 kV, gun angle 15^{o} and time 4 h.

Results

Microstructural Observations

Figure 2 shows a complete AM60 magnesium die casting with biscuit, runners, gates and overflows. Optical micrographs taken at positions A, B and C are shown in Figs. 3–6. In positions A and B, the grain structure at the centre consists of coarse grains surrounded by small grains, (*see* Fig. 3). Near the surface, fewer coarse grains are observed in these positions. Figure 4 shows that the coarse grained region is wider near the gate (position A) and covers nearly the entire cross-section.

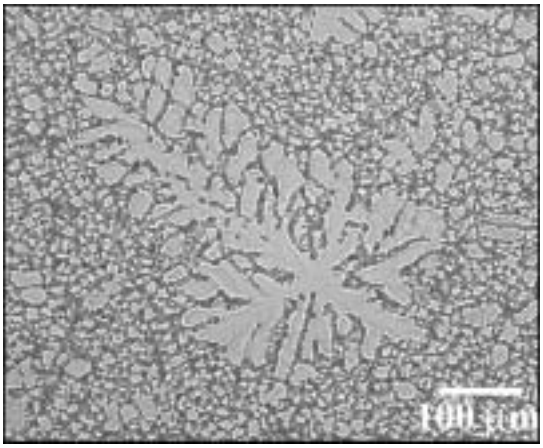

3 Optical micrograph of etched AM60 microstructure, showing coarse dendrite surrounded by fine equiaxed grains, as occasionally observed in position A and centre of cross-section at position B.

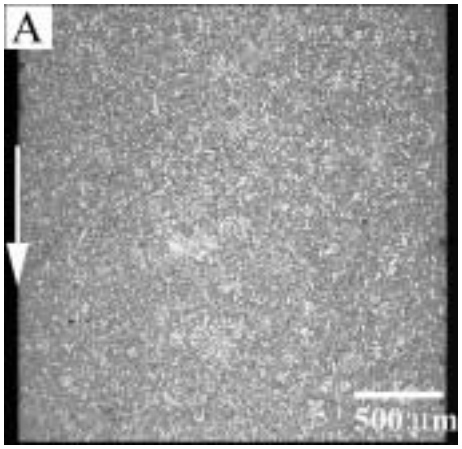

4 Optical micrograph of etched microstructure in position A (melt flow vertical, T_m=680°C).

Further from the gate (position B) the coarse grained region covers approximately half the section thickness, (*see* Fig. 5). The area fraction of coarse crystals is approximately 25% in the centre. Few coarse grains are found in position C (*see* Fig. 6). No cold flakes are generally observed.

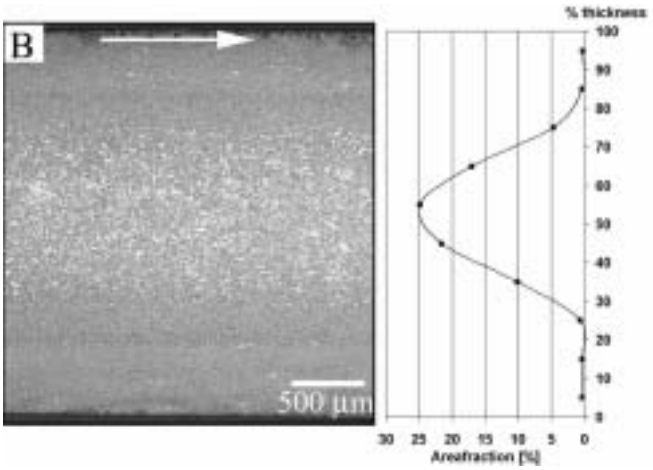

5 Optical micrograph of etched microstructure in position B (melt flow horizontal, T_m=680°C).

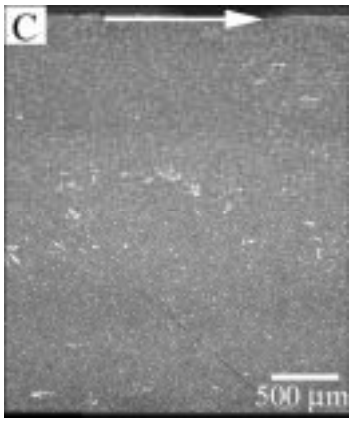

6 Optical micrograph of etched microstructure in position C (melt flow horizontal, T_m=680°C).

Grain Size Distribution at T_m=680^{o}C

The grain maps in Fig. 7 were taken from the centre and subsurface areas, i.e. approximately 300 σm from the surface, in both positions B and C. A fine grained microstructure with few coarse grains is observed in the subsurface maps of positions B (upper left) and C (upper right). In the centre of position B (lower left), many coarse grains are surrounded by fine grains, in contrast to the microstructure in the centre of position C (lower right) where only a few coarse grains are present.

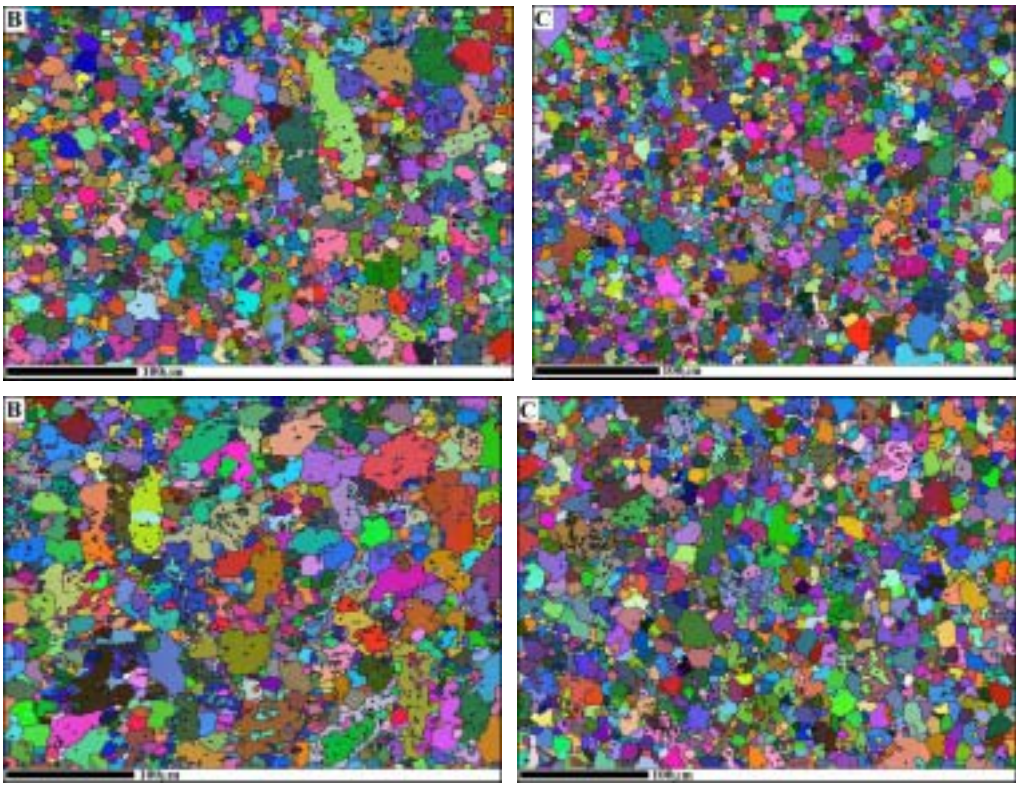

7 Grain size distribution maps: *upper left*: position B, subsurface, grain size ~11 σm; *lower left*: position B, centre, coarse and fine grain sizes 20–75 σm and 5–10 σm respectively; *upper right*: position C, subsurface, grain size ~11 σm; *lower right*: position C, centre, grain size ~10 σm.

Effect of Superheat on the Grain Size Distribution

To investigate the importance of initial melt superheat, boxes were cast with different initial melt temperatures of 640^{o}C and 710^{o}C, 21 and 91 K above T_l, respectively. In position B, (lower left and lower right images in Fig. 8), the region of floating crystals is centred in the cross-section. This region has a wider appearance for 710^{o}C than

640°C and covers approximately 75% of the section thickness. In the latter, the floating crystals are apparently more densely packed. In position C at 640°C (upper left image, Fig. 8), the floating crystals are distributed over nearly the entire cross section, in contrast to position C at 710°C (upper right micrograph), where a thin layer is observed in the centre.

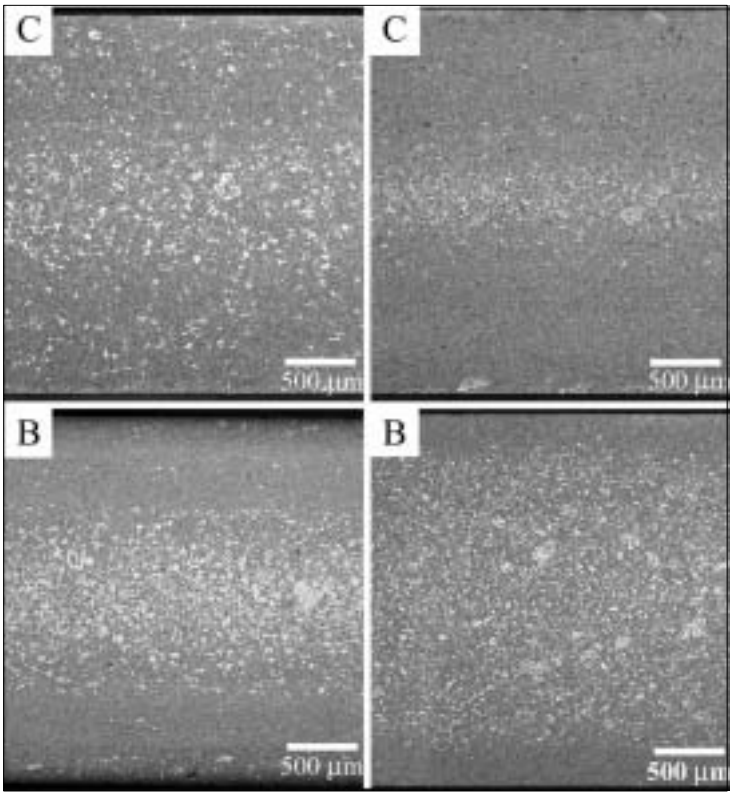

8 Effect of superheat on grain size: *upper left*: position C, T_m=640°C; *lower left*: position B, T_m=640°C; *upper right*: position C, T_m=710°C; *lower right*: position B, T_m=710°C.

Discussion

Grain Size Distribution at T_m=680°C

It can be deduced that the observed differences in grain size distribution encountered in the die cast box originate from the turbulent, non-isothermal conditions that prevail in the shot sleeve. As the cooling rate is significantly lower in the shot sleeve than in the die cavity, a coarse grained structure is expected compared to the die cast structure. It is therefore reasonable to assume that the different coarse grained structures observed in the die casting originate from different positions in the shot sleeve.

Closer to the runner end of the shot sleeve a solid layer is rapidly formed, analogous to aluminium die casting,[19] and a quiescent melt is established. The solid layer reduces the heat transfer rate through the sleeve wall and restricts further rapid growth of the solid. The solidification front establishes a constitutionally undercooled zone in which new crystals can be formed. These crystals are however not easily transported into the bulk of the liquid due to the stagnant conditions and lack of fluid flow. Locally a hot melt is present, i.e. $T_m > T_l$, induced by the temperature pattern in the shot sleeve,[20] which remelts the dendrite seeds that are formed.

At the plunger end of the shot sleeve, below the pouring hole, a turbulent condition rules in which new metal is continually washing over the water cooled plunger and the shot sleeve wall. Crystals can easily nucleate as a thermally undercooled zone is most likely present adjacent to the cylinder wall. Detachment and transportation of crystals is easily provided for by the flow and convective currents present.

According to Garber,[21] for example, with optimal first phase plunger movement and a fill fraction* of 0.5, the first metal to enter the runner system would be melt from close to the runner end of the cylinder. This metal, in which few floating crystals are present, freezes before the entire cavity is filled. Interrupted fill tests and flow modelling revealed stagnant conditions in position C resulting in the microstructure shown in Fig. 6. The last metal to enter the cavity would be melt, or mush, containing a large fraction of floating crystals originating from near the plunger and ending up close to the gate in the box (position A) as seen in Fig. 4.

To test the hypothesis that an increasing amount of floating crystals is entering the cavity with increasing plunger stroke, an interrupted fill test was conducted. The plunger was stopped at various strokes and the runners were investigated. In Fig. 9 the fill test and the corresponding runner microstructures are displayed. At 200 mm stroke before stopping the plunger, the metal front has approximately reached the gate (upper left image). Few floating crystals are observed (upper right micrograph) in a cross-section of the runner indicated by the arrow (upper left image). When the cavity is filled (lower left image), corresponding to ~320 mm plunger stroke, a large fraction of floating crystals is observed (lower right micrograph).

* Corrected from print in the journal.

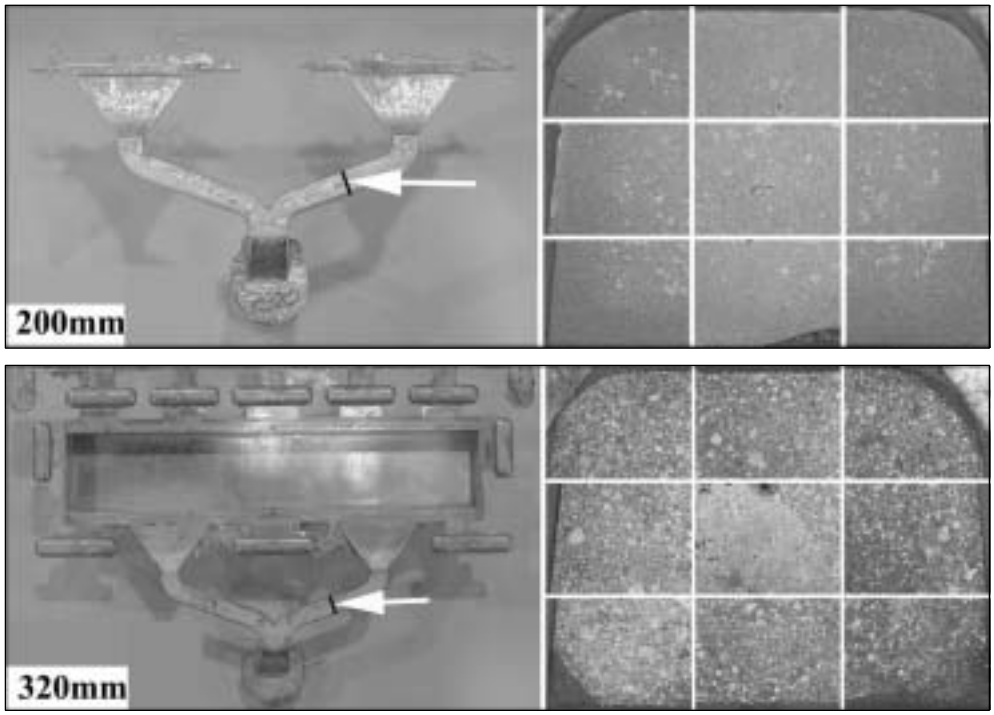

9 Fill tests and corresponding runner microstructures: *top*: interrupted movement at 200 mm plunger stroke; *bottom*: filled cavity at 320 mm plunger stroke.

Effect of Superheat on Grain Size Distribution

The observed differences in microstructure in position B can be explained by considering that a higher melt temperature (710^{o}C) decreases the growth rate of solid and therefore reduces the thickness of the solidifying layers at the die walls. Thus, a wider layer of metal containing floating crystals can flow in the centre during filling (lower right micrograph, Fig. 8). This is in contrast to a lower melt temperature (640^{o}C) where thicker solidifying layers can rapidly form at the die walls and restrict the metal arriving later to flow in a thin section in the centre. Hence, the coarser crystals in the centre are apparently more densely packed (lower left micrograph Fig. 8). However, the coarse crystals are not only constrained to the centre. Some coarse crystals are also present near the surface. This observation does not apply to the entire bottom section of the casting, and can result from deposition of small amounts of the metal flow front by rapid freezing at the die walls during filling. Some coarse crystals can be present at the flow front due to the low melt temperature.

In position C, floating crystals are distributed over almost the entire cross-section for the low melt temperature (640^{o}C) in contrast to the higher melt temperature (710^{o}C) where a thin layer is observed in the centre (*see* Fig. 8). This suggests that the first metal to enter the cavity, in which a certain volume freezes in position C during filling, has obtained a temperature sufficiently low for dendritic crystals to survive for the 640^{o}C casting. For the 710^{o}C experiment the metal in position C does not freeze entirely through the thickness during filling due to the high melt temperature. Solidification proceeds from the walls, while in the centre metal flows unimpeded. Thus this volume is continuously fed with melt containing floating crystals.

The floating crystals are occasionally centred in the cross-section as a plug, e.g. position B in Fig. 2. This is suggested to be as a result of lift forces[22] causing migration of the coarse particles towards the centre[23] during flow. In a crystal migration perspective, the effects of variations in viscosity, crystal morphology, size, density and distribution could be analysed. However, it is not within the scope of the present work to assess the importance of these parameters due to the inherent complexity of two-phase flow.

In the present context, solid redistribution is suggested to occur in the shot sleeve, and an additional mechanism can be proposed for the generation of centred crystals. As a skin is continually formed during filling of the die cavity, any metal entering later will flow within the solidified skin.[24] The thickness of the skin is directly dependent on the heat transfer conditions[25] and is also expected to depend on filling phase velocity, temperature of the melt and die temperature. The metal entering the cavity first possesses few floating crystals and the skin that forms is therefore free of floating crystals. The metal entering later possesses an increasing amount of floating crystals. This flow of mush can be forced to the centre due to the presence of solid, or material resisting movement, adjacent to the walls. Occasionally, the skin is not sufficiently thick to fully accommodate the centred position of the crystals. Thus, the centred crystals have been suggested to result from a combination of skin formation and crystal migration.[9] It is to be noted that work is in progress on flow and solidification behaviour of semi-solid material.

Conclusions

1. Large differences in grain sizes are present in the investigated AM60 box shaped die casting.
2. Plunger motion and shot sleeve temperature are most likely contributing to solid redistribution which results in inhomogeneous grain size distributions in the die casting.
3. Local melt flow characteristics are significant in the formation of the grain structure.
4. The distribution of floating crystals is affected by the amount of initial melt superheat.

Acknowledgements

The present work was funded by the project NorLight Shaped Castings, with the following partners: the Norwegian Research Council, Alcoa Automotive Castings, Scandinavian Casting Center ANS, Elkem Aluminium ANS, Fundamus AS, Hydro Aluminium Metal Products, Hydro ASA, NIMR, NTNU, and SINTEF (project responsible). The authors acknowledge the partners for financial support.

References

1. 'Vacural vacuum die casting process', 3–7; Müller Weingarten, Germany.
2. N. FANTETTI, O. HOLTA, J.B. RØNHAUG and D. ALBRIGHT: Proc. 19th Int. Die Casting Cong. & Exposition, 1997, NADCA, T97–054, 1-4.
3. P. PALIANI, L. ZALEWSKI, J. BARRETO, N. TSUMAGARI, J. BREVICK and C. MOBLEY: Proc. 18th Int. Die Casting Cong. & Exposition, 1995, NADCA, T95–046, 149–155.
4. D. RODRIGO, M. MURRAY, H. MAO, J. BREVICK, C. MOBLEY and R. ESDAILE: Proc. 20th Int. Die Casting Cong. & Exposition, 1999, NADCA, T99–064, 219–225.
5. L. WANG, T. NGUYEN and M. MURRAY: Proc. 21st Int. Die Casting Cong. & Exposition, 2001, NADCA, T01–014, 1-7.
6. W.P. SEQUEIRA, M. MURRAY, G. DUNLOP and D.H. STJOHN: Proc. 1997 TMS Annual Meeting, 1997, 169–185.
7. A. BOWLES, J.R. GRIFFITHS and C.J. DAVIDSON: Proc. Magnesium Technol., 2001, 161–168.
8. H.I. LAUKLI, A. GRACIOTTI, O. LOHNE, H. GJESTLAND and S. SANNES: Proc. 21st Die Casting Cong., 2002, NADCA, T02–035.
9. H.I. LAUKLI, O. LOHNE, L. ARNBERG, H. GJESTLAND and S. SANNES: 6th Int. Conf. on 'Magnesium alloys and their applications', Wolfsburg, Germany, November 2003, DGM, 182-189.
10. A. OHNO: 'Solidification – the separation theory and its practical applications', 51–60, 78; 1987, Springer Verlag, Germany.
11. B. CHALMERS: *J. Aust. Inst. Metals*, 1963, **8.3**, 255–263.
12. K.A. JACKSON, J.D. HUNT, D.R. UHLMANN and T.P. SEWARD: *AIME Trans*., 1966, **236**, 149–158.
13. B. CHALMERS: 'Principles of solidification', 171; 1967, John Wiley & Sons, USA.
14. C.S. ROBERTS: 'Magnesium and its alloys', 44; 1960, John Wiley & Sons, USA.
15. S. SANNES: 'Thermographic temperature control', Internal report O2C-AN4.LWP, Norsk Hydro, Porsgrunn, Norway, 2002.
16. 'Microstructure of magnesium based diecasting alloys', Diecaster Bulletin 3, Hydro Magnesium, Norway, 1999.
17. F.J. HUMPHREYS: *J. Mater. Sci*., 2001, **36**, 3833–3854.
18. HKL Technology Channel 5, HKL Technology, 2001.
19. Z. W. CHEN and M.Z. JAHEDI: Proc. 20th Int. Die Casting Cong. & Exposition, 1999, NADCA, T99–084, 295–303.
20. P. ROBBINS: Proc. 21st Int. Die Casting Cong. & Exposition, 2001, NADCA, T01–071.
21. L.W. GARBER: *Die Cast. Eng*., 1982, **26**, 14–22.

22. C. CROWE, M. SOMMERFELD and Y. TSUJI: 'Multiphase flows with droplets and particles', 95–97; 1998, CRC Press, USA.
23. A.K. DAHLE, S. SANNES, D.H. STJOHN and H. WESTENGEN: *J. Light Met*., 2001, **1.2**, 99–103.
24. S. SANNES, H. GJESTLAND, H.I. LAUKLI, H. WESTENGEN and O. LOHNE: Proc. SAE World Cong., 2003, 03M–192.
25. S. SANNES, H. GJESTLAND, H.I. LAUKLI and H. WESTENGEN: Proc. 6th Int. Conf. on 'Magnesium alloys and their applications', Wolfsburg, Germany, November 2003, DGM, 725-731.

ARTICLE 3

The Effect of Variations in Melt Temperature on the Grain Structures in an AM60 Die Casting

H.I. Laukli[1], O. Lohne[1], L. Arnberg[1], H. Gjestland[2], S. Sannes[2]

[1]Department of Materials Technology
Norwegian University of Science and Technology
N-7491 Trondheim
NORWAY

[2]Magnesium Competence Centre
Hydro Aluminium
N-3907 Porsgrunn
NORWAY

Proceedings of the 6th International Conference on Magnesium Alloys and Their Applications, 2003, vol.6, pp.182-189.

Abstract

The grain structures in cold chamber high pressure die castings (HPDC) of magnesium are complex and vary with position in the casting. A fraction of the metal solidifies in the shot sleeve before injection and the remaining melt rapidly freezes in the die cavity. The final grain structures can be described as a result of three different phenomena: a) melt solidified in the die, b) fragments of dendrites formed at the sleeve wall and c) crystals formed close to the sleeve wall during pouring and subsequent settling. The initial melt temperature and the conditions prevailing in the shot sleeve affect the contribution of each mechanism to the final grain structure. In the present work the grain structures in thin walled AM60 die castings produced at three different melt temperatures and at various shot sleeve temperatures, have been investigated. The grain morphologies are observed to depend strongly on initial melt superheat and the three different solidification mechanisms can to different extent contribute to the final grain structure.

Introduction

In the cold chamber high pressure die casting process (HPDC) a significant heat loss is experienced during filling of the melt into the shot sleeve. Occasionally all superheat has dissipated prior to the injection stage [1], thus initiating solidification. Shot sleeve solidification comprises the formation of a solid skin at the shot sleeve wall and equiaxed dendritic crystals in the melt. The skin can result in cold flakes in the casting[2]. A mixture of primary crystals, termed externally solidified grains [3] or floating crystals [4], and residual melt is injected into the cavity. The relatively cold die walls and thin walled geometry ensures rapid freezing which generates a bimodal grain size distribution [4-7].

The general understanding of floating crystals have been limited to being recognized as externally solidified crystals. The mechanisms by which the crystals are formed in HPDC have been questioned [6]. A review of the different mechanisms of nucleation of equiaxed crystals in aluminium alloy castings has been reported [8], and analogous mechanisms have been suggested to pertain to the solidification of magnesium alloys[9].

Generally, the solidification of alloys initiates with crystal nucleation on suitable substrates [10] at a sufficient undercooling of the melt. These crystals can then grow into dendrites with different order branches depending on the dendrite tip radius, the local thermal gradient, solute liquid diffusion and the constitutional conditions present. When the crystals start to interact, i.e. the thermosolutal diffusion fields encapsulating the crystals impinge on each other, peripheral growth is substituted by crystal coarsening [11]. The mechanisms of nucleation of equiaxed crystals in the absence of grain refiner additives are briefly as follows: Equiaxed dendritic crystals can form during pouring of metal into a permanent mould, as a result of nucleation and growth in the thermally undercooled region adjacent to the wall [12]. These crystals grow with a necked shape due to the constraints set up by the wall restricting solute diffusion at the root. The crystals are easily separated from the wall by convection. A similar mechanism is the nucleation and growth of equiaxed crystals, termed free chill crystals, in the thermally undercooled zone adjacent to the mould walls when pouring into a cold permanent mould [13].

During growth of solid at the wall, solute is rejected at the crystal interface creating a solute enriched zone. This results in a region with lower liquidus temperature than the bulk of the liquid. Simultaneously, heat is extracted from the growing solid and a

thermal gradient is established adjacent to the growing interface. A constitutionally undercooled zone is therefore generated in which suitable substrates can nucleate crystals [14]. When a layer of material solidifies at a mould wall, dendrites are rapidly formed growing into the liquid opposite and parallel to the direction of heat flow. The dendrite trunks develops branches in which segregated melt is interdendritically entrapped. These dendrites can be fragmented through remelting due to constitutional gradients, thermal conduction, solute solid diffusion or ripening phenomena [15]. The dendrite fragments then float or sink depending on the alloy constitution and convective conditions present. Another proposed mechanism is that due to heat radiation at the melt surface a thermally undercooled zone is generated adjacent to the melt surface in which dendrites can form. These crystals can be detached by breaking off [16].

A critical criterion for the survival of crystals is the magnitude of superheat in the melt. The present paper presents an investigation of the influence of melt temperature on the grain structures in thin walled AM60 box-shaped castings [17] produced in a Bühler 420-ton cold chamber HPDC machine.

Experimental

Approximately 15 boxes were cast to obtain a quasi-steady state temperature in the shot sleeve. These initial castings were thus produced with constant melt temperatures at the initiation of filling, at qualitatively increasing shot sleeve temperatures. At steady state a minimum of 30 castings were produced for each melt temperature with process parameters as listed in Table 1 (details in [6]). The steady state shot sleeve temperature has been estimated to be 250°C directly below the pouring hole and 300°C at the end[6].

Table 1. Process parameters used for producing AM60B die castings. ($T_{liquidus}$ of the AM60 alloy is 619°C[18]).

T_m [°C]	T_{die} [°C]	Fill fraction	v_2 [ms^{-1}]	P_3 [bar]
640, 680, 710	200	~0.5	4.5	600

Samples were prepared for optical microscopy [19] taken from two positions in front of one of the gates, A) close to the gate and B) farther away, and C) in an area midway between the gates in the bottom of the box [4,6]. Area fraction measurements of the floating crystals were performed with an equivalent circle diameter (ECD) threshold of 10σm, derived from image analysis [20].

Results

Effect of Melt and Shot Sleeve Temperature on the Grain Size Distribution

The micrographs in Figure 1 are obtained from a casting produced with an initial melt temperature of 640°C. The microstructure is generally coarser closer to the gate (position A), with the primary crystals distributed over the cross section. In position B the coarse crystals are principally centered with fewer and finer floating crystals distributed from the center to the surface. A more random distribution and fewer coarse crystals are present in position C.

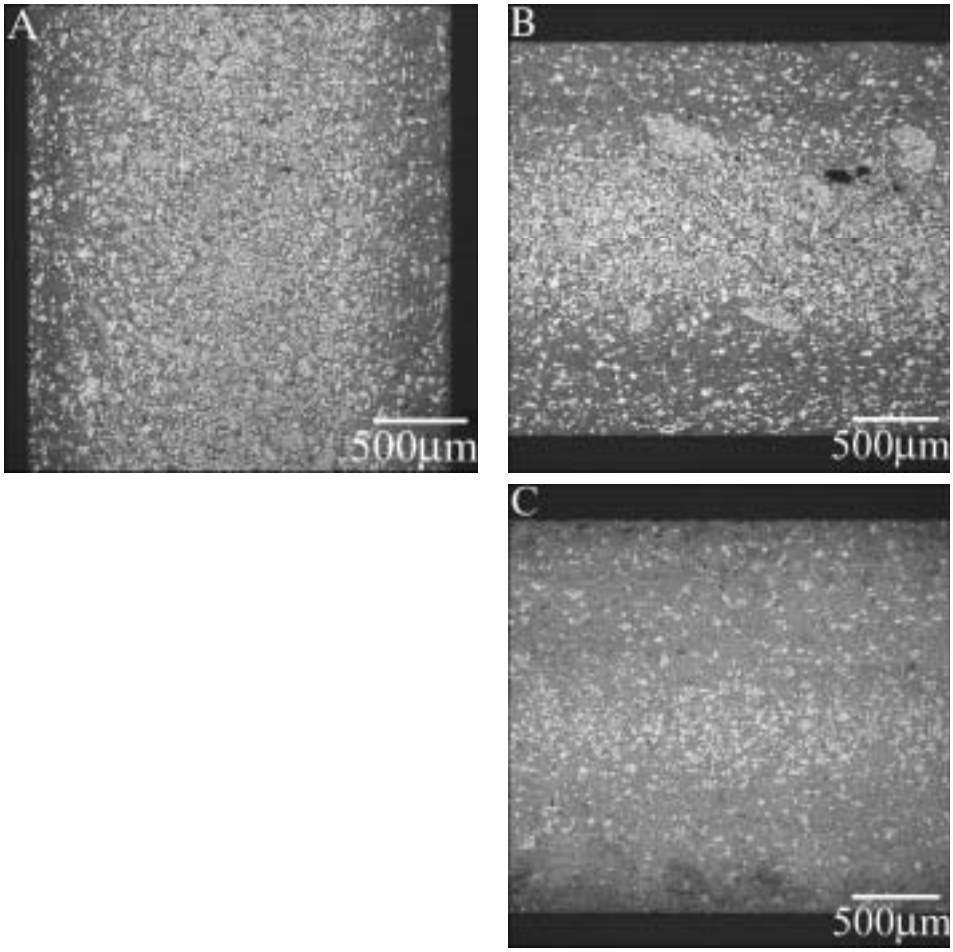

Figure 1: Optical micrographs of etched cross sections (2.5mm thickness) of a casting produced with low superheat T_m=640°C. Micrograph A: flow vertical. B: flow horizontal. C: flow horizontal.

The measurements of area fraction as function of thickness for the three melt temperatures are displayed in Figure 2. Consistent with the micrographs in Figure 1, the area fraction of floating crystals is decreasing with distance from the gate. In

position A (640°C), the floating crystals covers 35% of the area in 50% of the cross section thickness. At 680°C this drops to 30% in 30% of the thickness. At 710°C the area fraction of floating crystals is approximately 10% in 10% of the section thickness. A maximum in area fraction is present in the center of position B for all temperatures. At 640°C the area fraction is approximately 40%, at 680°C it is 35% and at 710°C 13%. A slight increase in area fraction is observed closer to the surface at 640°C. In position C a maximum in area fraction is observed at 640°C, i.e. 25%. At 680°C and 710°C the area fraction in position C is approximately 2-3%.

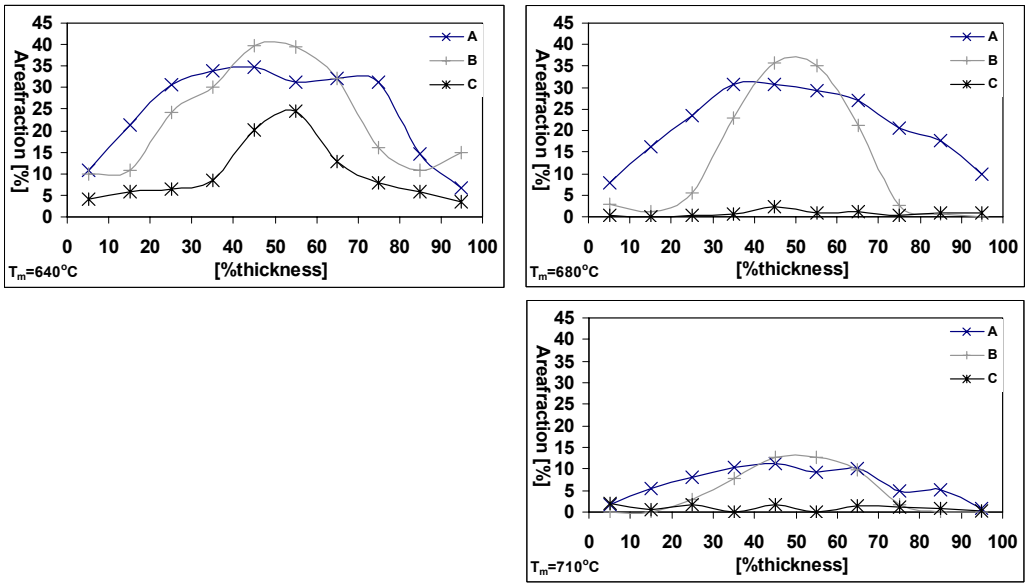

Figure 2: Area fraction of floating crystals in A, B and C for T_m=640°C (upper left), 680°C (upper right) and 710°C (lower right).

In Figure 3 micrographs from position B from a) a pre-steady state casting and b) a steady state casting are displayed. A coarser microstructure is present in Figure 3 a).

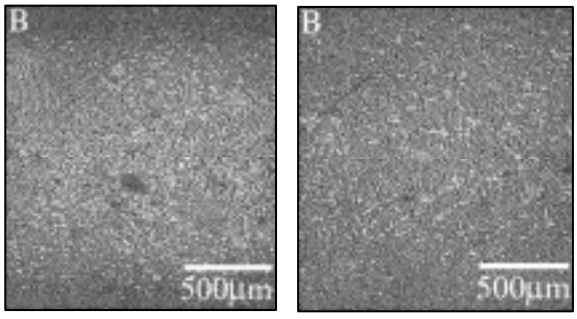

a) b)

Figure 3: Micrographs from position B. T_m=710°C. a) Lower $T_{shot\ sleeve}$ and b) at a quasi-steady state $T_{shot\ sleeve}$.

Effect of Superheat on the Crystal Morphology

The castings produced at a low superheat (640°C) revealed two distinct crystal morphologies. The floating crystals are observed to be coarse dendritic or rosette like, as observed in Figure 4 a), or globular in shape, Figure 4 b). The latter dominates in position C. At higher melt temperatures (680 and 710°C) the crystal morphology is generally elongated dendrite trunks or arms (Figure 4 c) or branched dendrites (Figure 4 d). The branched crystals dominate in the center of the cross sections and closer to the gate.

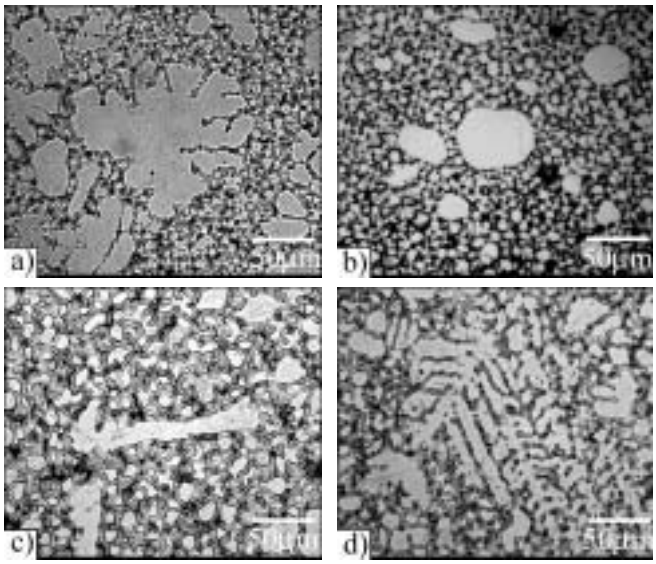

Figure 4: Floating crystal morphologies; a) Coarse dendritic/rosette like, b) globular (T_m=640°C), c) elongated trunks/arms, d) branched dendritic (T_m=680 and 710°C).

Discussion

Effect of Melt and Shot Sleeve Temperature on the Grain Size Distribution

In magnesium HPDC up to 20% of the metal can be solidified in the shot sleeve prior to injection as reported in [5], and a decreasing fraction of floating crystals from the gate has been observed [21]. This is analogous to the observations in Figure 1 and in Figure 2 and has been proposed to result from the non-isothermal conditions in the shot sleeve. Supported by work on plunger movement and wave behavior in the shot sleeve, the larger fraction of coarse crystals observed close to the gate in the casting has been proposed to originate from closer to the plunger. The lower fraction of crystals observed farther from the gate has been deduced to originate from closer to the runner end [4,6,18]. Pre-solidification is most likely susceptible to shot sleeve volume and fill ratios. Measurements of the area fraction of floating crystals (with an ECD threshold of

6.7σm) close to 0.5 have* been reported [5] using a small diameter shot sleeve with a fill fraction of 0.35.

It can be deduced that with a low melt temperature a larger undercooling can be rapidly established and a larger number of crystals are nucleated (640°C, Figure 2). Nucleation, growth and remelting of crystals depend on the degree of melt undercooling, and at higher melt temperatures the undercooling adjacent to the walls is reduced and fewer crystals are formed. Crystals that are nucleated later remelt due to the superheated liquid and hence fewer floating crystals are observed in the casting (Figure 2, 680°C and 710°C).

The floating crystals are occasionally centered in the cross section thickness, e.g. position B in Figure 2, which can be explained by a solid skin is rapidly formed at the die walls during filling. The skin alters the flow behavior locally by reducing the effective cross section thickness. The melt, or mush, arriving later is forced towards the center. Thus, a larger area fraction of floating crystals is observed in the center [6,18]. Occasionally, the skin may not be sufficiently thick to fully accommodate for the centered crystals and crystal migration can be an additional mechanism acting as proposed in [22]. Presently it is not clear if the observed plug flow is solely due to any one of these mechanisms, and work is in progress to increase the understanding of semi-solid flow.

It has been proposed that velocity and superheat is critical for the distribution of floating crystals in the cross section thickness [6]. The microstructure in position B (Figure 1) deviate from that reported and can partially be attributed to the different filling phase velocities, i.e. 4.5ms^{-1} in contrast to 6.5ms^{-1} [6]. A lower velocity can result in a greater fraction of metal freezing at the die walls during filling. Hence, the crystals distributed between the surface and the center are locked in this position. This can not be observed at higher melt temperatures as fewer floating crystals survive in the shot sleeve, and the crystals that first enter the cavity are less susceptible to be deposited closer to the surface as less metal freeze at the die walls.

The observed effect of decreased fraction of floating crystals with increased shot sleeve temperature can be deduced to result from the reduced number of crystals formed and

* Corrected from printed version.

the increased likelihood of remelting with superheated melt (Figure 3). To test the hypothesis that the thermal conditions in the shot sleeve affects the formation of floating crystals, a few castings were produced with coating in the interior of the shot sleeve. The coating was expected to exaggerate the effects observed in Figure 3. As depicted in Figure 5, only a few floating crystals are present in position A (close to the gate) despite that a longer cycle time was inevitably generated during coating.

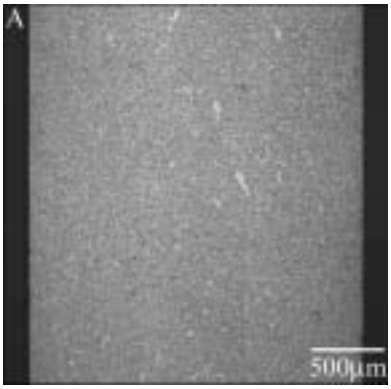

Figure 5: Micrograph from position A in a casting produced with coated shot sleeve. The coating procedure interrupted steady state and hence generated a slightly lower shot sleeve temperature. Initial T_m=680^oC.

Effect of Superheat on the Crystal Morphology

The diversity of dendrite morphologies observed is proposed to result from the variable cooling conditions and different nucleation mechanisms that prevail in the shot sleeve. At lower melt temperatures a less inclined temperature gradient and a larger thermal undercooling is established adjacent to the shot sleeve wall in which crystals can nucleate. During filling the crystals can be formed at the wall and eventually separate according to the theory outlined in [12], or resemble the nucleation of free chill crystals in the thermally undercooled region adjacent to the shot sleeve wall [13]. The "wall crystals", with a near-globular shape [12], are transported into the bulk of the liquid during filling by the flow of melt. The crystals survive as the melt is sufficiently cold and branching is restricted due to lack of undercooling. At a later stage a large number of floating crystals has formed and grown to the point of impingement followed by dendrite coarsening, which results in rosette like dendrites (Figure 4 a). The first wall crystals that were formed possess a globular morphology (Figure 4 b) and are distributed closer to the runner end of the shot sleeve and therefore end up far from the gate in the casting [4,6,18], e.g. in position C (Figure 1, right micrograph). As the globular crystals are associated with a lower melt temperature and dominate at lower

solid fractions at low superheat, e.g. position C, they are most likely not formed as a result of the high shear rates encountered in HPDC, as proposed in [5]. To obtain a globular microstructure shear is commonly applied for order of magnitudes longer times than the crystals are exposed to in HPDC [23].

At higher melt temperatures the temperature gradient adjacent to the shot sleeve wall during filling is steeper, and wall crystals are not expected to form as easily as the thermally undercooled region is reduced. Some crystals can form, but these are disposed to shrink and remelt as they are carried into the bulk of the superheated liquid. At a later stage crystals nucleate on the wall and grow as dendrites into the melt. Dendrites can be nucleated in the constitutionally undercooled zone at the growth front[14] or be fragmented due to dendrite arm remelting at the roots [15]. The latter mechanism is more probable as the morphology of many of the crystals resembles dendrite fragments (Figure 4 c and d). A cascade effect can be triggered as more fragmentation is initiated. The dendrite finds itself in superheated liquid, and arms are easily detached. In-situ solidification experiments, by means of X-ray imaging, have manifested the ease by which dendrite arms are fragmented during columnar dendritic growth in aluminium alloys, and convection is a major contributor in the fragmentation process [24]. Forced convection generated by the plunger movement can enhance fragmentation through dendrite arm remelting. Forced and free convection is set up by the melt flow during and after pouring and thermosolutal gradients, respectively. The crystals remain branched dendritic till injection is initiated, as an insufficient number of crystals are present to impinge on each other and generate coarsening.

It has been reported that dendrite fragments results from the high shear rates encountered in the gate [5]. If this mechanism pertains, a high fraction of branched dendritic crystals would be expected in the runner system. However, a large fraction of dendrite fragments is present on either side of the gate, as observed in the micrograph in Figure 6 obtained from a position in front of the gate. Metallic dendrites are not expected to break mechanically in a casting operation, but can be plastically deformed[25].

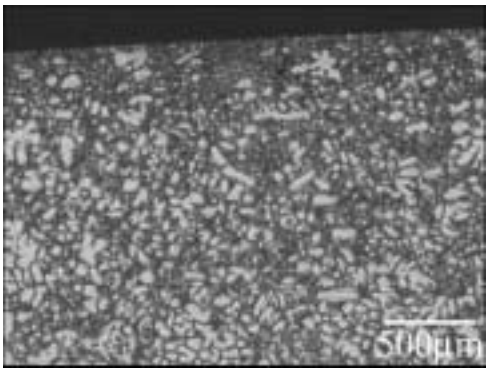

Figure 6: Microstructure of gate-section with dendrite fragments present.

The solidification in HPDC is highly non-idealised. Large differences in grain sizes, distributions and crystal morphology can be observed, depending on position in the casting, process conditions, thermal and constitutional variations, flow behaviour, volume fraction of pre-solidified metal and alloy type. An additional aspect can be the growth of floating crystals in the cavity, which is not within the scope of the present work. However, it can be argued that a higher melt temperature would generate a coarser microstructure due to a higher fraction liquid. Analogous, a low melt temperature and larger fraction of floating crystals would generate less melt to freeze, and coarsening would not occur. However, the floating crystals are coarser in the latter case. A higher melt temperature can improve the efficiency of the intensification pressure, and pressure effects (Claussius-Clapeyron) could be introduced generating a finer grain structure.

Conclusions

The initial melt temperature and the thermal conditions in the shot sleeve affect the distribution of floating crystals:

1. A larger area fraction of floating crystals is obtained with a low superheat and colder shot sleeve, which is attributed to the large number of floating crystals formed and the increased survival rate.
2. A lower area fraction of[*] floating crystals is obtained with a larger melt superheat or altered heat transfer conditions in the shot sleeve. This is proposed to result from fewer floating crystals are formed and fewer survive.

The floating crystal morphology is affected by the melt superheat:

1. With a low melt temperature wall mechanisms are proposed to dominate. This results in floating crystals with a coarse dendritic (rosette like) or globular morphology.
2. Branched and elongated dendrites are obtained with higher melt temperatures. This is attributed to extensive dendrite fragmentation in the shot sleeve.

Acknowledgements

The present work was funded by the project NorLight Shaped Castings and partners: the Norwegian Research Council, Alcoa Automotive Castings, Scandinavian Casting Center ANS, Elkem Aluminium ANS, Fundamus AS, Hydro Aluminium Metal Products, Norsk Hydro ASA, NIMR, NTNU and SINTEF (project responsible). The authors acknowledge[*] the partners for financial support.

[*] Corrected from printed version.

References

[1] Z.W. Chen, M.Z. Jahedi, Int. J. C. Met. R., 1998, 11, 129-138.

[2] D. Rodrigo, M. Murray, H. Mao, J. Brevick, C. Mobley, R. Esdaile, NADCA Trans., 1999, 219-225.

[3] D. StJohn, A.K. Dahle, T. Abbott, M.D. Nave, M. Qian, Proc. Mg Tech., 2003, 95-100.

[4] H.I. Laukli, A. Graciotti, O. Lohne, H. Gjestland, S. Sannes, NADCA Trans., 2002, T02-035, 1-5.

[5] W. Sequeira, PhD thesis, The University of Queensland (Brisbane), 2000.

[6] H.I. Laukli, O. Lohne, S. Sannes, H. Gjestland, L. Arnberg, Int. J. C. Met. R., 2003, 16, 515-521.

[7] A. Bowles, J.R. Griffiths, C.J. Davidson, Proc. Magnesium Techn., 2001, 161-168.

[8] J. Hutt, D. StJohn, Int. J. C. Met. R., 1998, 11, 13-22.

[9] A.K. Dahle, Y.C. Lee, M.D. Nave, P.L. Schaffer, D.H. StJohn, J. Light Met., 2001, 1, 61-72.

[10] L. Bäckerud, M. Johnsson, Proc. Light Met., 1996, 679-685.

[11] W. Kurz, D.J. Fisher, Fundamentals of Solidification, Trans Tech. Publications, 1998, 85-89.

[12] A. Ohno, Solidification - The sep. theory and its practical applic., Springer Verlag, 1987, 51-60, 78.

[13] B. Chalmers, J. Aust. Inst. of Metals, 1963, 8, 255-263.

[14] W.C. Winegard, B. Chalmers, Trans. ASM, 1954, 46, 1214-1224.

[15] K.A. Jackson, J.D. Hunt, D.R. Uhlmann, T.P. Seward, Trans. AIME, 1966, 236, 149-158.

[16] R.T. Southin, Trans. AIME, 1966, 239, 220-225.

[17] S. Sannes, H. Gjestland, H. Westengen, H.I. Laukli, Proc. Mg Alloys & Appl., 2003, 725-731.

[18] S. Sannes, H. Gjestland, H. Westengen, H.I. Laukli, O. Lohne, SAE Trans., 2003, 03M-192.

[19] H.I. Laukli, O. Lohne, L. Arnberg, Proc. Mg Alloys & Appl., 2003, 232-235.

[20] Adobe Photoshop, 7.0, Adobe, 2002.

[21] P.D.D. Rodrigo, V. Ahuja, Proc. Int. Conf. Mag. Sci. Techn., 2000, 97-104.

[22] A.K. Dahle, S. Sannes, D.H. St. John, H. Westengen, J. Light Met., 2001, 1, 99-103.

[23] Y. Ito, M.C. Flemings, J.A. Cornie, Rheol. & microstr. of AlSi6.5 in *Nature and prop. Of SSM*, TMS, 1991.

[24] R.H. Mathiesen, L. Arnberg, K. Ramsøskar, T. Weitkamp, C. Rau, A. Snigirev, Met. Mat. Trans. B, 2002, 33B, 613-623.

[25] A. Hellawell, S. Liu, S.Z. Lu, JOM, 1997, 18-20.

ARTICLE 4

Effects of Grain Refiner Additions on the Grain Structures in HPDC A356 Castings

H.I. Laukli

Department of Materials Technology
Norwegian University of Science and Technology
N-7491 Trondheim
NORWAY

Submitted for publication in: *Metallurgical and Materials Transactions A*, 2004.

Abstract
In the cold chamber high pressure die casting process (HPDC) solidification begins when the metal is poured into the shot sleeve and impinges on the relatively cold shot sleeve wall and plunger. Therefore, a mixture of liquid and externally solidified crystals (ESCs) is injected into the die cavity. The mechanisms that control the formation of ESCs are not fully comprehended. In the work presented here, the microstructures of thin walled A356 aluminium alloy die castings have been investigated. The castings were produced with variations in melt superheat and constitutional conditions, and it was found that: 1) the area fraction of ESCs increases with a decrease in the melt superheat; 2) a low superheat generates coarser, more globular ESCs, whilst a larger superheat results in branched, dendritic crystals; 3) additions of Ti in solution increase the fraction of ESCs; 4) additions of AlTi5B1 grain refiner enhance the formation of globular, coarse ESCs and generate a finer grain size in the casting. The results are discussed with special emphasis on the shot sleeve solidification conditions and the mechanisms that control the formation of the ESCs.

Keywords: A356, grain refinement, pre-solidification, high pressure die casting (HPDC).

Introduction

When the metal is poured into the shot sleeve in the cold chamber high pressure die casting (HPDC) process, the superheat is quickly dissipated. The metal is therefore in a semi-solid state when it becomes exposed to the greater cooling rate in the die cavity. The microstructure eventually possesses a duplex grain structure which consists of fine grains and coarse externally solidified crystals (ESCs). In magnesium [1-3] and aluminium HPDC [4], a large volume fraction of ESCs is typically present near the gate in the casting, whilst, further away, there is a significantly lower fraction of ESCs. The conditions for solidification and feeding are influenced, and the ability to successfully transmit the after-pressure can be affected. The mechanisms responsible for the inhomogeneous distribution of ESCs are described in [2,4].

There are great interests in further development of shot sleeve technology with particular emphasis on reducing the amount of ESCs. It is therefore necessary to improve the understanding of the formation of ESCs and assess the solidification mechanisms in detail: The solidification of alloys begins when crystals are nucleated on suitable substrates [5] at a sufficient undercooling of the melt. These crystals can evolve into dendrites, and eventually, the thermosolutal [6] diffusion fields encapsulating the dendrites impinge on each other, and peripheral growth is substituted by crystal coarsening [7].

In the dynamic nature of the casting process, crystals can be formed without the chemical addition of inoculants. The mechanisms are reviewed by Hutt and StJohn [8], and are briefly as follows: During the filling of a die, crystals are nucleated in the thermally undercooled region at the wall. The crystals possess a necked shape because solute diffusion at the root is restricted by the wall. This provides easy separation from the wall, by convection, as outlined by Ohno [9]. Chalmers [10] proposed that free chill crystals are formed in the thermally undercooled region adjacent to the die wall, whilst Southin [11] argued that heat radiation at the melt surface generates a sufficient thermal undercooling for nucleation and growth of crystals which detach by breaking off. Jackson [12] proposed that dendrite fragments can be formed by ripening phenomena, i.e. the dendrite dissolves at the root where the curvature is greatest. Winegard [13] explained that, in an alloy, (with a eutectic phase diagram), solute rejection at the crystal interface and simultaneous release of latent heat generates a constitutionally undercooled zone at the growth front in which suitable substrates can nucleate crystals.

In order to establish a better understanding of the mechanisms which control the nucleation of ESCs, thin walled A356 aluminium alloy die castings were produced with variations in melt superheat and with additions of Ti and AlTi5B1 grain refiner. The resulting grain distributions and the mechanisms responsible for the ESC morphologies are discussed.

Experimental

Generic, box shaped cold chamber high pressure die castings were produced. A complete casting, with biscuit (B), runners (R) and overflows (O), is shown in Fig.1. Metallographic investigations were done in locations A, B and C.

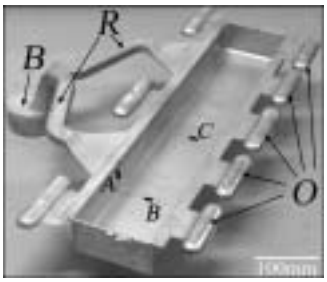

Figure 1: Complete box shaped casting with biscuit (B), runners (R) and overflows (O). Samples for microstructural investigations were taken from the locations marked A, B and C. Wall thickness: 2.5mm.

Alloys

Three variants of the A356 aluminium alloy were utilised: (1) A356 with a relatively low Ti content (0.007); (2) A356+AlTi5B1, (same batch as (1), but AlTi5B1 added as rod to the melt in a ratio of 10g to 1kg less than 60 seconds prior to HPDC to avoid fading); (3) A356+Ti, with a relatively high Ti content (0.13), in solution, (added during ingot production). This was intended to study the principal effects of Ti in solution and the effects of additions of grain refiner particles. The high iron content is usually added to prevent soldering in the die.

Table 1. Alloy compositions based on average batch contents [wt%].

Alloy	Si	Mg	Mn	Fe	Ti	Sr	B	Al
A356	7.2	0.35	0.66	0.66	0.007	0.013	0.002	Balance
A356+AlTi5B1	7.2	0.35	0.66	0.66	0.060^{+}	0.013	0.012^{+}	Balance
A356+Ti	7.2	0.37	0.68	0.47	0.130	0.018	0.002	Balance

$^{+}$The higher Ti and B contents are in the form of particles, (added as AlTi5B1 grain refiner).

The temperature as a function of fraction solid-curves for the A356 and A356+Ti alloys, as determined by phase diagram calculations using the computer model Alstruc [14], are shown in Fig.2. A discrepancy at low fractions solid is present: the liquidus temperature of the A356 alloy (T_{liq}å609°C) is approximately 4K less than T_{liq}å613°C for the A356+Ti alloy. However, the estimated variations in the melt temperature measurements is ~5K, and furthermore, the calculations are also disposed to some uncertainty due to the inherent complexity of calculating the solidification behaviour of multi-component alloy systems. It has therefore been assumed that equal melt temperatures induce approximately similar superheats. Additionally, it was assumed that the addition of AlTi5B1 to the A356 alloy, (which gave the A356+AlTi5B1 alloy - A356 with grain refiner particles), generated a negligible effect on the T_{liq}, and possessed a similar solidification behaviour.

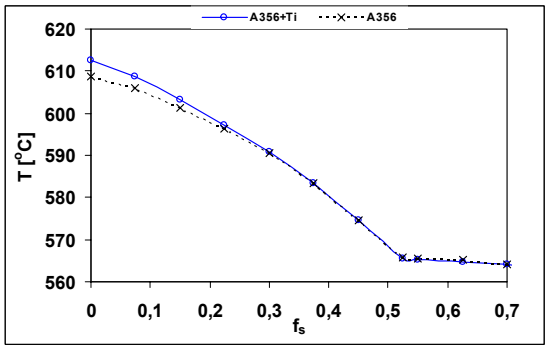

Figure 2: Temperature as function of fraction solid for the A356 and A356+Ti alloys as predicted by the computer model Alstruc [14]. Isothermal solidification at the eutectic temperature, T_{eut}=565°C.

Casting Procedure

Batches, each of ~100kg, of the A356 and A356+Ti alloys were held in a furnace, where the temperature was controlled with a thermocouple. A steel ladle with thermally insulating coating, (pre-heated by immersing into the melt), was used for pouring the melt (~1kg) into the shot sleeve of the die casting machine. The A356+Ti alloy was held at a temperature of approximately 700°C for at least 2 hours prior to casting, to assure that the Ti was kept in solution. Samples were regularly extracted from the melt during the casting operation, and compositional analysis revealed relatively homogeneous compositions throughout the batches. Castings were produced, and scrapped, until a steady state shot sleeve temperature (250-300°C) was reached [4]. The A356 and A356+AlTi5B1 castings were produced with superheats of ~65K and ~95K, whilst the A356+Ti castings were produced with ~25K, ~65K and ~95K superheats.

Microstructure Characterisation

Metallographic samples, taken from castings produced at steady state with representative production data, (i.e. velocity, pressure and timing), were prepared for optical microscopy and SEM investigations. The samples were ground, mechanically polished and etched in a modified Murakami etchant (60ml distilled H_2O, 10g NaOH and 5g $K_3Fe(CN)_6$). Chemical etching was replaced with ion milling in the preparation of the SEM-samples. To resolve the fine grained microstructure, electron backscattering diffraction measurements (EBSD) in SEM was used. In a few polished samples, the local composition was measured with electron probe micro analysis (EPMA).

Results

ESC Morphologies

Three different ESC morphologies are typically observed in the castings: 1) globular crystals, 2) elongated trunks and 3) branched dendrites. The globular crystals (Fig.3a) are associated with a low superheat. They are isolated, near-spherical crystals that are generally present farther from the gate as well as in intermediate positions in the cross section, (i.e. near the surface). The elongated trunks (Fig.3 b) are observed at all superheats and are typically present near the surface. The branched dendritic crystals (Fig.3 c), are coarser at low superheats, and are observed in the centre of cross sections and dominate near the gate.

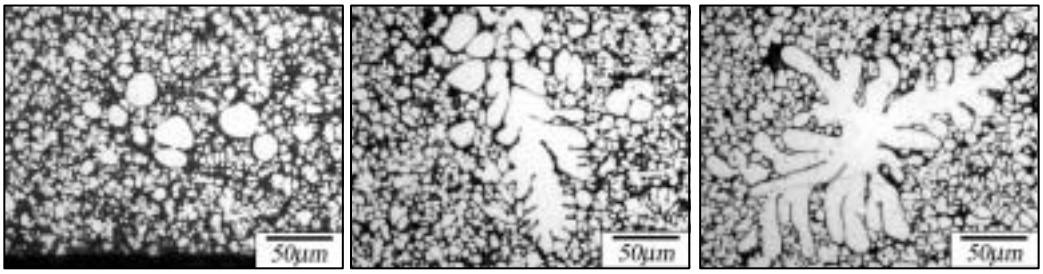

a) b) c)

Figure 3: Different ESC morphologies; a) Globular; b) Elongated trunks; c) Branched dendritic. The ESCs are surrounded by a fine grained microstructure. Alloy: A356+Ti.

The castings produced with the A356 alloy possess dendrites resembling the ESC in Fig.3 c), with thinner branches. When the AlTi5B1 grain refiner was added, the ESCs became coarser and globular ESCs were present in similar positions as those observed in the A356+Ti castings produced at a low superheat (Fig.3 a).

To gain further information on the ESC-morphologies the microstructures were investigated in the SEM with the EBSD technique. This technique allows the crystallographic orientation of the grains to be determined by scanning the sample surface with the electron beam. The different crystallographic orientations can be processed to appear as grain maps, where a specific colour indicates a grain. Grains with misorientations greater than a specific value, e.g. 15^{o}, are separated by grain boundaries, (delineated as black lines). Fig.4a shows an elongated trunk and a few coarse ESCs positioned in a fine grained matrix. An agglomerate-like ESC, (greyish colour with the circumference marked as a red line), which possesses dendrite arms with approximately similar colour, i.e. crystallographic orientation, is shown in Fig.4b. The vague, dark lines mark the borders between the dendrite branches, whilst the white areas are non-indexed grid points which can result from particles or a non-uniform ion milling.

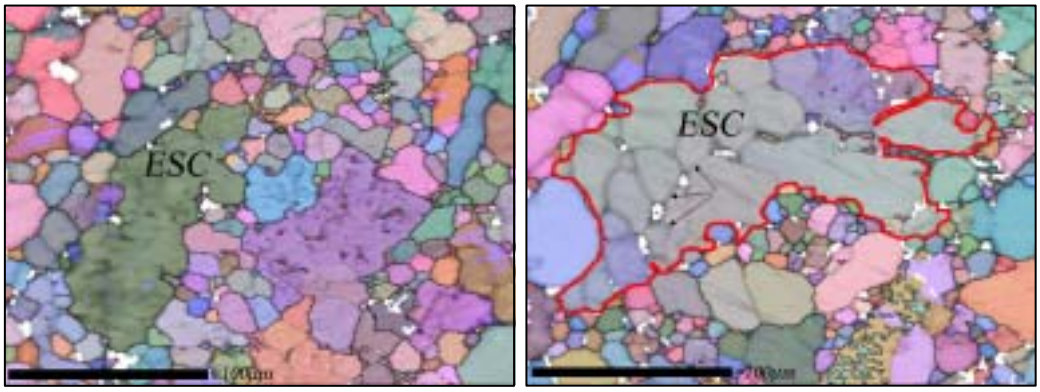

a) b)

Figure 4: Grain orientation maps obtained from EBSD measurements in SEM. a) Elongated trunk (A356); b) Coarse agglomerate-like crystal (A356+Ti). The white spots are non-indexed grid points. The arrows marks the lines separating the dendrite branches.

Effect of Superheat on the Distribution of ESCs

The average area fraction of ESCs decreases when moving at further distances away from the gate. This is clearly demonstrated in the micrographs in Fig.5 a-c, (A356+Ti, ~25K superheat), and in the diagram in Fig.5d. In the casting produced with a superheat of 25K, the average area fraction of ESCs is approximately 20% in position A (near the gate) and decreases to 6% in position C. At a superheat of 65K, the average area fraction is 13% in position A and ~3% in C. In the castings produced with a superheat of ~95K, the average area fraction is 10% in position A and decreases to 2% in position C.

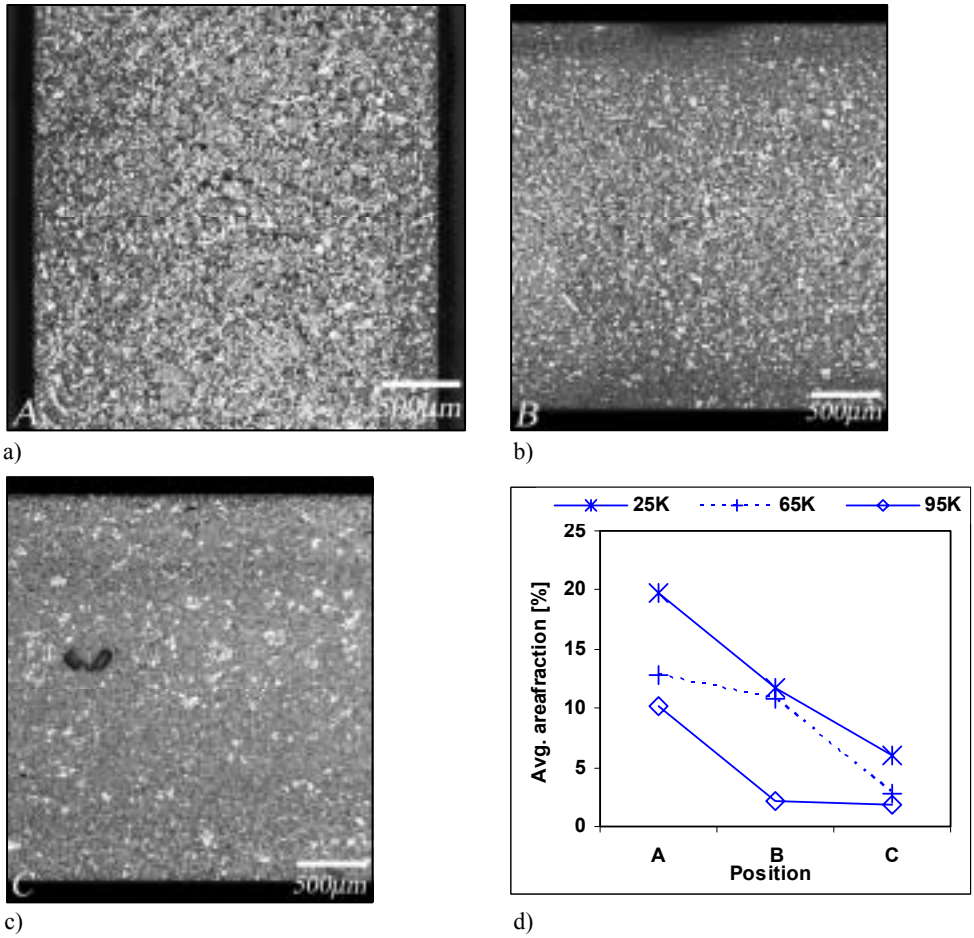

a) b) c) d)

Figure 5: Cross sectional micrographs from an A356+Ti casting (~25K superheat) at locations a) A, b) B and c) C. Flow directions: vertically (A); horizontally (B and C), parallel to the page. d) Measurements of the average area fraction of ESCs, (white particles in the micrographs), as a function of position for different superheats in the A356+Ti castings.

The measurements of the area fraction of ESCs as a function of thickness for the three different superheats are shown in the diagrams in Fig.6. Each measurement represents the average area fraction of ESCs in an area of ~250x2500σm (thickness). There are three principal features to note: 1) The area fraction of ESCs generally decreases from positions A to C as shown in Fig.5d. 2) A significant reduction in the area fraction of ESCs is found at a higher superheat. 3) The ESCs are segregated to the centre in location B, whilst the peak is broader in A.

Specifically, at 25K superheat the maximum area fraction of ESCs is 25% in position A and ~19% in B. At a superheat of 65K, the area fraction of ESCs is ~17% in A and in B it is ~19%. In position C, the ESCs are distributed relatively homogeneously in the cross section at superheats of 25K and 95K, (5-9% and 1-3%). Contrarily, at 65K superheat a defined peak is present in the centre with an area fraction of ESCs of approximately 6%.

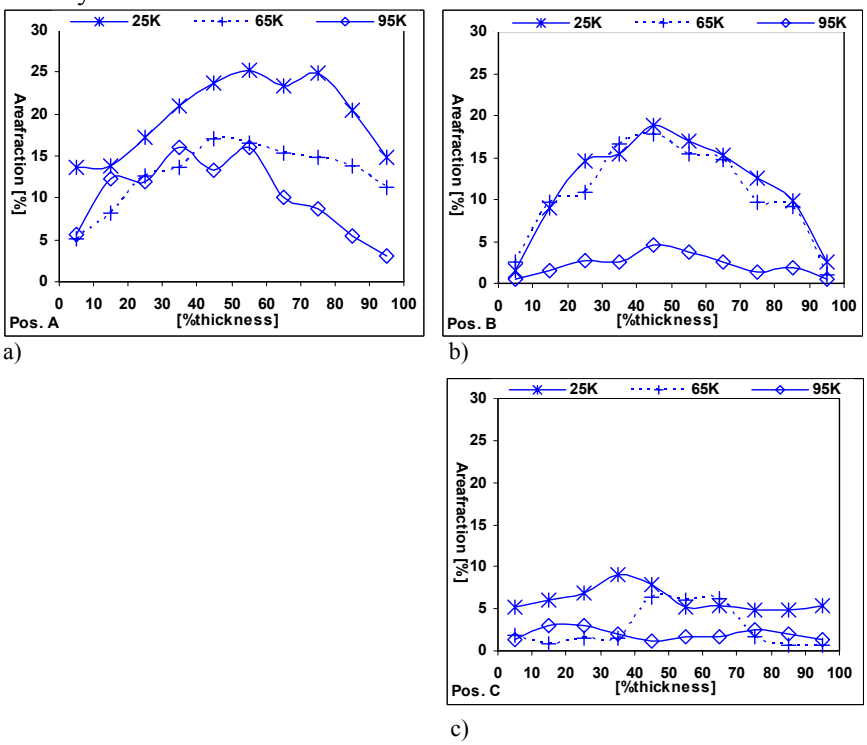

Figure 6: Measurements of the area fraction of ESCs as a function of the thickness in positions a) A, b) B and c) C in A356+Ti castings produced with superheats of 25K, 65K and 95K.

Effect of Grain Refinement on the Distribution of ESCs

Micrographs from location A, (from the surface to the centre of the cross sections), in the A356 and A356+Ti castings produced with 65K superheat are shown in Fig.7a and b. Despite that position A (near the gate) is typically associated with a higher fraction of ESCs, a relatively low fraction of ESCs is present in the A356 casting, (Fig.7 a). The ESCs are segregated to the central region of the cross section where the area fraction of ESCs is approximately 4%, (Fig.7 c). In the A356+Ti casting, there is a larger fraction of ESCs (Fig.7 b), and the area fraction is approximately 18% (Fig.7 c) in the centre. Near the surface, the area fraction of ESCs is 6-10%.

The measurements of the Ti content are included in the diagram in Fig.7 c. The measurements were done from the surface to the centre of the cross sections in defocus mode, (i.e. 50σm probe size) and represent the average of 3 parallel lines. The amount of Ti increases towards the central region in the A356+Ti casting, (line marked A356+Ti_Ti), and furthermore, the Si content, (Fig.7 c), decreases markedly from the surface to the ESC-rich central region (A356+Ti_Si). This is less pronounced for the A356 casting, (A356_Si), which possesses a lower fraction of ESCs. The scatter in the measurements of the Si content is inherently related to whether the probe was positioned in Al-Si eutectic or a primary crystal. An example of an EPMA map is shown in Fig.7 d, where the Al and Si contents are qualitatively illustrated with dark and red, respectively.

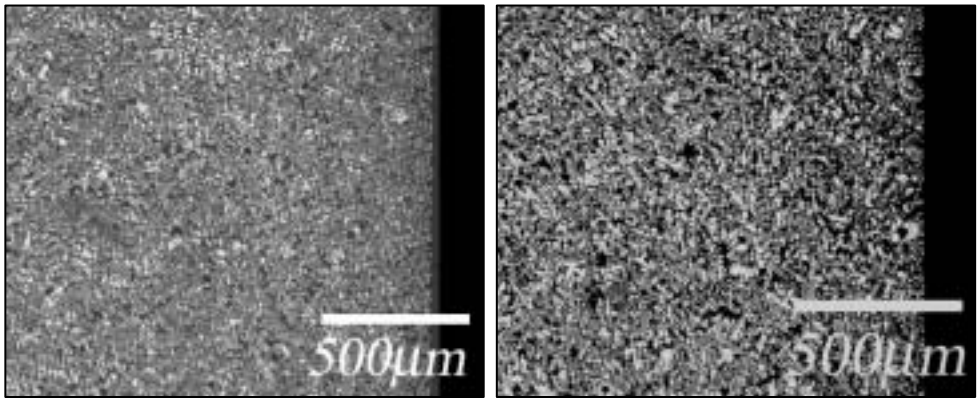

a) b)

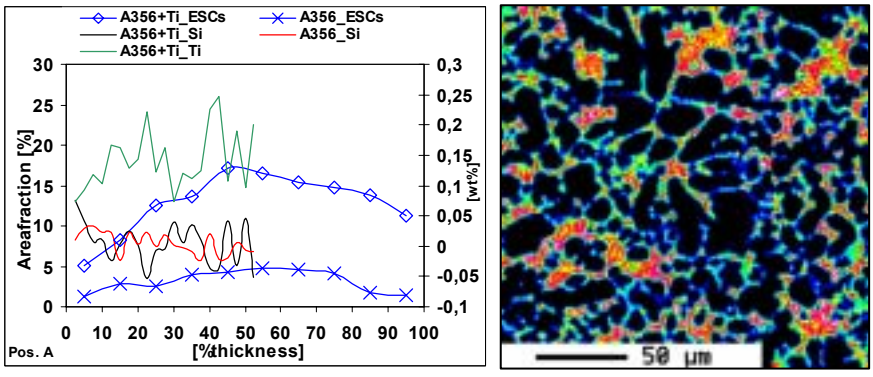

c) d)

Figure 7: Micrographs from position A, (from the surface to the centre of the cross sections), in castings produced with a superheat of ~65K: a) A356 alloy; b) A356+Ti alloy. Flow direction: vertically and parallel to the page; c) Measurements of the area fraction of ESCs and EPMA-measurements of the Si and Ti contents; d) EPMA map from position A in an A356 casting produced with 65K superheat. Primary Al appears dark and Al-Si eutectic appears red. (Probe size: 1σm; step size: 0.5σm; acc.voltage: 15kV; probe current: $30*10^{-9}$Amp).

Micrographs from location B in A356 castings produced with 65K superheat are shown in Fig.8. A relatively large fraction of the ESCs are segregated to the central region in Fig.8 a, (A356+AlTi5B1), whilst a relatively dispersedly distributed and significantly lower fraction of ESCs is present in Fig.8 b, (A356). The measurements of the area fraction of ESCs as a function of the thickness are shown in the diagram in Fig.8 c. The A356+Ti castings possess a similar ESC-distribution as the A356+AlTi5B1 castings with a maximum area fraction of approximately 18%, whilst the A356 casting possesses a significantly lower area fraction of ESCs (~4%). Additionally, the ESCs in the A356+AlTi5B1 casting are more centred. However, a few ESCs are occasionally observed near the surface, which is a result of some ESCs being deposited in the surface layer that forms at the wall during filling [15].

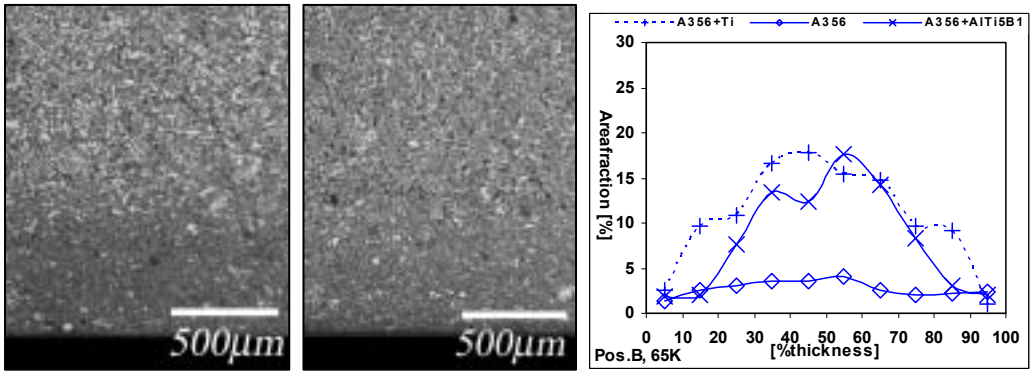

a) b) c)

Figure 8: Micrographs from location B, produced with 65K superheat: a) A356+AlTi5B1 and b) A356 castings. Flow direction horizontal, parallel to the page. c) Diagram of the area fraction of ESCs as a function of the thickness.

Effect of AlTi5B1 on the Fine Grained Microstructure

The effect of AlTi5B1 grain refiner in the A356 alloy, on the grain structures formed from the solidification of the residual melt in-situ in the die cavity is shown qualitatively in Fig.9. A micrograph from an A356 casting (65K superheat) is shown in Fig.9 a, whilst a micrograph from an A356+AlTi5B1 casting (65K) is shown in Fig.9b. Micrographs from the A356 and A356+AlTi5B1 castings, (95K superheat), are shown in Fig.9 c and d. A significantly finer grain size is present from the surface to the centre in the AlTi5B1 grain refined castings, (Fig.9 b and d).

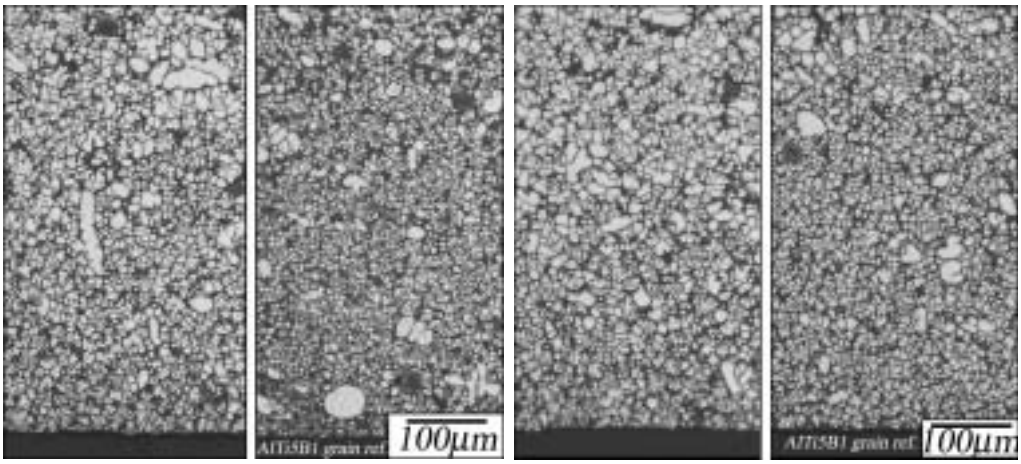

a) b) c) d)

Figure 9: Micrographs from location B in castings produced with superheats of 65K: a) A356 and b) A356+AlTi5B1; and 95K: c) A356 and d) A356+AlTi5B1. A significantly finer grain size is present in b and d.

Discussion

General Remarks

Before the results are analysed the solidification modes will be considered. Without any shot delay time, the filling of the shot sleeve and the initial phases of the plunger movement typically take 4-5 seconds, (i.e. the plunger movement starts immediately after the metal pouring is completed). Solidification thus progresses, and the fraction solid increases. The effect of 2 seconds shot delay time, (i.e. delay of 2 seconds before the plunger movement initiates), is shown in the micrographs in Fig.10 from A356+Ti castings, (location B). In spite of the large superheat (95K) a qualitatively larger fraction of ESCs is present in Fig.10 a, (shot delay time of 2 seconds), compared with Fig.10 b from an A356+Ti casting produced with conventional parameters, i.e. no shot delay time.

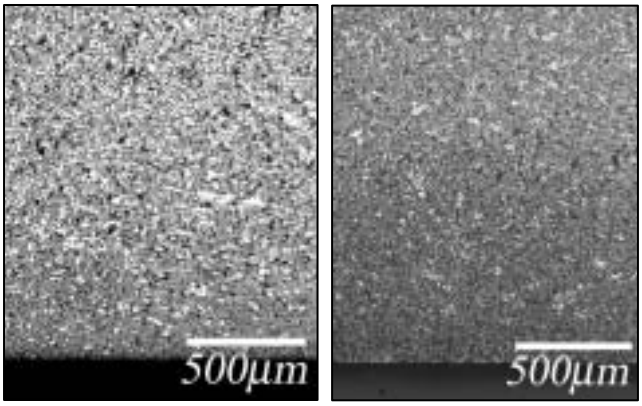

a) b)

Figure 10: Micrographs from location B in A356+Ti castings produced with 95K superheat and a) shot delay time 2 seconds and b) conventionally cast (i.e. no shot delay time).

When the melt is filled into the shot sleeve, the superheat and eventually the latent heat of fusion is conducted in the shot sleeve wall. Thus, the initial amount of superheat affects the amount of heat absorbed in the shot sleeve wall, which can ultimately affect the further progress of the solidification. In the present context, however, it is assumed that there is not sufficient time for the differences in the amount of superheat to significantly affect the mechanisms that control the formation of crystals.

Furthermore, the metal injection takes ~20ms, and it can be argued that the crystals will not extensively evolve in this period. The large shear rates encountered in the gate does not affect the crystal morphology to a noticeable extent. Similarly, it is proposed that no significant ESC coarsening occurs when the die filling is completed. Any coarsening of the ESCs would be exaggerated when increasing the superheat, because more latent heat and a lower fraction of ESCs would be present when the filling was completed. The ESC morphologies reveal that the opposite situation is present. In the work presented here, it is therefore assumed that the crystal morphologies and distributions are principally a result of the shot sleeve conditions.

Segregation of ESCs

The slight shift in the position of the peak in the area fraction of ESCs from the centre in location A (Fig.6 a) is attributed to the flow into the die. When the semi-solid metal flows through the gate, it rapidly experiences a 90^{o} bend. Thus, the metal impinges directly on the die wall. An additional 1mm further into the casting, it is expected that

the momentum persists and forces the metal towards the inside of the box, and a larger fraction of ESCs is therefore measured. When a lower fraction of ESCs is present (95K superheat), the flow conditions are similar. However, a larger amount of metal dilute in ESCs flows through which ultimately alters the ESC distribution.

The ESCs are less dispersed and segregates to the central region in the A356+AlTi5B1 castings, (Fig.8). In [15] it is shown that the ESCs segregate to the central region of the cross section till a maximum packing is reached which is proposed to depend on the coherency point for the alloy. The coherency point is a function of the crystal morphology, and branched dendrites obtain coherency at a lower fraction solid than finer crystals [16]. The maximum packing can therefore be variable within a casting because the ESC morphology varies with location in the casting. It can therefore be proposed that the area fraction of ESCs in the centre of location B (Fig.8 c) has not reached maximum packing because they are finer than in position A, of e.g. the A356+Ti alloy, where the area fraction is simultaneously greater (Fig.6 a). Similarly, the larger maximum area fraction of ESCs measured in [15] can result from a greater initial fraction of ESCs.

It has been shown that the die temperature and the fraction of ESCs affects the position of defect bands in A356 die castings, and the responsible mechanisms are described in detail in [17]. The ESC distributions can therefore be important for the interpretation of the mechanisms that controls the formation of defect bands as well as the segregation of crystals to the central region. For later work, a polynomial curve fitting was therefore established, as shown in Fig.11.

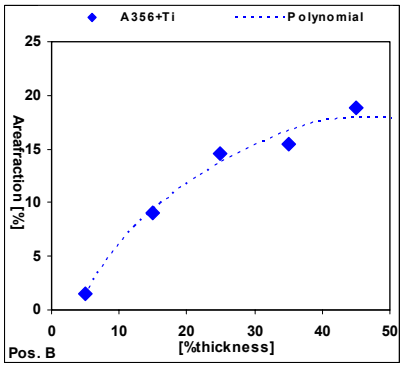

Figure 11: Diagram with area fraction of ESCs as function of thickness. Experimental data for A356+Ti casting (25K superheat) and polynomial curve fitting.

ESC Morphologies

It is necessary to assess the role of the cooling conditions and the different nucleation mechanisms in the shot sleeve to explain the diversity of dendrite morphologies that are present: During the filling of the shot sleeve, the formation of ESCs is restricted to the thermal undercooling of the melt near the plunger and the shot sleeve wall [9,10]. The melt temperature when pouring into the shot sleeve affects the nucleation events, because a low superheat gives a leaner temperature gradient and a larger thermal undercooling.

These ESCs possess a globular shape (Fig.3 a), and are transported into the bulk of the liquid during filling by the flow of melt. Therefore, they enter the die cavity early during metal injection [4], and end up in locations in the casting which are relatively far from the gate, e.g. position C (Fig.5). The efficiency of this mechanism is strengthened with the additions of grain refiners, i.e. the A356+AlTi5B1 alloy, where globular crystals are observed in castings produced with a relatively large superheat (65K). Without grain refiner additions, the globular ESCs are principally associated with lower melt temperatures and dominate at locally lower fraction solid. At larger superheats, where the shear rates are expected to be comparable with lower superheats, they are generally absent. Thus, the globular ESCs are not a result of the high shear rates encountered in HPDC as proposed in [18]. Globular crystals can be obtained when a slurry is exposed to shear for order of magnitudes longer times than in HPDC [19].

Eventually, the shot sleeve wall and plunger become covered with a solid layer and the wall-mechanisms are less disposed to be active. Solidification progresses and further nucleation can occur in the constitutionally undercooled zones encapsulating growing ESCs. A greater fraction solid is obtained and the ESCs can grow to the point of impingement which results in coarse dendritic ESCs, as shown in Fig.4 b.

At larger superheats the thermal gradient adjacent to the shot sleeve wall and plunger during filling is steeper, and the ESCs are impeded to be formed by wall mechanisms. If a few ESCs are formed, they dissolve and remelt when carried into the superheated liquid. When the filling is completed and a surface layer has formed, the solidification proceeds from the shot sleeve wall and plunger, and dendrites can be nucleated in the constitutionally undercooled zone at the growth front [13] and/or be fragmented due to dendrite arm remelting [12]. The morphology of the majority of the ESCs resembles dendrite fragments (Fig.3 b and c) and the latter mechanism can therefore be the most

frequent occurrence. The ESCs remain branched dendritic because the fraction solid is not sufficient to generate crystal coarsening.

The solidification of aluminium alloys have been investigated real-time with X-ray imaging. Those experiments show the ease by which dendrite arms are fragmented by partial melting during columnar dendritic growth, principally as a result of convection [20]. In this context, forced convection generated by the plunger movement can enhance the fragmentation process as well as the convection induced by the melt flow and the thermosolutal gradients that are present.

Effect of Superheat on the Distribution of ESCs

The survival rate of crystals in a superheated melt has been discussed theoretically in [21] and for the A356 alloy in [22]: At melt temperatures below the thermosolutal transition temperature, (T_{trans}), the crystals dissolve by relatively time-consuming solute diffusion, whereas above T_{trans}, they instantaneously remelt. The heat content in the melt at the time of injection is therefore critical for the survival rate of the ESCs. An increase in the melt superheat generates a reduction in the fraction of ESCs in the castings, as shown in the diagrams in Fig.5 and Fig.6, and with a lower melt temperature the superheat dissipates quickly, which results in a greater fraction of ESCs. Furthermore, a low superheat generates a leaner thermal gradient adjacent to the shot sleeve wall and plunger, and more crystals are therefore formed compared with a larger superheat, where a steeper gradient is present, and fewer crystals are formed.

Effect of Grain Refinement on the Distribution of ESCs

When Ti is added to an Al-Si alloy, the solidification path becomes complex. It follows from the Al-Si phase diagram that Si is inherently rejected at the crystal interface, and from the Al-Ti phase diagram that Ti is attracted. Furthermore, the volumetric segregating power of Ti is much stronger than for Si, and 0.05wt%Ti has an equivalent segregating power as 2wt%Si [23]. If Ti in excess of 0.15wt% is present, aluminium crystals can be nucleated on Al_3Ti particles through a peritectic reaction at 665^{o}C [24]. Furthermore, the peritectic reaction can occur at lower Ti contents when the amount of Si is increased [25]. The Ti content was less than 0.15wt% and the melt temperature was kept well above 665^{o}C. The following arguments are therefore provided for the role of Ti in solution:

Firstly: the ESCs in the A356 castings possess thinner branches compared with the A356+Ti castings, where they are generally coarser. The tip of a dendrite perceives less constraint during growth when strongly segregating elements are absent. This results in thinner dendrites because they are able to penetrate into un-saturated melt. Contrarily, the presence of strongly segregating elements, (e.g. Ti and Si), retard the growth front and peripheral growth is substituted with coarsening which results in coarser dendrites.

Secondly: the A356+Ti castings were expected to generate a greater constitutional undercooling effect due to the segregating power of Ti [26], and hence, a larger fraction of ESCs. In contrast, fewer ESCs would be formed in the A356 castings, which possess small amounts of Ti in solution. However, at a similar melt superheat the total fraction solid should be approximately equal, (cf.Fig.2), which implicitly would induce a greater fraction pre-solidified material left in the biscuit and runner system of the A356 castings. However, there were no microstructural evidence that this occured when the microstructures in the biscuits were investigated.

Furthermore, there is negligible difference in the average Si content in the A356 and A356+Ti castings and therefore no macro-segregation effects can be observed in location A. However, the Si content decreases markedly from the surface and to the centre in the A356+Ti casting, (Fig.7 c), and the lower Si content is therefore associated with the ESCs. This effect is less pronounced in the A356 casting because it possesses a lower fraction of ESCs. The increase in the Ti content in the central region and a decrease near the surface in the A356+Ti casting is also associated with the ESCs.

Thirdly: despite that the Ti was expected to primarily be in solution in the melt in the A356+Ti alloy, fine resolution EPMA-mapping was done to investigate the possible presence of Al_3Ti particles in the castings. This revealed that the Ti was principally in solution in the ESCs, whereas a few TiFeMn particles were observed, located in the Al-Si eutectic. It is also to be noted that the higher Fe-content in the A356 castings compared with the A356+Ti castings did not significantly contribute to the formation of ESCs.

It is therefore proposed that the significant differences in the area fraction of ESCs in the A356 and A356+Ti castings are a result of the enhanced constitutional undercooling effect of Ti. Hence, a larger constitutional undercooling generates more

frequent nucleation and more crystals. Furthermore, the EPMA measurements were done in castings produced with an initial superheat of ~65K. It follows that the melt temperature would eventually be below the Al_3Ti peritectic temperature (665^oC) in the shot sleeve. The same situation would arise in casting with 25K superheat. Because the EPMA measurements did not reveal any Al_3Ti particles it is assumed that the differences in the fraction of ESCs principally result from the variations in initial melt superheat and not by nucleation on Al_3Ti particles at lower superheats.

Effect of AlTi5B1 on the Fine Grained Microstructure

When inoculants were added to the melt, (AlTi5B1 in the A356 alloy, i.e. the A356+AlTi5B1 alloy), an increase in the fraction of ESCs was generated, (Fig.8). It is an established perception that grain refiner additives require a lower critical undercooling for nucleation [27], and thus, the increased fraction of ESCs is attributed to the effective nucleation on the suitable grain refiner particles that were present in the melt in the A356+AlTi5B1 alloy.

It is a common perception that grain refining by chemical additions is not necessary in HPDC because a fine grained microstructure is achieved when the melt experiences the very large cooling rate in the die. However, it is evident that when AlTi5B1 was added to the melt, there was also a complimentary effect on the microstructure. A significantly finer grain size was achieved from the solidification of the residual melt in the die cavity, which shows that grain refinement is important in the formation of the final grain structure in aluminium high pressure die casting.

Conclusions

A356 aluminium alloy die castings have been produced with variations in the thermal and constitutional conditions. It has been found that the distributions of the externally solidified crystals (ESCs) are greatly affected by the melt superheat and the additions of Ti and AlTi5B1 grain refiner:

1. The area fraction of ESCs is largest near the gate. This is attributed to the conditions under which pre-solidification occurs and the inherent metal behaviour during plunger movement and die filling.
2. The area fraction of ESCs increases with a decrease in the melt superheat on pouring and decreases with an increase in the melt superheat.

3. Additions of Ti in solution increase the formation of ESCs.
4. Additions of AlTi5B grain refiner enhance the formation of ESCs and generate a finer grain size in the casting.

The morphology of the ESCs is affected by the thermal undercooling gradient in the shot sleeve, the constitutional conditions and thus the mechanisms that are responsible for the formation of ESCs:

1. A low superheat, and a leaner thermal gradient, generates coarser, more globular ESCs. A larger superheat, and a steeper thermal gradient, results in branched, dendritic crystals.
2. Grain refiner additions to the melt are shown to enhance the nucleation of globular, coarse ESCs.

Acknowledgements
The present work was funded by the project NorLight Shaped Castings and partners: the Norwegian Research Council, Alcoa Automotive Castings, Scandinavian Casting Center ANS, Elkem Aluminium ANS, Fundamus AS, Hydro Aluminium Metal Products, Norsk Hydro ASA, NIMR, NTNU and SINTEF (project responsible). The author acknowledges the partners for financial support.

The following Hydro Aluminium research centres are acknowledged for additional support: (1) Research and Development Materials Technology (RDM) for supplying the A356 alloys; (2) Magnesium Competence Centre for place at disposal a die casting machine.

Professor Otto Lohne, Professor Lars Arnberg and Professor emeritus Nils Ryum from the Department of Materials Technology at NTNU are acknowledged for comments and discussions on the present work. Mr. Raimo Helenius is acknowledged for assistance in preparing metallographic samples.

References

[1] P.D.D. Rodrigo, V. Ahuja, Proc. Int. Conf. Mag. Sci. Techn., 2000, 97-104.

[2] H.I. Laukli, O. Lohne, S. Sannes, H. Gjestland, L. Arnberg, Int. J. C. Met. R., 2003, 16, 6, 515-521.

[3] H.I. Laukli, O. Lohne, L. Arnberg, H. Gjestland, S. Sannes, Proc. Mg. Alloys & Appl., 2003, 182-189.

[4] H.I. Laukli, A. Graciotti, O. Lohne, H. Gjestland, S. Sannes, NADCA Trans., 2002, T02-035.

[5] L. Bäckerud, M. Johnsson, Proc. Light Met., 1996, 679-685.

[6] G. Hansen, A. Hellawell, S.Z. Lu, R.S. Steube, Met. Mat. Trans. A, 1996, 27A, 569-581.

[7] W. Kurz, D.J. Fisher, Fundamentals of Solidification, 1998, 85-89.

[8] J. Hutt, D. StJohn, Int. J. C. Met. R., 1998, 11, 13-22.

[9] A. Ohno, Solidification - The sep. theory and its practical applic., 1987, 51-60, 78.

[10] B. Chalmers, J. Aust. Inst. of Metals, 1963, 8, 255-263.

[11] R.T. Southin, Trans. AIME, 1966, 239, 220-225.

[12] K.A. Jackson, J.D. Hunt, D.R. Uhlmann, T.P. Seward, Trans. AIME, 1966, 236, 149 -158.

[13] W.C. Winegard, B. Chalmers, Trans. ASM, 1954, 46, 1214-1224.

[14] A.L. Dons, E.K. Jensen, Y. Langsrud, E. Trømborg, S. Brusethaug, Met. Mat. Trans. A, 1999, 30A, 2135-2146.

[15] H.I. Laukli, C.M. Gourlay, A.K. Dahle, Migration of Crystals During the Filling of Semi-Solid Castings, 2004, *submitted*.

[16] A.K. Dahle, L. Arnberg, Acta Mat., 1997, 45, 547-559.

[17] C.M. Gourlay, H.I. Laukli, A.K. Dahle, Met. Mat. Trans. A, 2004, *accepted*.

[18] W. Sequeira, PhD thesis, The University of Queensland (Brisbane), 2000.

[19] Y. Ito, M.C. Flemings, J.A. Cornie, Rheol. & microstr. of AlSi6.5 in *Nature and prop. of SSM*, 1991.

[20] R.H. Mathiesen, L. Arnberg, K. Ramsøskar, T. Weitkamp, C. Rau, A. Snigirev, Met. Mat. Trans. B, 2002, 33B, 613-623.

[21] Q. Han, A. Hellawell, Met. Mat. Trans. B, 1997, 28B, 169-173

[22] H.I. Laukli, PhD thesis, Norwegian Univ. of Science & Technology (Trondheim), 2004.

[23] D.H. St. John, A.K. Dahle, M. Easton, J.E.C. Hutt, N.L.M. Veldman, Mat. Forum, 1999, 23, 137-152.

[24] M.M. Guzowski, G.K. Sigworth, D.A. Sentner, Met. Trans. A, 1987, 18A, 603 618.

[25] P.A. Tøndel, PhD thesis, Norwegian Institute of Technology (Trondheim), 1994.

[26] M.A. Easton, D.H. StJohn, Acta Mat., 2001, 49, 1867-1878.

[27] A.L. Greer, A.M. Bunn, A. Tronche, P.V. Evans, D.J. Bristow, Acta mat., 2000, 48, 2823-2835.

ARTICLE 5

Migration of Crystals During the Filling of Semi-Solid Castings

H.I. Laukli[1], C.M. Gourlay[2], A.K. Dahle[2]

[1]Department of Materials Technology
Norwegian University of Science and Technology
N-7491 Trondheim
NORWAY

[2]CRC for Cast Metals Manufacturing (CAST)
Division of Materials
The University of Queensland
Brisbane, QLD 4072
AUSTRALIA

Submitted for publication in: *Metallurgical and Materials Transactions A*, 2004.

Abstract

In cold chamber high pressure die castings (HPDC), the microstructure consists of coarse externally solidified crystals (ESCs) that are commonly observed in the central region of cross sections. In the present work, controlled laboratory scale casting experiments have been conducted with particular emphasis on the flow and solidification conditions. An A356 aluminium alloy was used to produce castings by pouring semi-solid metal through a steel die. Microstructures similar to those encountered in HPDC have been produced and the resulting microstructure is found to depend on the melt and die temperature: 1) the fraction of ESCs determines the extent of migration to the central region; 2) a maximum packing determines the area fraction of ESCs in the centre; 3) the die temperature affects the position of the ESCs – a higher die temperature can induce a displaced ESC distribution. It is found that the migration of crystals to the central region requires a flow which is constrained at all melt/die interfaces. Furthermore, potential lift mechanisms are discussed. An assessment of the Saffman lift force on individual particles shows it has no significant effect on the migration of ESCs.

Keywords: Pre-solidification, crystal migration, high pressure die casting (HPDC).

Introduction

In many modern casting processes the material injected into the die cavity is partially solid so that the die fills by semi-solid flow where the material behaviour is generally non-Newtonian [1]. In the case of semi-solid casting processes such as rheocasting and thixocasting, the solid fraction and microstructure are carefully controlled before injection. In these processes a solid fraction of 50% is typically used.

In cold chamber high pressure die casting (HPDC), solidification begins when superheated metal is poured into the shot sleeve and impinges on the relatively cold shot sleeve wall and plunger. When the plunger moves forward, a mixture of externally solidified crystals (ESCs) and melt is injected into the die cavity. The nature of solidification in the shot sleeve leads to a variable fraction of ESCs being injected into the die, so there is less control over the solid fraction injected in HPDC than in semi-solid casting. Solid fractions up to 20% have been reported in magnesium cold-chamber HPDC [2].

In HPDC microstructures, ESCs are commonly compacted in the casting cross section. A typical example of this is shown in Fig.1a which is a HPDC aluminium casting made with A356. It contains a fine grained surface layer and a central region containing a mixture of ESCs and fine grains [3]. In bends of the castings, the ESCs tend to be compacted in the central region as shown in Fig.1 b. Bands of segregation following the contour of the casting are also often observed [4]. The inhomogeneous microstructure has been found to significantly improve corrosion resistance of high pressure die cast Mg-Al alloys [5], and may also influence the wear- and mechanical properties.

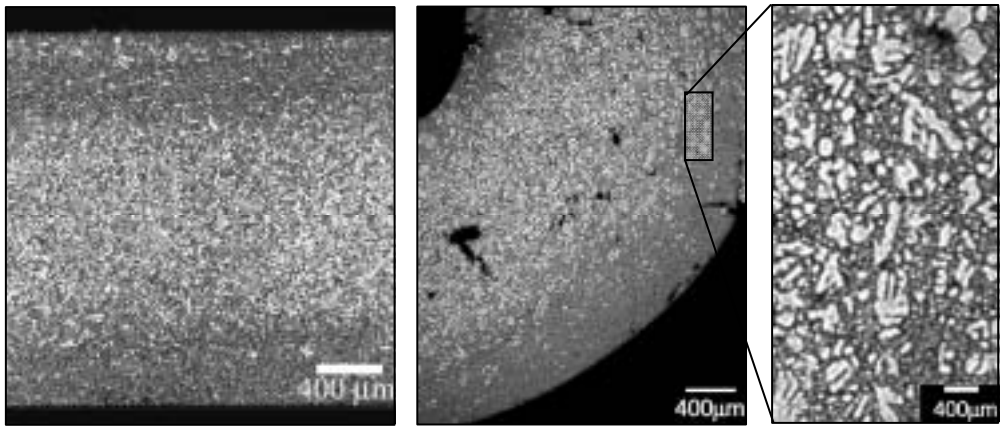

a) b) c)

Figure 1: Typical HPDC microstructures obtained from box-shaped die castings containing externally solidified crystals (ESCs): a) Straight section, flow direction to the right and parallel to the page; b) Bend, flow direction vertical; c) Magnification of the microstructure in the bend.

The externally solidified crystals (ESCs) are not equivalent to the cold flakes [6] that occasionally form due to the breaking up of the solid layer at the chamber wall, but instead are single-crystal dendrites. The reported terminology is somewhat inconsistent, and floating crystals [3, 7], externally solidified dendrites [8], externally solidified grains (ESG) [9] and, in the case of gravity pour casting, intrinsic crystals [10] are occasionally used.

Whilst centred crystals are commonly observed in semi-solid cast and HPDC components, the phenomenon has never been assessed in detail. Two brief explanations have been proposed in HPDC: Firstly, in a rheological framework put forward to explain the formation of banded defects in HPDC, it was suggested that fluid-dynamic forces induce particle migration towards the centre of the cross-section [11]. During flow, the primary crystals experience a translational force, which results in a central region with a higher density of primary crystals. This is schematically shown in a quasi-Lagrangian approach in Fig.2, where the window of reference follows a volume of melt with crystals immersed in it. The crystals are initially homogeneously distributed. At a later stage the crystals have been forced to the centreline, CL.

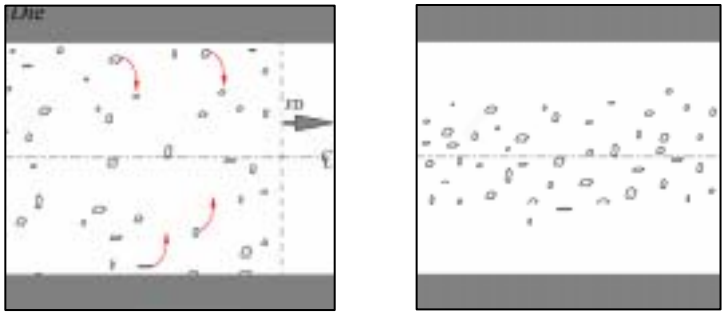

Figure 2: Schematic outline of crystal migration towards the centreline, CL. Initially: Uniform distribution of crystals; At a later stage: Particles migrated towards the CL. FD: Flow direction.

Secondly, it has been proposed that the distribution of ESCs in a die casting results from the solidification conditions present in the shot sleeve and in the die cavity in the HPDC process [7]. An inhomogeneous temperature distribution is inherently present in the shot sleeve resulting in non-uniform solidification conditions. This results in a variable distribution of ESCs in the castings, with a higher fraction of ESCs near the gate and lower fractions farther from the gate. Additionally, a solidifying surface layer forms, which constricts the metal to flow in the centre. This is schematically illustrated in Fig.3. The metal in position II, far from the gate, possesses a thermal history originating from the hotter shot chamber end and therefore contains few ESCs. The metal in position I (closer to the gate) originates from closer to the plunger and contains a larger fraction of ESCs (as shown in the micrograph, far left in Fig.3). The surface layer, made up of the first metal to enter the die, possesses few ESCs and forces later metal, with a larger fraction of ESCs, to the central region.

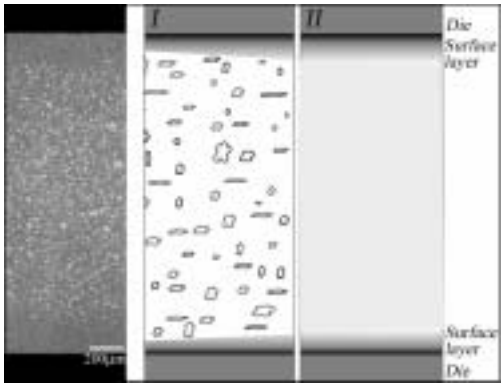

Figure 3: Illustration of surface layer formation and ESC distribution. Melt with a low fraction of ESCs solidifies at the die walls forming a surface layer. Later, the metal which flows in the same cross section is consequently forced to the centre. Reproduced with data from [12].

A mutual assumption for both these hypotheses is that some solidification forms a surface layer during filling of the die cavity. In the modelling of fluid flow and solidification in magnesium HPDC, it has been shown how a surface layer can form during the filling process [13], and it has been suggested that the surface layer may not fully account for the centred crystals [14].

Due to the nature of the commercial HPDC process, it is difficult to accurately reproduce the combined flow and solidification behaviour during die filling. Thus it has not been possible to validate the mechanisms presented earlier using HPDC. This has led us to take a new approach to studying the behaviour of ESCs during simultaneous flow and solidification: Controlled laboratory scale casting experiments have been conducted using semi-solid aluminium A356 alloy cast into an open ended steel die by gravity pouring. The effects of melt and die temperature on the microstructure are assessed with special emphasis on the distribution of ESCs.

Experimental

The A356 alloy, with composition shown in Table 1, has a liquidus temperature of ~615^{o}C as determined by phase diagram calculations using the computer model Alstruc [15].

Table 1. Principal alloy constituents [wt%], according to the A356 batch composition.

Alloy	Si	Mg	Fe	Ti	Sr
A356	6.80	0.35	0.07	0.016	0.0033

The alloy was first heated in a 1l graphite crucible to a superheat of 90K. The crucible was then removed from the furnace and allowed to cool in air whilst being vigorously stirred using a boron nitride coated and preheated impeller. A rotation rate of 600rpm was used as it was found to be high enough to cause significant dendrite fragmentation and some spheroidisation so that the material had a low enough viscosity for pouring. At a lower stirring rate the dendrites became large and branched and were found to impede flow. The superheat dissipated in approximately 3 minutes and the cooling rate in the solidification range was approximately 3.8Kmin^{-1}. When the desired fraction solid (f_s) was obtained, stirring was stopped and the metal was poured into a steel die within 3 seconds.

The solidification behaviour of the alloy, (approximated as Al-7wt%Si), was estimated by the Scheil-equation. The temperature as a function of f_s is shown in Fig.4. The different melt temperatures that were used and the corresponding f_s, are indicated with dashed lines.

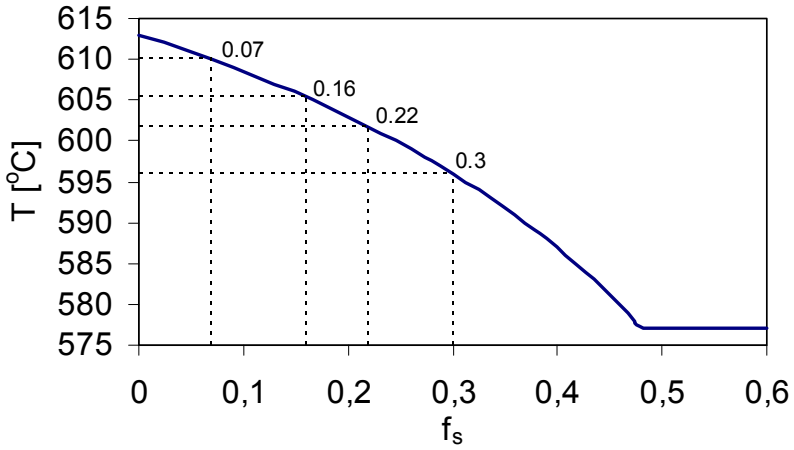

Figure 4: Solidification behaviour of the A356 alloy as estimated by the Scheil-equation. Isothermal solidification at the eutectic temperature, T_{eut}=577°C. Solidification completed at T_{sol}=553°C.

The elbow-shaped steel die (Fig.5) was first pre-heated in an air-circulating furnace where the temperature was controlled with a thermocouple probe to +/-5K. The die has an open end (Fig. 5) and, during casting, the metal therefore flowed continuously through the cavity until flow arrested due to solidification. To further assist in the movement of the slurry, the die was tilted 8°. The cooling rate of the die was approximately 8Kmin^{-1} in the ambient temperature range (T_{air}=21°C at 33% humidity) and the heat dissipation from the die was therefore negligible during casting.

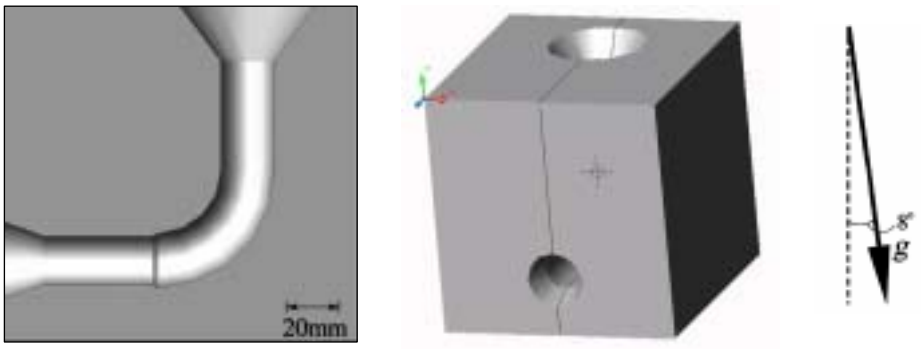

Figure 5: Transverse drawing of the die cavity and drawing of complete die.

The five different die temperatures that were used are listed in Table 2. A constant fraction of ESCs of 0.16 was used in these experiments to simulate the f_s injected in cold chamber HPDC. These conditions induced a significant amount of flow through the die, which is assumed to be essential to observe pronounced effects. The die temperatures used were chosen based on initial casting trials that generated observable differences in the microstructure.

Table 2. Castings produced with f_s~0.16 and a range of die temperatures.

T_{die} [^oC]	130	180	270	350	450
f_s	0.16	0.16	0.16	0.16	0.16

A set of experiments were also conducted with an Mg-6wt%Al alloy as this is similar to the common AM60 magnesium die casting alloy. The experiments were similar to those reported above, with a fraction of ESCs of 0.16 and a die temperature of 270^{o}C.

The samples were ground, polished and electrolytically etched with a 5%HBF_4-solution. Macrographs and micrographs were obtained with an optical macroscope and an optical microscope, respectively. Area fraction measurements were obtained by image analysis.

Results

General Observations

A longitudinal section of the casting cut along the parting plane typically revealed a microstructure similar to that in Fig.6 a. In the vertical section of the casting a surface layer with no ESCs can be observed on the right-hand side. This corresponds to the region where the melt directly impinged on the die wall during pouring. On the left-hand side of the vertical section, the ESCs are positioned near the surface. In the bend, the ESCs are positioned in the centre region following the curvature of the bend. Through the contraction, the segregation of the ESCs is well-defined and follows the contour of the casting. In the horizontal part of the casting the ESCs are also centred. A few ESCs are present in the upper surface layer at the end of the horizontal section of the casting. Fig.6 b is a photograph of the casting at a lower magnification. The arrow indicates the plane where microstructural samples, used in the majority of this paper, were taken from.

a) b)

Figure 6: a) Macrographs of a longitudinal section of an A356 casting produced with T_{die}=270°C and f_s~0.16. The ESCs appear as large primary dendrites (white). The fine grains and the Al-Si eutectic comprising the matrix appears as dark grey; b) A photograph of the casting. Microstructural samples were taken from the plane marked with an arrow.

In all the castings, a large area fraction of ESCs is present in the central region of the cross section, and the microstructure typically appears as shown in Fig.7 a with coarse pre-solidified dendrites (ESCs) and interdendritic Al-Si eutectic present. In the central region, large pools of Al-Si eutectic were occasionally observed between the dendrites and a significant fraction of the dendrites possess an agglomerate-like morphology. There is a slight tendency for smaller, less agglomerated ESCs to be present farther from the centre, as observed in Fig.7 b, although this is somewhat inconsistent. In this area there is a transition from a central region that possesses a high area fraction of ESCs to a surface layer with few ESCs. The surface layer is observed to have a refined branched dendritic microstructure as a result of the higher cooling rate in the die, as shown in Fig.7 c.

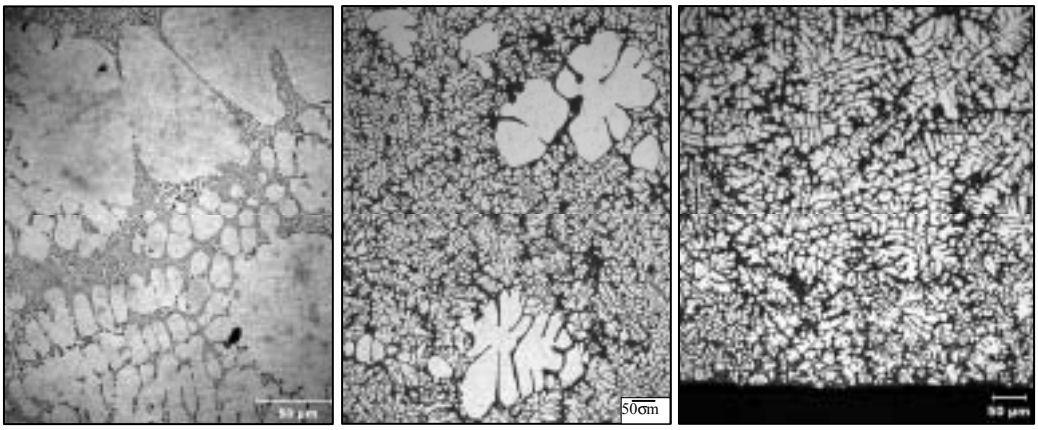

a) b) c)

Figure 7: Optical micrographs of the microstructures obtained from different positions in the cross section. a) In the central region: large agglomerated ESCs and Al-Si eutectic; b) In the transition between the central region and the surface layer: smaller ESCs surrounded by fine dendrites; c) Near the surface: a fine dendritic microstructure.

Effect of Die Temperature on ESC Distribution

Microstructures of samples produced with a variable T_{die} and a constant f_s~0.16 are shown in Fig.8. At a low die temperature of 180°C (Fig.8 a) the ESCs are positioned in the centre of the cross section. A casting produced with a die temperature of 270°C is shown in Fig.8 b. The ESCs are centred with a few ESCs positioned near the upper edge. At a die temperature of 350°C (Fig.8 c) the ESCs are principally located in the upper part of the cross section but the ESCs are still segregated away from the surface. At higher die temperatures (e.g. 450°C) the metal did not fill the entire cross section, as shown in Fig.8 d, and few ESCs are present.

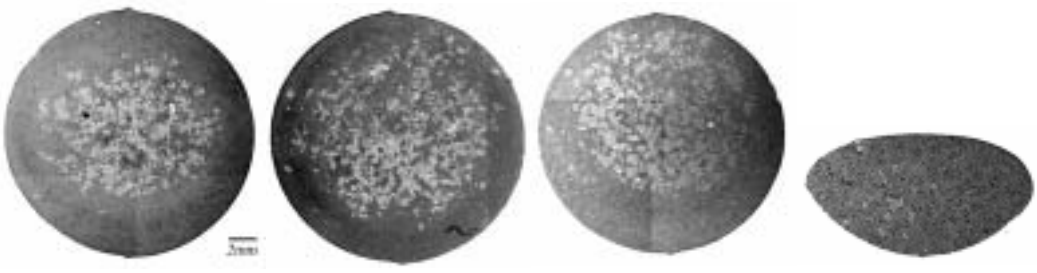

a) b) c) d)

Figure 8: Micrographs of castings produced with f_s~0.16 and variable die temperatures: a) 180°C; b) 270°C; c) 350°C; d) 450°C. ESCs appear as large white dendrites.

Effect of Variable f_s on ESC Distribution

The effect of variable f_s on the distribution of ESCs is shown in Fig.9. The ESCs are distinctly centred in the cross section at $f_s = 0.07$ (Fig.9 a) and the ESCs were found to be more centred at lower fractions of ESCs. At $f_s = 0.16$ (Fig.9 b), the central ESC containing region covers a larger area of the cross section. In the castings produced with $f_s = 0.22$, the ESCs are more dispersed (Fig.9 c), and when $f_s = 0.3$, the metal did not fill the entire cross section as shown in Fig.9 d. However, a relatively thin surface layer free from ESCs is present adjacent to the surface in the bottom part of the casting.

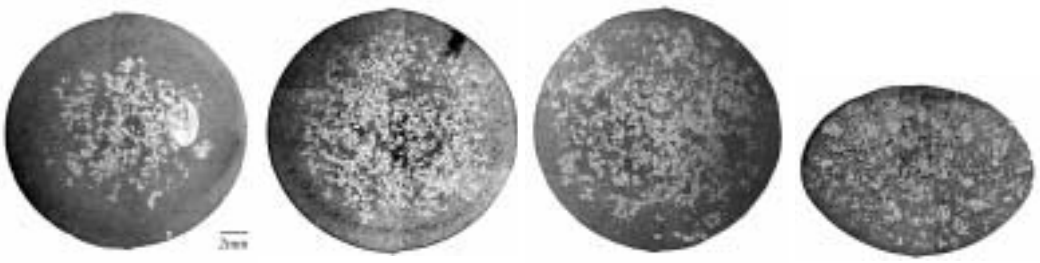

a) b) c) d)

Figure 9: Micrographs of castings produced with a T_{die}~250^{o}C, (a-c; d slightly higher), and variable f_s: a) 0.07; b) 0.16; c) 0.22; d) 0.3.

In some of the micrographs, a segregation band following the contour of the casting can be observed, e.g. Fig.9 b. The segregation band forms when slip occurs between the immobile surface layer and the movement of material adjacent to this, and is described in detail by Gourlay et al. [16].

The micrographs indicate differences in the local area fraction of ESCs in the central region. Measurements of the area fraction of ESCs conducted at higher magnification, indicate that the local area fraction in the centre is typically ~0.35-0.4. No significant variations in the ESC packing fraction in the centre occur irrespective of the bulk ESC fraction used.

A quantitative assessment of the variations in distance from the casting edge to the ESC-rich central region was conducted. The local area fraction of ESCs as a function of the diameter, D, is shown in Fig.10 a, for the castings produced with f_s of 0.07 and 0.22. Each measurement represents the average area fraction in an area of 200x860σm. The central ESC-rich area becomes larger and therefore moves towards the surface with increased f_s. The lower area fraction of one data point in the central region of the

0.07 sample is a random effect and can be attributed to the local variations in f_s as a result of large pools of eutectic in the regions analysed. To determine the variations in distance from the edge to the ESCs, a line following the apparent interface was drawn between the ESC-free surface layer and the ESC-rich centre region, as shown in Fig.10 b. The average distance from the ESCs to the surface was measured, (Fig.10 a), and found to decrease from 3.5mm to ~1mm with an increase in the fraction of ESCs from 0.07 to 0.22.

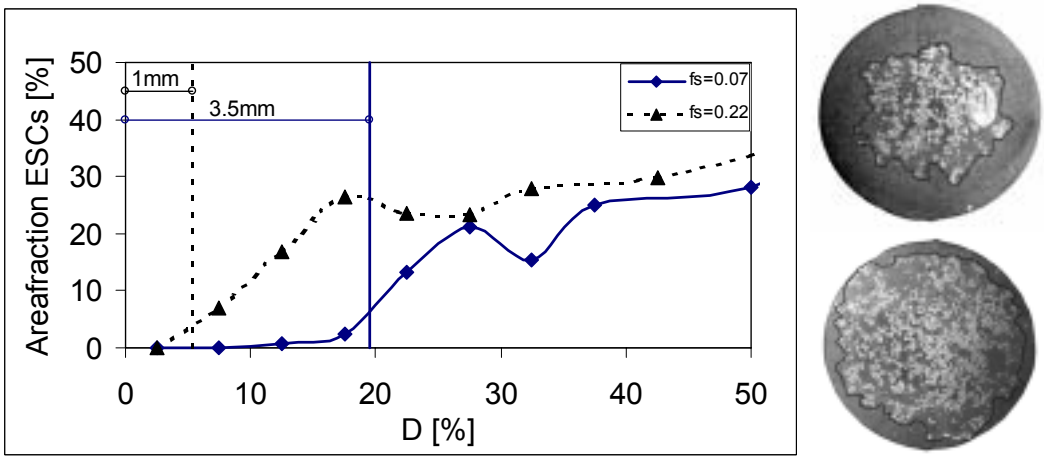

a) b)

Figure 10: a) Measurements of the local area fraction of ESCs as a function of the diameter (D) from the edge of the samples (from left to right). The vertical lines indicate the average distance from the edge to the central ESCs. b) Micrographs of the samples with superimposed lines to distinguish the surface layer and the centre region. The upper micrograph is from a casting with f_s~0.07. The bottom micrograph is from a casting with f_s~0.22. Die temperature ~150^{o}C.

Further casting experiments were conducted with a binary Mg-6wt%Al magnesium-aluminium alloy. This was intended to resemble the casting of the common AM60 HPDC-alloy. With a similar metal preparation procedure as for the A356 alloy, finer ESCs were obtained, and few dendrite agglomerates were observed. This is analogous to observations in HPDC of the AM60 [14] and the A356-alloys [3]. A similar microstructure as observed in Fig.6a and Fig.1b (HPDC), was obtained with the Mg-Al alloy (Fig.11): the ESCs are centred in the longitudinal cross section. It is therefore proposed that there is no significant effect of particle size on the ESC migration.

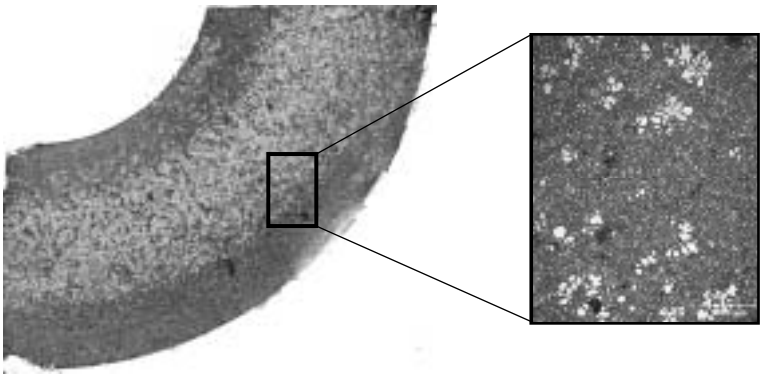

Figure 11: Macrograph from a longitudinal section in a binary Mg-6wt%Al alloy casting. An increased fraction of ESCs is observed towards the centreline analogous to the A356 castings. Casting produced with an initial f_s of ~0.16 and a die temperature of 270°C. The magnified area reveals relatively fine ESCs.

Discussion

There are large inherent differences between gravity die casting and cold chamber HPDC such as velocity, after-pressure, filling time and casting geometry. The melt velocity through the gate in HPDC is typically 30-50ms^{-1}, the pressure approximately 600bar, filling time 10-100ms and casting thickness 2-5mm. The differences in cooling rate and flow conditions are therefore expected to result in very different microstructures, affecting the grain size and eutectic structure, morphology and distribution. However, typical HPDC microstructural phenomena have been produced in gravity die castings in the present work, and in the forthcoming sections the microstructure is discussed with special emphasis on the distribution of ESCs.

Beforehand, it is necessary to assess the casting method: it could intuitively be expected that the solid is separated in the crucible and that segregated liquid enters the die first during pouring. This would be an analogous argument to the suggested mechanisms for the metal behaviour in the shot sleeve in HPDC outlined in the introduction [3]. However, the relative density between the solid and liquid, which is of the order ψ_s/ψ_l ~1.07, indicates that significant settling of the solid would not be expected during the few seconds of pouring. The forced and free convection should furthermore enhance a more homogeneous bulk material. Additionally, the temperature measurements during stirring revealed that no significant thermal gradients were present in the crucible. It was therefore concluded that the metal poured contained a

relatively uniform distribution of ESCs and an amount corresponding to the measured temperature.

To test the hypothesis that an approximately uniform mixture of liquid and ESCs was poured during the casting operation, the first metal that flowed through the die was quenched in a crucible. The resulting microstructure in the quenched material is shown in Fig.12 a. This metal contains a qualitatively similar area fraction of ESCs as originally aimed at. A micrograph from the central region of a casting produced with similar f_s and die temperature as in a, is shown in Fig.12 b. A slightly higher area fraction of ESCs is present in b.

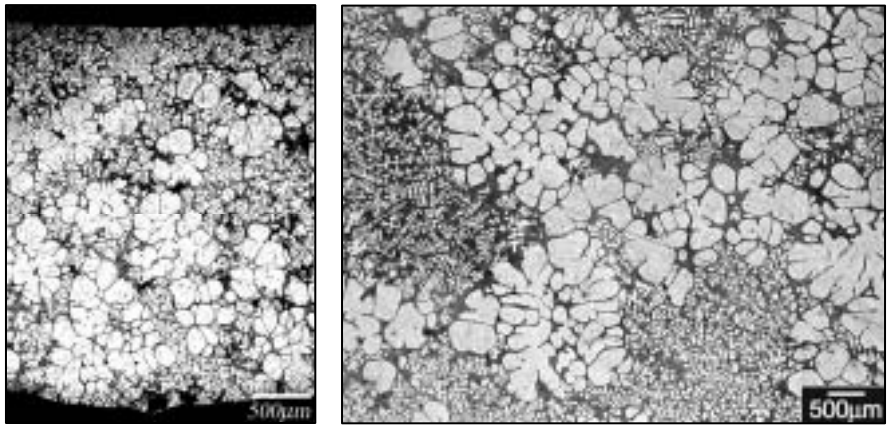

a) b)

Figure 12: a) Microstructure of metal that contains ESCs quenched in a steel crucible produced with an initial f_s~0.16 and a die temperature of 250^{o}C; b) From central region of casting produced with similar parameters.

Effect of Die Temperature on ESC Distribution

The changes in the distribution of ESCs with die temperature shown in Fig. 8 can be explained by considering the effect of die temperature on the degree of wall-constrained flow and the shape of the filling flow front: At a low die temperature, enough solidification occurs at the die wall to constrain the flow such that the flow front fills the entire cross section during die filling. With increasing die temperature the fluidity increases because less solidification occurs at the die walls and it is therefore also a decrease in the degree of constraint to flow at the walls. The wall constraint decreases first at the upper die surface because of gravity, and the degree of upper die wall constraint therefore decreases with increased die temperature.

The effect of the degree of wall constraint on the behaviour of ESCs is illustrated in Fig.13. In Figures 8a and b, the casting cross section is circular suggesting the die temperature was low enough for complete wall constraint to be achieved. With similar constraint from all parts of the die wall, lift forces towards the centre of the cross section are symmetrical in the cross section resulting in the ESC distributions of Figs. 8a and b. This is illustrated in Fig 13a.

The cross section of Fig 8c is not perfectly circular (the top of the cross-section has not completely filled) suggesting that, at a die temperature of 350^{o}C, there was only partial upper wall constraint. The driving force for the ESCs to migrate towards the centreline from the top is then smaller than the migration force from the bottom wall and the compacted ESCs are displaced upwards in the cross-section as shown in Fig 8c and illustrated in Fig. 13b.

The microstructure in Fig.8d shows that at a die temperature of 450^{o}C, there is no upper wall constraint at all. In this case, there is only a migration force from the bottom die wall forming a layer which contains few ESCs at the bottom wall. On top of this mushy surface layer, the slurry, containing the majority of the ESCs, continuously flows through the die. Flow stops after the whole crucible has been poured into the die and few ESCs exist in the final microstructure (Fig.8 d). This is illustrated in Fig. 13 c.

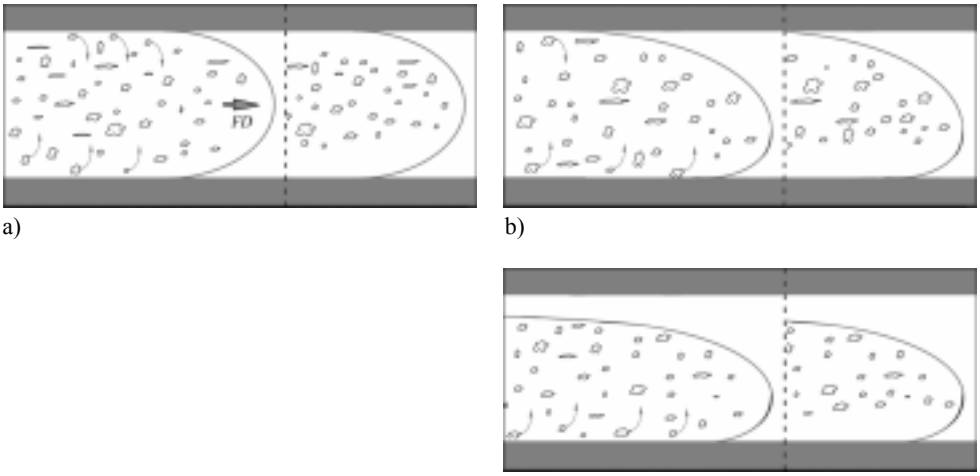

Figure 13: Qualitative flow front appearance with variations in die temperature. a) Low die temperature, e.g. 130^{o}C; b) Higher die temperature, e.g. 350^{o}C; c) Very high die temperature, e.g. 450^{o}C.

Effect of Variable f_s on ESC Distribution

The local area fraction of ESCs in the central region remains relatively constant with variations in the bulk f_s. A fraction of ESCs in the range 35-40% is slightly greater than the coherency point reported for this alloy [17] which depends on the morphology and size of the primary crystals [11]. It is therefore proposed that a maximum packing of ESCs is present in the centre and that it is related to the rheological properties of the alloy. A larger flow rate or a reduction in cross sectional area would be expected to exaggerate this phenomenon and possibly result in a denser packing of ESCs in the centre. An investigation on the effects of different die geometries therefore deserves further attention.

The sample cast with f_s=0.3 did not fill the whole casting (Fig. 9d) and no metal flowed out of the die. This suggests that the increasing viscosity of the solidifying slurry stopped flow before the casting was full. It is likely that, for ESCs of the size and morphology used in this work (Fig 7a), the apparent viscosity of the slurry at f_s=0.3 requires little further solidification to arrest flow. Arrest of flow at a solid fraction close to maximum packing can be expected as the dendrites can no longer freely rearrange themselves. Furthermore, the ESCs are distributed almost evenly in this casting (Fig. 9d) except for the thin ESC-free layer at the casting surface. This is likely to be because the bulk ESC fraction (0.3) is close to the local ESC fraction (0.35-0.4) found at the centre of all the castings and therefore little compaction is possible.

Potential Mechanisms Responsible for ESC Distribution

Wall Solidification

Similar to HPDC, it is assumed that a surface layer rapidly forms during die filling. ESCs are occasionally observed near the casting surface and whilst this is rare at low f_s, it occurs to a greater extent with increasing fraction of ESCs (Fig.9). It could therefore be anticipated that ESCs become trapped near the surface as a result of solidification fronts advancing from the die walls. In order to consider this effect, it is necessary to assess the surface layer in detail: The growth of a surface layer can exert a pressure on the interior. This is analogous to the principles on particle-solidification front interactions, e.g. [18]. The pressure is a function of the interactions between the mushy wall-layer and the ESCs. If the ESCs behave similar to a particle, they will experience both repulsive and attractive forces from the solidification front. The growth rate of the front determines when the ESCs are encapsulated [19].

In the present work, the ESCs are not stationary ahead of the growth front, but they are carried in the liquid which flows parallel to the solidifying wall layer. This could intuitively impede entrapment. Furthermore, the surface layer is relatively thin compared with the size of an ESC making entrapment more difficult. In addition, the ESCs are typically located in the central region of the cross sections, far from the surface of the casting suggesting that migration occurs at a greater rate than the surface layer is growing. It is therefore proposed that the ESCs segregate/migrate towards the centreline primarily by mechanisms other than pushing from the solidifying wall layer.

Flow-Related Lift Mechanisms

The migration of particles towards the centreline has been observed in tube (Poiseuille) flow in a number of fields. It is observed at low Reynolds numbers (Re) and the equilibrium particle position typically depends on different ratios of properties between the particles and the liquid such as density, particle size and velocity, as well as particle distributions, morphology, and viscosity [20]. The research in this area has generally been associated with observations of flow through transparent tubes with a liquid, with a specific viscosity and flow rate, containing immersed particles with different physical characteristics.

Despite particle migration being well documented in other fields, the authors know of no reports confirming that these mechanisms occur in semi-solid metals. The Reynolds numbers involved in metal casting are typically much higher than those used in the past migration experiments [20]. This is largely due to the very low viscosity of the liquid phase in semi-solid metals (similar to that of distilled water in the case of aluminium) so that the rheological behaviour is determined largely by the solid phase. The potential lift mechanisms with respect to the flow behaviour of ESCs during semi-solid filling are discussed in the following:

<u>*Saffman Lift*</u>:

In practice, two-phase flow incorporates a distribution of particles. The problem, however, can be simplified and can be outlined for a single particle as follows: In a laminar flow regime, with no-slip conditions at the walls, the velocity profile generally follows the contour of a parabola with the region of lowest stress at the peak of the parabola. In a turbulent flow regime, the velocity gradient adjacent to the wall is steeper and the velocity profile is blunted in the centre. For a Newtonian fluid, the velocity profile (du/dy) can be approximated as a linear relation, du_x/dy adjacent to the

wall, as shown in Fig.14. The induced shear stress, ϑ, is proportional to the velocity gradient, ϑ=σdu$_x$/dy, scaled by the dynamic viscosity, σ.

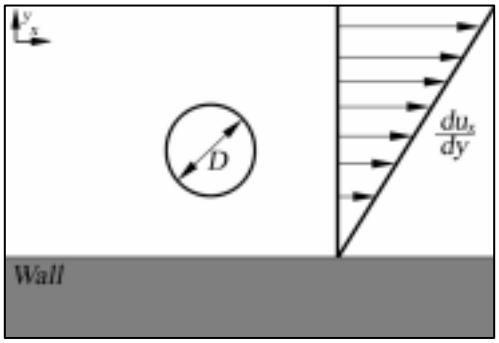

Figure 14: Spherical particle, of diameter D, in fluid flow with a linear velocity profile du$_x$/dy adjacent to the wall.

As a result of the shear gradient present, a lift force can be induced. The ratio between the shear stress on each side of the particle can be sufficient to lift the particle towards regions of lower shear stress. The relationship between the velocity difference between the particle and fluid (V-V_p) and the induced Saffman lift force (F$_s$) per unit mass is [21]:

$$F_S \mid \frac{2K\tau^{1/2}\psi D_{ij}}{\psi_d d/D_{lk}D_{kl}0^{/4}}/V\,4\,V_p 0 \qquad (1)$$

where: K: constant; D$_{ij}$: deformation tensor [s^{-1}]; ψ] fluid density [kgm^{-3}]; ψ$_d$: particle density [kgm^{-3}]; τ] kinematic liquid viscosity [m^{2}s^{-1}]; d: particle diameter [m]; V_p: particle velocity [ms^{-1}].

An assessment of the Saffman lift force was carried out by numerical simulations with the computer model Fluent. It was assumed that neglecting the heat transfer from the melt to the die during flow would not affect the validity of the calculations. Spherical aluminium crystals, with a diameter of 250σm, were introduced into an aluminium melt physically equivalent to the flow conditions in the casting experiments. The melt was allowed to flow through a die similar to the experimental set-up (assuming a constant tube diameter of 20mm). A bulk flow rate of approximately 2x10^{-4} m^{3}s^{-1} was used, and the flow was considered turbulent. It was found that the flow pattern is non-uniform and not fully developed. This is shown in Fig.15 a, where the velocity profiles at different locations in the die cavity are indicated. The inlet velocity profile is approximated as a plug.

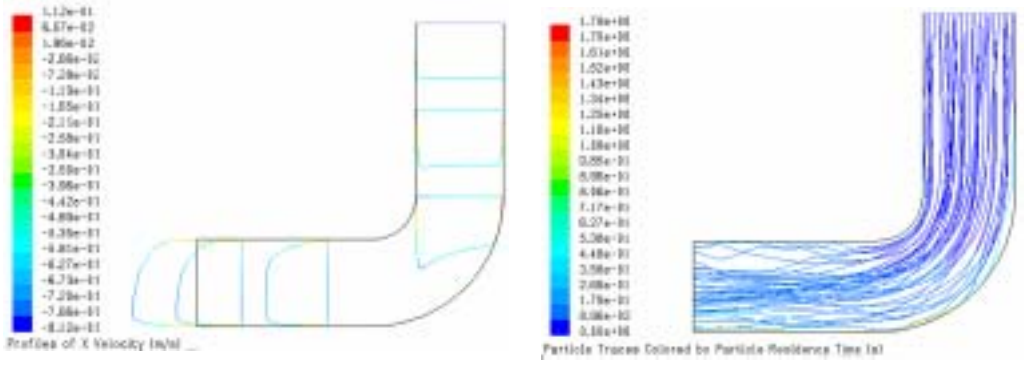

a) b)

Figure 15: a) Velocity profiles at different locations in the die cavity; b) Crystal trajectories. Scale bar indicates particle residence times. Obtained with numerical calculations of the flow with the computer model Fluent.

No significant Saffman lift-induced migration of individual particles was observed in the simulations, as shown by the crystal trajectories in Fig.15 b. It is therefore concluded that Saffman lift did not cause the segregation of crystals observed in the castings [22]. Other mechanisms must therefore be considered.

The Effect of a Non-Linear Velocity Gradient:

When a particle is positioned in a non-linear velocity gradient, as schematically illustrated in Fig.16, the fluid flow velocity is larger than the particle velocity by an amount $\div v_t$ on the top of the particle. On the bottom, however, the particle velocity is larger than the fluid flow velocity by an amount $\div v_b$. The particle is thus forced away from the wall as a result of liquid being pushed from the front towards the wall [23]. Careful assessment of the flow conditions and resulting velocity profiles is required to allow a detailed analysis of the contribution from this migration mechanism. This is beyond the scope of the present paper.

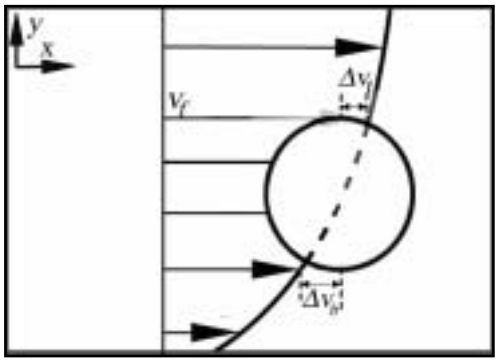

Figure 16: Lift due to the fluid-particle velocity difference between the bottom and the top of the particle.

Magnus Lift Force:
Particle rotation which results from interactions between particles, collisions with a wall or from velocity gradients can also induce migration of particles. Rotation of a particle can entrain fluid and cause a relative difference in velocity across the particle. A lift force is therefore established moving the particle towards regions of higher velocity (lower shear stress). For a spinning sphere, the Magnus lift force (F_M) per unit mass in a uniform flow field can be expressed as [24]:

$$F_M \mid \frac{3}{4}\mathrm{T}_d \Delta V_r \tag{2}$$

where V_r is the local fluid rotation rate and T_d is the angular particle velocity.

Both the Magnus lift force and a non-linear velocity gradient could contribute to the migration of the ESCs observed in the castings. An assessment of these mechanisms, however, requires extensive investigations and analyses of the flow conditions and particle interactions, which is not within the scope of the present paper.

Wall Effects:
A lubricating layer of liquid commonly forms near a wall of a tube carrying a suspension [25]. However, this effect is only expected to occur close to the die walls. For example, it has been proposed that wall-effects result in solid grains segregating to the centre of the flow channel in semi-solid casting when the diameter of the die is less than 10-15 times the particle diameter [25]. In the present study, the die diameter (20mm) is at least 80 times the typical ESC diameter, ie. outside the regime where this mechanism is expected.

Hydrodynamic Diffusion:
A mechanism for shear-induced particle migration operating when the solid fraction is sufficiently high for the particles to regularly collide has also been reported [26]. The collision frequency between the particles is proportional to the shear rate. In the velocity profile associated with tube flow, the shear rate is greatest near the tube wall. The collision frequency is therefore greatest near the wall and this results in a net flux of particles from the wall region towards the centre (from a region of high shear stress to low) [26]:

$$Flux \mid K_{\vartheta} \frac{f_s^{\,2}}{\vartheta} \frac{d\vartheta}{dy} \nu r^2 \tag{3}$$

where: K_θ: dimensionless parameter that depends on concentration; f_s: fraction of solid particles; ϑ: local shear stress; y: distance from the tube wall; $\dot{\nu}$: shear rate; r: particle radius.

This phenomenon is often termed hydrodynamic diffusion and requires very low Reynolds number (typically $1x10^{-4}$) and a solid fraction greater than about 0.3. In the present study, ESC migration occurs at solid fractions below 0.1. The irregular morphology of the ESCs may result in the suspension behaving similar to a greater solid fraction of spheres [11]. However, the flow is in the turbulent regime, i.e. the Reynolds number is of the order of $7x10^3$.

The experiments using Mg-6wt%Al (Fig. 11) indicate that there is no significant effect of particle size on ESC migration in this work. All of the migration mechanisms discussed above depend on particle size. It is possible, however, that the ESC size difference is not sufficient to significantly affect the migration. Additionally, the effect of agglomeration is not known. EBSD analysis of the ESC region is in progress and may give further knowledge on the dynamics of ESC plug formation mechanisms in semi-solid casting.

Conclusions

Microstructures typically associated with cold chamber HPDC have been reproduced in controlled laboratory scale casting experiments. The major results are:

1. A novel method to study flow and solidification phenomena in die castings has been developed.
2. The externally solidified crystals (ESCs) segregate/migrate towards the centreline.
3. The migration of crystals results in a symmetrical ESC distribution in a central region when flow is constrained at all metal-die interfaces. When flow is less constrained at an interface, the migration force away from that interface is reduced.
4. The position of the ESCs is affected by the die temperature because it affects the degree of metal-die flow constraint.
5. The distribution of the ESCs is affected by the bulk f_s, and becomes strongly compacted in the cross section at lower f_s. At higher f_s, the ESCs occupy a larger area in a centre region which becomes wider and is therefore moved towards the surface with increasing bulk f_s.

6. A maximum packing of ESCs in the centre of the cross sections occurs during flow. The packing fraction compares well to those measured rheologically for similar microstructures.

Possible lift mechanisms responsible for the movement of ESCs to the centre of the cross-section have been presented, and an assessment of the Saffman lift force of individual particles indicates it has no significant effect on the ESC migration. Further work is required to identify the dominating migration mechanism in semi-solid casting.

Acknowledgements

The present work was funded by: - The project NorLight Shaped Castings and partners: the Norwegian Research Council, Alcoa Automotive Castings, Scandinavian Casting Center ANS, Elkem Aluminium ANS, Fundamus AS, Hydro Aluminium Metal Products, Norsk Hydro ASA, NIMR, NTNU and SINTEF (project coordinator). The author acknowledges the partners for financial support.

- The authors would also like to acknowledge the support of the Cooperative Research Centre for Cast Metals Manufacturing (CAST). CAST was established and is supported by the Australian Government's Cooperative Research Centres Program.

- The Dr.Ing. Håkon Styri Fellowship administered by Polyteknisk Forening is greatly acknowledged by one of the authors (H.I. Laukli) for financial support.

Prof. Otto Lohne and Prof. Lars Arnberg (Department of Materials Technology, NTNU) are acknowledged for comments and discussions on the present work. Dr. Stein T. Johansen (SINTEF Materials) is acknowledged for discussions on particle migration in two-phase flow and Dr. Harald Laux (SINTEF Materials) for discussions on two-phase flow and for carrying out the computer simulations.

References

[1] A. D. Figueredo, *Science and technology of semi-solid metal processing*, NADCA, **2001**.

[2] W. Sequeira, PhD thesis, The University of Queensland (Brisbane), **2000**.

[3] H. I. Laukli, A. Graciotti, O. Lohne, H. Gjestland, S. Sannes, in *21st Die Casting Congr. & Tabletop Expo.*, NADCA, Rosemont, Ill., USA, **2002**, T02-035.

[4] C. M. Gourlay, H. I. Laukli, A. K. Dahle, in *ICAA9 - 9th int. conf. on aluminium alloys*, Brisbane, Australia, **2004**.

[5] G. Song, A. Atrens, M. Dargusch, *Corr. Sci.*, **1999**, 41, 249-273.

[6] M. Gershenzon, P. W. Rohan, M. T. Murray, in *20th int. die casting congr.&expo.*, NADCA, Cleveland, Ohio, USA, **1999**, 305 315.

[7] H. I. Laukli, O. Lohne, S. Sannes, H. Gjestland, L. Arnberg, *Int. J. Cast Met. R.,* **2003**, *16*, 6, 515-521.

[8] T. Abbott, M. Easton, *Mat. Forum,* **2001**, *25*, 181-201.

[9] D. StJohn, A. K. Dahle, T. Abbott, M. D. Nave, M. Qian, in *Magnesium Techn.,* (Ed.: H. I. Kaplan), TMS, **2003**, 95-100.

[10] Q. Han, A. Hellawell, *Met. Mat. Trans. B,* **1997**, *28B*, 169-173.

[11] A. K. Dahle, D. H. StJohn, *Acta Materialia* **1998**, *47*, 31-41.

[12] S. Sannes, H. Gjestland, H. Westengen, H. I. Laukli, O. Lohne, *SAE conf.,* Detroit, Michigan, USA, **2003**, 03M-192.

[13] S. Sannes, H. Gjestland, H. Westengen, H. I. Laukli, in *Magnesium alloys and applic.*, DGM, Wolfsburg, Germany, **2003**, 725-731.

[14] H. I. Laukli, O. Lohne, L. Arnberg, H. Gjestland, S. Sannes, in *Magnesium alloys and applic.*, DGM, Wolfsburg, Germany, **2003**, 182-189.

[15] A. L. Dons, E. K. Jensen, Y. Langsrud, E. Trømborg, S. Brusethaug, *Met. Mat. Trans. A,* **1999**, *30A*, 2135-2146.

[16] C. M. Gourlay, H. I. Laukli, A. K. Dahle, *Met. Mat. Trans. A,* **2004,** submitted.

[17] A. K. Dahle, L. Arnberg, *Acta Mat.* **1997**, *45*, 547-559.

[18] A. Mortensen, I. Jin, *Int. Mat. Rev.*, **1992**, 37, 101-128.

[19] J. W. Garvin, H. S. Udaykumar, in *Proc. of ASME Int. Mech. Eng. Congr.&Expo.*, ASME, New Orleans, Louisiana, USA, **2002**, 1-10.

[20] A. Karnis, H.L. Goldsmith, S.G. Mason, *J. of Chem. Eng.*, **1966**, august, 181-193.

[21] P.G. Saffman, J. Fluid Mech., **1965**, 22, part 2, 385-400.

[22] H. Laux, **2003**, *Communication*.

[23] S. T. Johansen, **2003**, *Communication*.

[24] C. Crowe, M. Sommerfeld, Y. Tsuji, Multiph. Flows Dr. Part., *CRC Press*, **1997**, 97-99.

[25] G. K. Sigworth, *Int. J. Cast Met.R.,* **1996**, *9*, 113-123.

[26] D. Leighton, A. Acrivos, *J. Fluid Mech.,* **1987**, *181*, 415-439.

ARTICLE 6

Segregation Band Formation in Al-Si Die Castings

C.M. Gourlay[1], H.I. Laukli[2], A.K. Dahle[1]

[1]CRC for Cast Metals Manufacturing (CAST)
Division of Materials
The University of Queensland
Brisbane, QLD 4072
AUSTRALIA

[2]Department of Materials Technology
Norwegian University of Science and Technology
N-7491 Trondheim
NORWAY

Metallurgical and Materials Transactions A, 2004. Accepted.

Abstract
Banded defects are often found in high pressure die castings. These bands can contain segregation, porosity and/or tears and changing casting conditions and alloy are known to change the position and make-up of the bands. Due to the complex, dynamic nature of the HPDC process, it is very difficult to study the effect of individual parameters on band formation. In the work presented here, bands of segregation similar to those found in cold chamber high pressure die cast aluminum alloys have been witnessed in laboratory gravity die castings. Samples were cast with a range of fraction solids from 0 to 0.3 and the effect of die temperature and external solid fraction on segregation bands has been investigated. The results are considered with reference to the rheological properties of the filling of semi-solid metal and a formation mechanism for bands is proposed by considering flow past a solidifying immobile wall layer.

Keywords: Segregation, high pressure die casting (HPDC), segregation bands.

Introduction

In many commercial casting processes some solidification occurs during filling and, increasingly commonly, material is semi-solid before filling begins. Therefore, the flow behavior of the solid and liquid phase in combination with solidification will produce the as-cast microstructure. In these processes, there is an increasing solid fraction during flow and, whilst the dramatic increase in apparent viscosity with fraction solid is widely reported [1], it is also important to consider the semi-solid microstructures at different fraction solids. It is these structures which give rise to the mechanical response of the mushy zone whether it be the apparent viscosity, the mechanism of flow or the permeability of a solid network. Therefore, understanding the rheological behavior of semi-solid alloys during flow is important in developing solidification models for commercial casting processes.

The developing microstructure with increasing fraction solid gives rise to two points at which there are marked changes in mechanical response [2]. Material of fraction solid below the coherency point (f_s^{Ch}) has no mechanical strength [3] and flows as a suspension of solid crystals in liquid. The coherency point marks the point where stresses begin to be transmitted between solid particles, a solid network begins to form and shear strength development initiates [2]. Coherency typically occurs in the fraction solid range 0.1-0.3 [3,4]. On further cooling, dendritic reorientation in response to a stress becomes more difficult as there is less liquid and the semi-solid strength increases until the dendrites are sufficiently large and branched that they interlock such that they can no longer reorient. This marks the second distinct change in mechanical response: the maximum packing fraction (f_s^{Pk}) which usually occurs in the fraction solid range 0.3-0.6 [3,5]. Above this point the increase in shear strength is much greater[3] and the structure often deforms by fracture of the network [5] because the response to stress is to pack the well-interconnected network tighter together. f_s^{Pk} also marks the onset of tensile strength development [6].

Dahle and StJohn [2] used this rheological framework to begin to describe the formation of the banded defects often found in high pressure die cast (HPDC) components. The presence of banded defects has been noted by a number of researchers in a range of casting processes and alloys [7-11] and are typically made up of bands of segregation, gas porosity, interdendritic porosity and/or tears following the contour of the casting [8]. Due to the macroscopic nature of these defects, they cannot be removed during heat treatment and the form they take during solidification remains in the cast product.

Aluminium alloys are high pressure die cast by the cold chamber process in which solidification begins when superheated metal is introduced into a relatively cold shot sleeve. In the time the metal spends in the shot sleeve, further nucleation, growth and/or remelting occur depending on the thermal, constitutional and flow characteristics in the shot sleeve. When the plunger moves forward, a mixture of liquid and free-floating externally solidified crystals (ESCs) is then injected into the die so that filling occurs by semi-solid flow [12]. Typically, the volume fraction of ESCs in cold chamber HPDC (f_s^{ESC}) is around 20%**.**

Dahle and StJohn [2] suggest that defect bands form by a combination of a fraction solid gradient away from the die walls brought about by heat transfer into the relatively cold mould, and the migration of ESCs to the centre as a result of lift forces on the solid. They point out that this results in a region of lower fraction solid between a solidifying wall layer and the central ESCs, and that deformation will be concentrated in the lower fraction solid region, which could then form a shear plane. They argue that the defects formed would be dependent on the local fraction solid in the shear plane during flow: If this was below f_s^{Ch} for much of the filling, bands of segregation would appear; whereas if a greater extent of solidification occurred in the plane, the band could be made up of pores or tears. No study has yet tested the rigor of this formation mechanism.

Defect bands are most commonly reported in the literature for HPDC Mg alloys because the bands are typically porous or torn in these alloys and are therefore a striking feature in the microstructure [9]. An example is given in Figure 1a. In Al-Si alloys, the defects are usually bands of segregation and, whilst not mentioned regularly in the literature, they are also common. An example of segregation bands in a HPDC aluminium component is shown in Figure 1b:

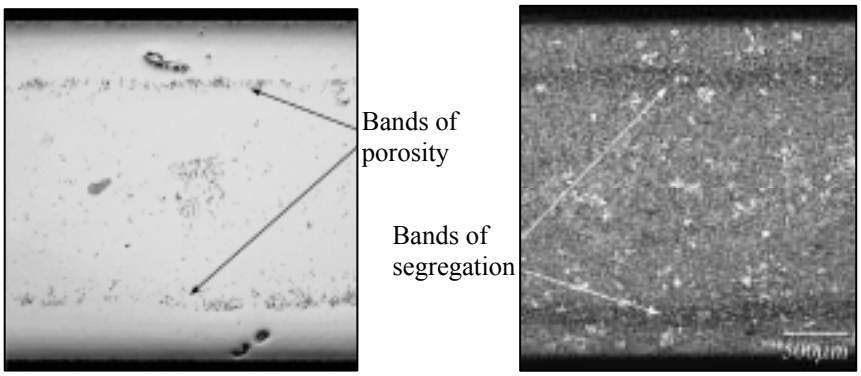

a) b)

Figure 1: Defect bands following the contour of the casting in HPDC 'U' shaped boxes. The flow direction is to the right, parallel to the page. (a) Pore bands in Mg alloy AM60 and (b) segregation bands in Al alloy A356. Further details of the castings are given in (a) reference [12] and (b) reference [13].

Some researchers have attempted to study these defects by changing parameters in commercial die casting processes [9-11,14]. These studies have shown that changing casting conditions and alloy can alter both the composition of bands (whether torn, porous and/or segregated) and also their position in the cross section. However, due to the complex, dynamic nature of commercial die casting processes, it has not been possible to isolate and study individual parameters in detail. In the work presented here, defect bands have been studied in controlled laboratory experiments from which a defect band formation mechanism has been developed.

Experimental Method

Metal Preparation

Aluminum alloy A356 was used in this investigation. The alloy composition is shown in Table 1.

Table 1: Composition of the A356 alloy used [wt%].

Al	**Si**	**Mg**	**Fe**	**Ti**	**Species**
Balance	6.80	0.35	0.07	0.016	Wt %

In order to inject similar material to that in the cold chamber HPDC process, material with fraction solid $0< f_s <0.3$ was prepared: A 1kg melt, held in a graphite crucible, was heated in an electric resistance furnace to 700^{o}C which is approximately 85K above the liquidus temperature of this alloy. The temperature was allowed to stabilize measured by a K-type thermocouple. The crucible was then removed from the furnace, placed on a refractory brick and stirred with a steel impeller from 90K above the liquidus temperature. The melt cooled in air whilst being stirred at a rate of 600rpm until the temperature corresponding to the desired solid fraction was reached. The Scheil equation was used to calculate the solid fraction from temperature because stirring caused significant convection in the liquid. Whilst stirring is not expected to cause the ESCs to obtain an isostructure in this short time, the time the material spent in the mushy zone was very similar for all castings with the same f_s^{ESC} as the cooling conditions were the same each time. In this way reproducible ESC containing feedstock was produced.

Gravity Die Casting

An elbow shaped steel die of dimensions shown in Figure 2a was modified to have an open end to allow flow through the die.

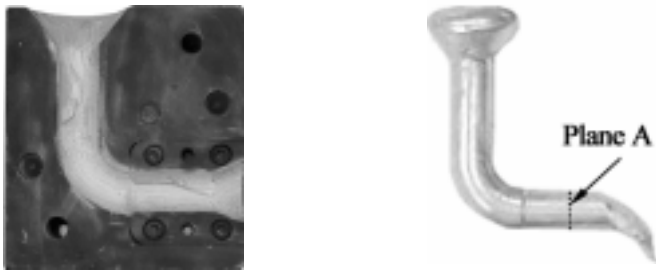

a) b)

Figure 2: Photographs of (a) the steel elbow-shaped die used in this investigation and (b) a casting produced from this die showing plane A used for characterization.

The die was preheated for more than two hours in an air furnace to homogenize the temperature within the die. The die was then removed, placed on a refractory brick and the temperature was measured at the top of the die using a K-type surface thermocouple. Once the die had cooled to the desired temperature, semi-solid metal was poured into the die until either the die was filled and fed or the crucible was empty. No die coat was used to minimize the resistance to interfacial heat transfer and also to simulate HPDC conditions.

Characterization

The castings were sectioned through plane A, as indicated in Figure 2b, where the diameter of the cross-section is 18mm. Throughout this paper "the cross-section" will refer to plane A, unless otherwise indicated. Samples were then ground and polished before being electrolytically etched with a 5%HBF_4 solution.

Results

General Remarks

Two typical macrostructures observed in the cross-sections are shown in Figures 3a and 3b and both display two striking features: a dark band of material following the contour of the casting and large grains in the central region.

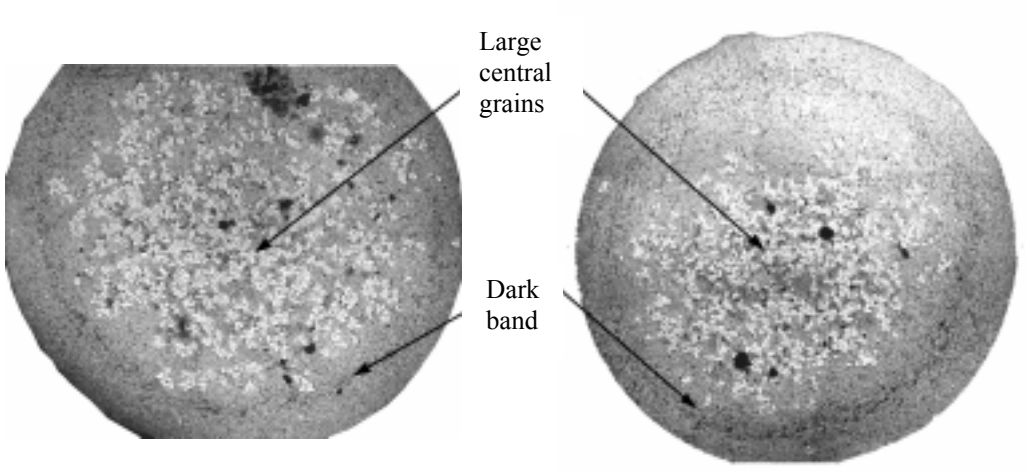

Figure 3: Macrographs of the cross-section showing dark bands following the contour of the casting and large central grains. Casting conditions were (a) f_s^{ESC} = 0.16 and T_{die}=270°C and (b) f_s^{ESC} = 0.11 and T_{die}=270°C.

Including the material between these features, the macrostructure contains four distinct regions. Typical microstructures from within these regions are shown in Figures 4a ⇓ 4d where the white phase is ζ-Al and, at this scale, the eutectic appears black. The outer region (Figure 4a) has a fine microstructure and a number of small eutectic pathways. The band region (Figure 4b) typically contains ζ-dendrites similar to those in Figure 4a and a significantly larger fraction of eutectic. As the eutectic is black, we therefore observe a dark band following the contour of the casting at the macro scale (Figures 3a & 3b). The region inside from the band (Figure 4c) is generally similar to that outside the band. These three regions are discussed in more detail later.

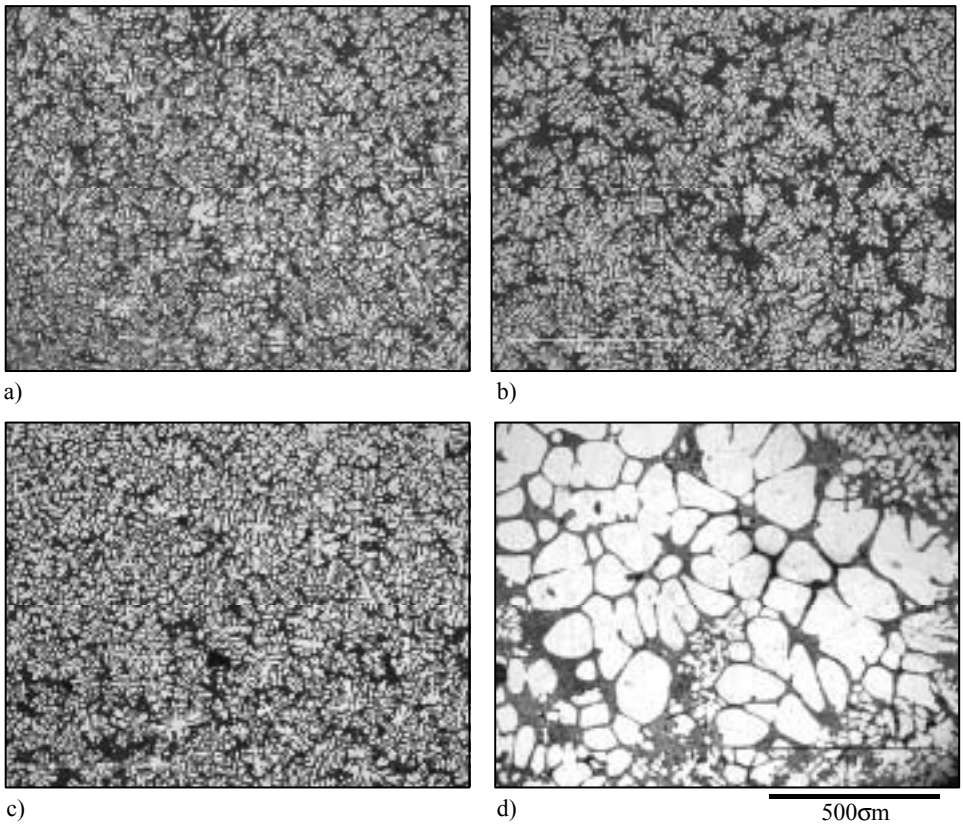

Figure 4: Typical microstructures from the four macroscopic regions of the cross-section. (a) Outside the band, (b) the band, (c) inside the band and (d) the centre of the casting. a-d have the same magnification.

The nature and distribution of the ESCs (the second striking feature) are discussed in detail elsewhere [15]. In the context of this paper, we only point out that the ESCs are large and agglomerated (Figure 4d), and that there are also pools of eutectic in the central region, much of which was probably liquid entrapped by the agglomerates. The important point to note is that the ESCs are concentrated towards the centre of the cross-section and that there is a network of ESCs in a central plug during flow (Figures 3a and 3b).

Nature of the Bands

In order to quantify the band, the microstructure was examined by two methods: A JEOL JSM-646OLA scanning electron microscope was used to carry out EDS and determine average silicon compositions across the cross-section. 50,000 pixels were measured in areas of 140 x 100σm and the average silicon concentration was then calculated. In this way the local average silicon composition could be determined with respect to position in the cross-section. Quantitative optical microscopy was also used to calculate the area fraction of the eutectic. Figure 5 shows the variation in silicon content and area fraction eutectic in the 4mm from the bottom of the cross-section towards the centre by these two methods. The two techniques are in good agreement and show a distinct peak in the region of 1.1- 2.6mm from the bottom edge. Note, that the peak is broad and its edges are difficult to define. Furthermore, within the peak, there are distinct variations in silicon content.

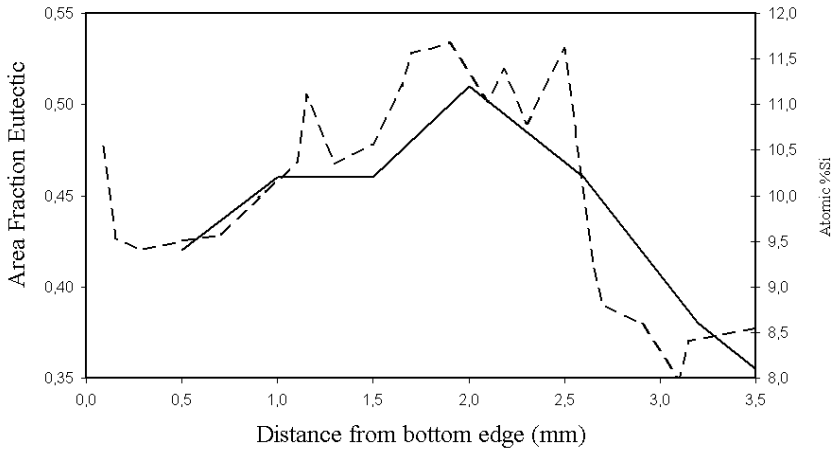

Figure 5: Area fraction of eutectic (solid line) and atomic % silicon (dashed line) versus distance from the bottom of the cross-section. The sample is the same as that shown in Figure 3b.

Whilst, in general, the band can be defined as an area of higher fraction eutectic, the microstructures in Figures 6a⇓ 6d highlight further features of the band. Figure 6a shows a feature most commonly observed at sharp directional changes: pathways of eutectic leading from the inner material to the band as tributaries (marked [i]). Figure 6b shows a complex interconnected series of eutectic pathways (marked [ii]) and Figures 6c and 6d show distinct flow or possibly slip paths (the directions of these paths are marked [iii] and [iv]).

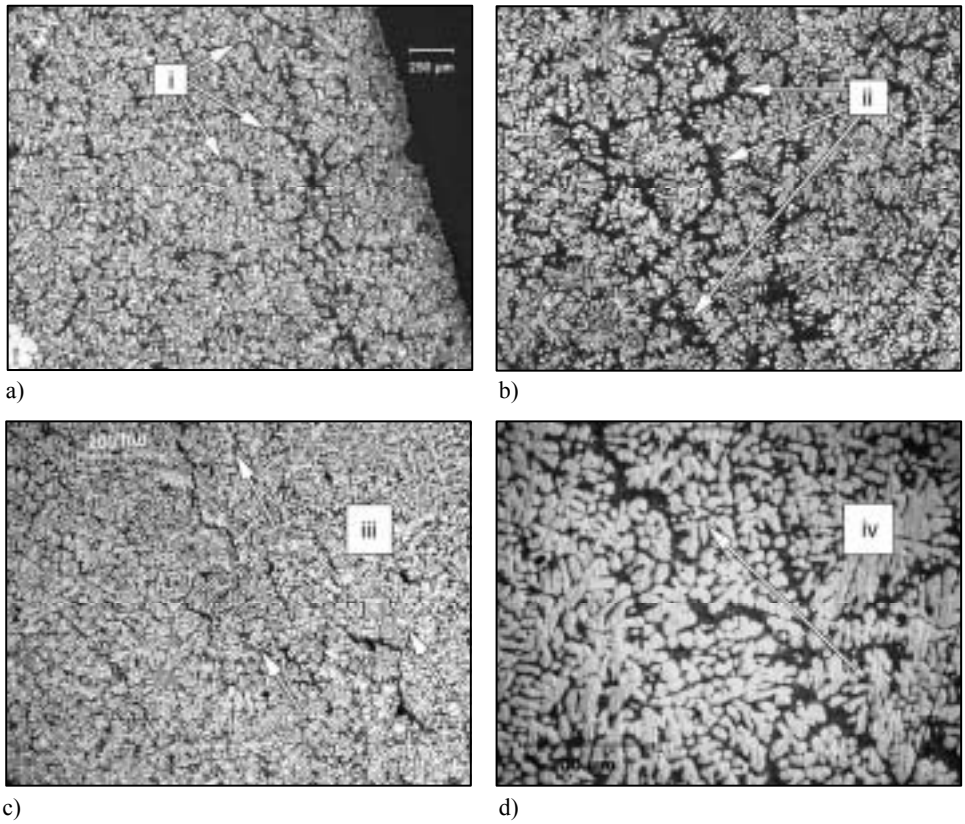

a) b)

c) d)

Figure 6: Micrographs showing significant features of segregation bands: [i] eutectic tributaries leading to the band; [ii] interconnected eutectic pathways within a band; and [iii] and [iv], the direction of flow or slip paths within a band. Casting conditions were: (a) and (c): $f_s^{ESC} = 0.16$, $T_{die} = 270^oC$ and (b) and (d): $f_s^{ESC} = 0$, $T_{die} = 88^oC$. All micrographs are taken from the cross section except (a) which is from a longitudinal section at the bend.

Figures 7a and 7b show how the local fraction eutectic varies across the whole cross-section for the samples shown in Figures 3a and 3b respectively. Each data point represents the area fraction of eutectic in a 500x500σm area of material and was calculated by quantitative metallography using optical micrographs. The area studied in each measurement is depicted by the horizontal bars on Figures 7a and b. The arrows indicate the position of the segregation bands.

The large size of the ESCs present at the centre of the cross section has resulted in peaks and troughs in this region due to the measurement area being either in a large agglomerate or in a pool of eutectic. This region encompassing the ESCs is highlighted by a shaded box. Outside the ESC containing region, each data point was obtained from a micrograph typically containing more than 30 ζ-Al dendrites and is therefore

representative of the local microstructure. The micrographs used for Figures 7a and b were taken at the same magnification as Figure 6d, where it can be seen that the eutectic and the ζ-Al phase are well approximated as two distinct colors and are therefore easily distinguishable by quantitative metallography. The error associated with distinguishing between two distinct colors depends chiefly on the discrimination parameters chosen in the software. For the discrimination parameters used in all measurements, the error in distinguishing between two distinct colors is less than 1%. The smallest significant measured changes in the area fraction of eutectic outside the ESC region are greater than 0.05 (at least 10%). It is therefore reasonable to measure changes in area fraction eutectic by this method. This is further supported by the fact that changes in fraction eutectic are large enough to be observed clearly by eye in Figures 4a, b and c and also that the area fraction eutectic measurements are in good agreement with EDS measurements in Figure 5.

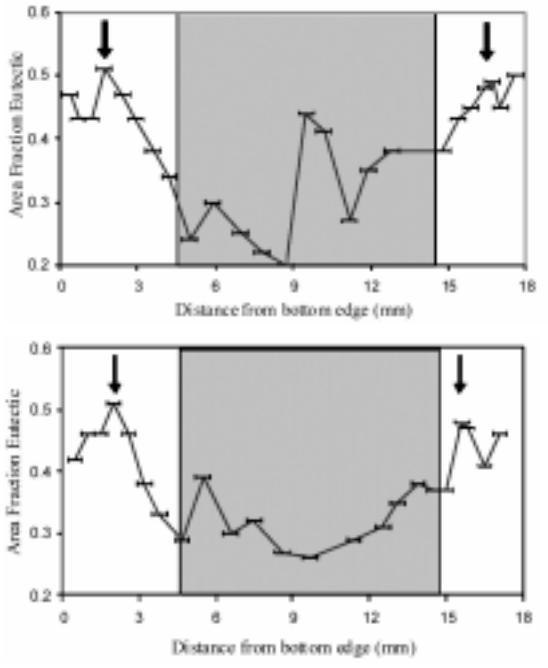

Figure 7: Plots of the area fraction of eutectic versus distance from the bottom of the cross-section across the diameter. Casting conditions: (a) $f_s^{ESC} = 0.16$ and $T_{die} = 270^oC$ and (b) $f_s^{ESC} = 0.11$ and $T_{die} = 270^oC$. The positions of the segregation bands are indicated by arrows. The corresponding microstructures are shown in Figure 3a and 3b respectively.

Considering the regions outside the ESC-rich central region, there are three important points to note: First, in both samples the peak in fraction eutectic is more pronounced at the bottom band than at the top. Second, the decrease in eutectic fraction away from the eutectic peak is much greater towards the centre of the sample than towards the

edge. Third, the eutectic area fraction decreases quite steadily for a relatively long distance from the band peak towards the centre. This could indicate the lateral segregation of liquid and is discussed later.

Whilst the edges of the band are difficult to define, the band centre is relatively simple to identify in an optical microscope. This is confirmed by noting the obvious peak in Figures 7a and 7b but the diffuse nature of the peak edges. The position of the band is defined as the distance from the centre of the bottom band to the flash mark at the bottom of the cross-section, because the band is at its most distinct at this location. The band position was measured using the ruler bar on an optical microscope at 200x magnification.

The Effect of Casting Variables on the Bands

Die Temperature

Samples cast with a die temperature exceeding 350^{o}C did not contain segregation bands. These samples did not fill the cross-section and contain a large amount of porosity suggesting a high velocity and turbulent flow. Generally, samples cast with a die temperature less than 350^{o}C contain segregation bands and Figure 8 shows how the band position varies with die temperature. Whilst the accuracy of the band position is estimated at only +/-0.1mm, the fact that the band is observed to move outwards by 1mm in an increasing die temperature range of 220^{o}C, is a significant result.

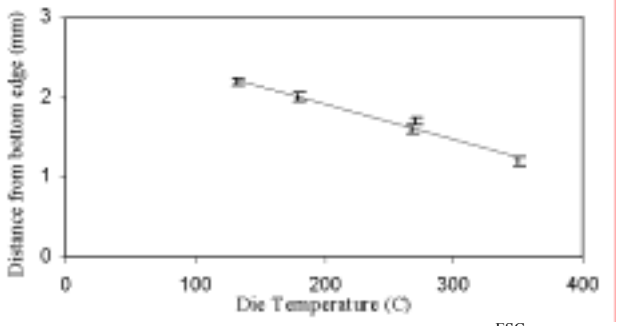

Figure 8: Band position as a function of die temperature for samples of $f_s^{ESC} = 0.16$.

Fraction of ESCs

To obtain accurate values for f_s^{ESC}, the actual ESC fraction in the cross sections studied was calculated by quantitative metallography. Samples cast into a 270^{o}C die with a range of fraction solids showed a change in the nature of the bands with f_s^{ESC} as summarized in Table 2. At the lowest values of f_s^{ESC}, multiple bands were formed.

With increasing fraction solid, single bands formed and above a critical value there were no bands. The approximate f_s^{ESC} ranges are shown in Table 2 and examples of microstructures are given in Figures 3a, 9a and 9b. Furthermore, bands in samples cast with a larger f_s^{ESC} are more distinct than those formed with lower f_s^{ESC}. This can be confirmed by comparing Figures 3a and 9a.

Table 2: A summary of the change in the nature of the bands with f_s^{ESC}.

Approximate f_s^{ESC} range	Nature of bands	Example
$f_s^{ESC} < 0.1$	Multiple	Figure 9a
$0.1 < f_s^{ESC} < 0.25$	Single	Figure 3a
$f_s^{ESC} > 0.25$	No band	Figure 9b

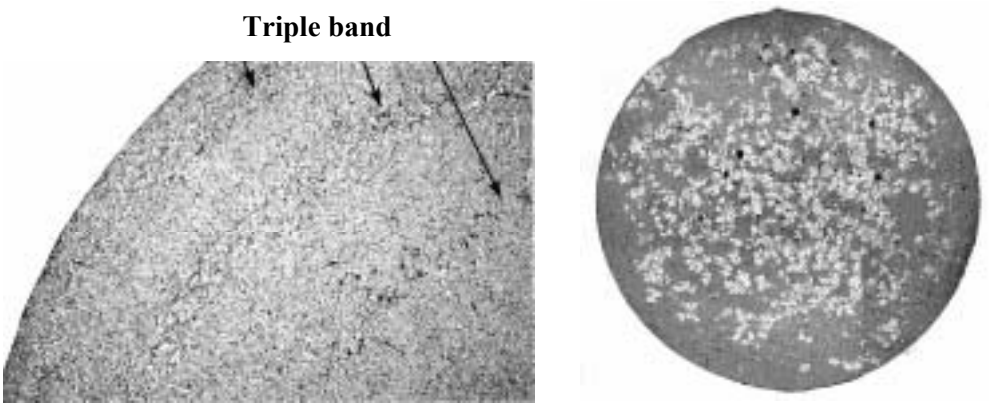

a) b)

Figure 9: (a) A triple band was produced under conditions of f_s^{ESC}= 0.06, T_{die} = 270°C. (b) No band formed under conditions of f_s^{ESC}= 0.28, T_{die}= 270°C.

The band position was measured for samples with a single band, and the results are plotted against f_s^{ESC} in Figure 10. This shows that the band is moved towards the die wall with increasing fraction ESCs. A 1mm change in band position over the range of f_s^{ESC} studied is significant when compared to the estimated error in the measured band position of +/-0.1mm.

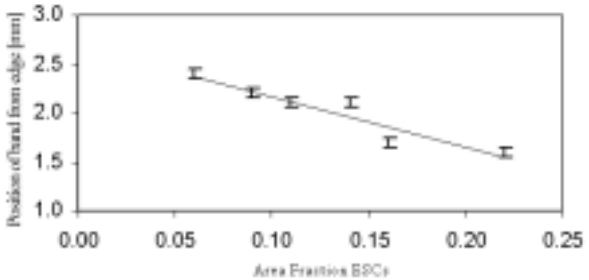

Figure 10: Band position as a function of f_s^{ESC} for samples cast with a die temperature of 270 °C.

Discussion

General Remarks

By comparing the band following the contour of the casting in Figures 1b and 3, it can be concluded that the bands of segregation found in the gravity die castings appear to be similar to those found in cold chamber HPDC Al alloys. To examine further if this superficially similar macrostructural feature forms by the same mechanism in the gravity and high pressure die casting processes, a number of castings were made using Mg-Al alloys because HPDC Mg alloys contain bands of porosity as discussed in the introduction [9,10]. Castings were made by the procedure outlined for the Al-Si castings, although a small superheat, and thus no ESCs, was required to fill the castings. Figure 11 shows that a pore band following the contour of the casting forms in Mg-6wt%Al gravity die cast by this procedure. Therefore, by using a different alloy, the defect has been found to change in nature from a segregated band to a band of interdendritic porosity in the same way that it does in the HPDC process. This strongly implies that the defect found in these gravity die castings forms by a similar mechanism as those in commercial HPDC castings.

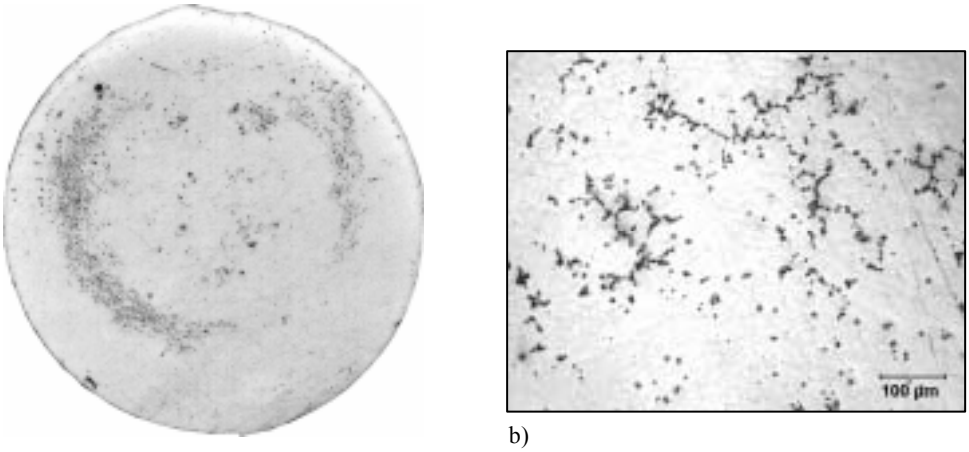

a) b)

Figure 11: As-polished micrographs from the cross-section of a sample of binary Mg-6wt%Al (similar to AM60). Casting conditions were: Superheat = 5K, T_{die} =360°C. (a) Shows a band following the contour of the casting, (b) shows the band to be made up of interdendritic porosity.

These defects have formed in the gravity castings without the high shear rates during filling or the highly non-equilibrium conditions associated with the HPDC process. The evidence of flow and slip in and around the bands suggest that rheology is important in understanding banded defects and therefore supports the rheological approach adopted by Dahle & StJohn [2].

Before the results are analyzed, the mode of solidification in these experiments will be considered: The ESCs are shown to migrate towards the centre of the cross-section early during filling [15]. Solidification proceeds from the relatively cold die walls resulting in a thermal gradient emanating from the die wall and a fraction solid gradient in the solidifying surface layer with a higher fraction solid nearer to the die wall. However, it is unlikely that flow was stopped by the wall layers impinging on the ESCs in the centre for samples of $f_s^{ESC} < 0.3$ because all of these castings filled completely. More likely, equiaxed crystals ripped from the solidifying wall layer during flow were carried in the liquid with the ESCs and flow was arrested by the increasing volume fraction of crystals carried at the flow tip [16]. This mechanism is especially likely as the flow cross-section is large. Furthermore, tip freezing has been identified as the flow arresting mechanism in fluidity tests carried out on alloys of similar composition [17]. Thus, flow is likely to have stopped before the whole cross section of plane A had solidified. Figure 12 depicts the situation shortly before flow arrests by tip freezing.

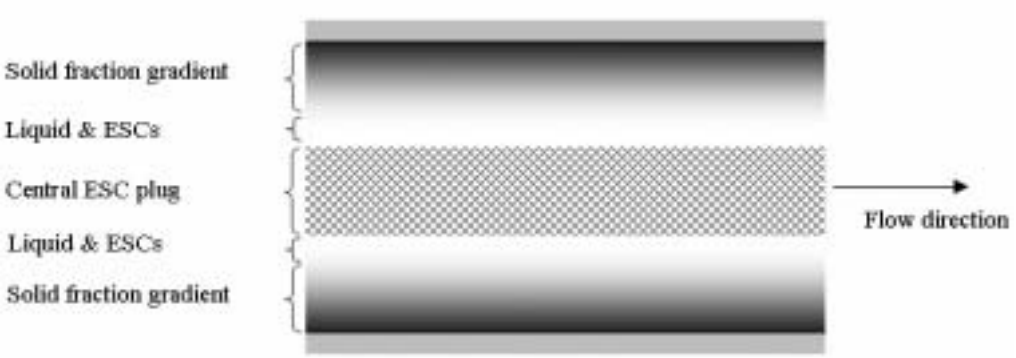

Figure 12: A schematic diagram of the distribution of solid phase at a late stage during flow. The diagram represents the plane perpendicular to plane A in Figure 2b . Solid fraction gradients exist from the die walls and ESCs have formed a network at the centre of the cross-section. Darker tones signify a greater fraction solid.

The Effect of Die Temperature

In this study, changes in the rate of heat transfer are largely governed by changes in die temperature. Changing the die temperature alters the thermal gradients emanating from the die wall as well as the resulting solid fraction gradient. Thus, the fact that the band position is observed to change with die temperature (Figure 8), highlights the importance of surface layer solidification in band formation.

This relationship implies the band forms either at the edge of the solidifying wall layer or within the layer itself. If segregation bands form at the wall layer edge, the result suggests the bands move inwards with decreasing die temperature because the wall layer becomes thicker. If, however, the bands form within the solidifying layer, it suggests they form at a similar solid fraction contour at each die temperature, which would also move the band inwards with decreasing die temperature.

No segregation bands were found in castings with a die temperature exceeding 350^{o}C. This is most likely because the smaller temperature gradient resulted in a small f_s gradient away from the die wall. Segregation bands were not formed below a critical fraction solid gradient in commercial centrifugal castings in another study [7], suggesting the f_s gradient formed using a 450^{o}C die in our study could be too small for the formation mechanism to operate. The facts that the cross-section was not completely filled and the flow was highly turbulent are also likely to have been contributing factors in these experiments.

The Effect of f_s^{ESC}

The ESCs migrate to the central region [15], and the band often forms relatively far away from the ESCs (see Figure 3b). Despite this, altering f_s^{ESC} was found to shift the band position (Figure 10).

There is some evidence that the centered ESCs play a role in the segregation of enriched liquid to the band: The tributaries in Figure 6a suggest that liquid has segregated over significant distances and this is further supported by the decrease in fraction eutectic from the band to the centre (Figure 5). Furthermore, the bands are more distinct at higher f_s^{ESC} when the ESCs have formed a better developed network than at very low f_s^{ESC} when the network is less developed. This could be because the hydrostatic pressure during flow compresses the well-developed viscoelastic ESC network and squeezes liquid out towards the wall [18]. This liquid is likely to be highly enriched with solute as it was saturating the solidifying ESCs. The hydrostatic pressure and compression would increase the driving force for lateral liquid flow resulting in castings with a higher f_s^{ESC} having a more defined band. This driving force is in addition to the pressure drop due to solidification contraction causing inverse segregation towards the die wall.

It is important to note, however, that segregation bands were also observed when samples were cast with no ESCs (i.e. a small superheat). The ESCs therefore appear to

affect the position and nature of the segregation bands, but they are not an essential part of the formation mechanism.

Whilst the results here support the rheological approach to studying shear band formation, they also show the need to modify the framework put forward by Dahle & StJohn [2]. This is because there are features in the microstructure, which suggest the formation of the band is not due to deformation localizing in the lowest fraction solid region between the central plug and the solidifying wall layer: First, the band does not form at the edge of the ESC plug, as there is a region of fine-grained material between the band and the ESCs. Second, the band consists of a number of eutectic pathways that may be interconnected, see Figures 6a-d. Third, the segregation band can be wide (up to 1.5mm), which would not be required of a localized slip plane lubricating flow in the manner described by Dahle & StJohn.

A New Mechanism for Band Formation

Before a mechanism for the formation of banded defects in HPDC is proposed, the flow behavior of the solidifying semi-solid slurry must first be considered. A flow field imparts shear stresses on a body, and the response of a semi-solid to shear stress is strongly dependent on both the solid fraction and the structure of the solid phase [3]. The solid phase is not distributed evenly in the solidifying casting of this work as has been described, but takes the form depicted in Figure 12 due to a combination of ESC migration and wall solidification. The solid distribution can then be split into three regions, each of which will respond to the applied stress differently: At the centre of the flow is a network of ESCs which is carried in the liquid at the centre of the casting by plug flow[1]. As we move from the centre towards the wall, there is next a low solid fraction region flowing as a suspension carrying the plug. This suspension will contain some ESCs which have not formed part of the ESC network and also some crystals which have been ripped off the growing immobile wall layer. The third region is a largely immobile solid fraction gradient from about $f_s=f_s^{Ch}$ where the crystals of the flowing suspension begin to form a network to $f_s=1$ at the die wall. The response of an immobile solid fraction gradient to stresses induced by fluid flow will now be considered:

[1] The proximity and entangled nature of ESCs in the central network will result in most ESCs having the same velocity. The ESC network will therefore flow as a porous visco-plastic plug.

Flow past and through the f_s gradient region is similar to the well known case of flow driven by feeding in a directionally solidifying casting. However, whilst the flow direction due to feeding in a directionally cooled casting is up the solid fraction gradient, flow is perpendicular to the solid fraction gradient when flow occurs past a solidifying wall layer (Figure 13). Therefore, flow through the solid fraction gradient of this study is likely to be by mechanisms similar to the feeding mechanisms proposed by Campbell [19].

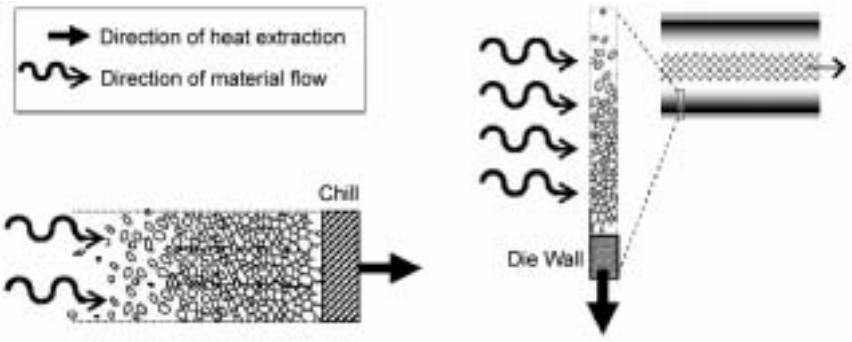

Figure 13: Schematic diagrams of flow in solidifying material. (a) Flow due to feeding in a directionally cooled melt: material flow is largely in the same direction as heat extraction. (b) The case in this study: flow past and through a solidifying layer at a die wall. Material flow is largely perpendicular to the direction of heat extraction.

Consider the response of material in different parts of the f_s gradient starting with the near-liquid region and then material of progressively greater solid fraction towards the die wall. The first material is of solid fraction below the coherency point and flows as a suspension of ζ-Al dendrites in the liquid analogous to mass feeding. As the fraction solid increases above the coherency point, however, the shear strength increases rapidly as a dendrite network begins to form [3]. Once a network has become partially interconnected, liquid may be able to flow through interdendritically. The response to stress is then the forcing of liquid through the dendrite skeleton analogous to interdendritic feeding. The interdendritic flow rate depends on the network permeability and the driving pressure. Just beyond the coherency point there are many pathways for interdendritic flow and the volumetric flow rate is likely to be able to exceed the deformation rate.

The fraction solid increases towards the die wall, the network becomes more entangled and compacted and the permeability decreases because liquid flow paths become smaller and more tortuous. Furthermore, the shear stress caused by fluid flow increases

up the fraction solid gradient. This is a result of the velocity profile, with a maximum velocity and minimum stress near the ESC network and an increasing shear stress towards the die wall.

Despite the increasing shear stress, a critical fraction solid exists where the volumetric flow rate of the liquid through the dendrite network is unable to exceed the deformation rate due to the free-flowing material and plug. The material response at this point depends on the strength of the network. If the network strength is exceeded by the applied stress, deformation could occur by local slip of the network itself. At this point the material is most likely around the maximum packing fraction and, therefore, there may still be enough liquid remaining to allow grain sliding and rolling[20]. The ease of sliding and rolling is a strong function of the dendrite shape (due to the degree of interlocking) and the grain size (the displacement required for a grain to slide past another) [5].

The heavily branched dendrites are likely to be interlocked and slip occurs between groups of dendrites. The strength of the network varies locally due to variations in the degree of entanglement and slip is expected to occur at the weakest local region. Once slip occurs in the dendrite network, it will be accompanied by some liquid flow if an interdendritic flow path exists because the sliding of grains past one another in a compacted network must cause some interdendritic regions to increase in volume, creating a pressure drop. This mechanism has been witnessed in work on shear cell experiments, where liquid was found to have segregated to the shear plane as grains rearranged away from the plane of slip [5].

With a greater concentration of liquid in these slipped regions, the resistance to deformation is reduced. Further slip will only occur if the new local configuration, now lubricated by a larger liquid film, is the weakest local region. If further slip occurs in the same region, more liquid would flow between the grains. The strength of the region would then be decreasing with each slip event and the mechanism would be one of positive feedback producing a distinct band.

However, it is also possible that once a group of dendrites had slipped past another, the new structure could be heavily interlocked and a separate, weaker region could slip elsewhere. In this case a region of segregated liquid could become isolated. If a pathway exists between a slipping area and an isolated region of liquid, liquid could be drawn into the new area of sliding dendrites. In this way a number of interconnected

paths containing enriched liquid could form a diffuse band. It is suggested that the tributaries and paths of eutectic in Figure 6a formed in this manner.

The mechanism outlined above has some similarities to the burst feeding hypothesis proposed by Campbell [19]. Burst feeding was suggested to occur as a series of bursting events when small barriers to flow in a solid skeleton are broken. Whereas the driving force for feeding is solidification shrinkage, in the present model, it is the fluid flow due to filling. Dahle et al [21] developed an analytical expression for the build-up of shear stress due to shrinkage induced fluid flow (feeding). They found that these stresses can be of similar magnitude to the dendrite network strength and that network collapse due to fluid flow in a dendrite network is possible. As the interdendritic flow rate is expected to be high in the case of flow past a solidifying wall layer, it is reasonable to suggest network collapse could also occur here.

It is therefore proposed that local slip in the dendrite network would occur in a band between a region of higher f_s where the shear stress is accommodated viscoelastically by the dendrite network and a region of lower f_s where the permeability is low enough for the volumetric flow rate of interdendritic fluid to exceed the deformation rate. This is shown pictorially in Figure 14:

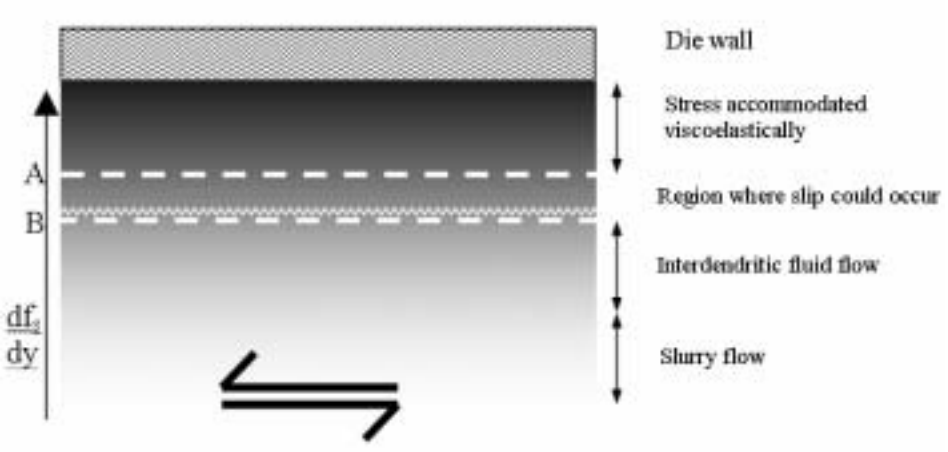

Figure 14: A schematic diagram of a solid fraction gradient emanating from a die wall where the darker tone signifies a greater fraction solid. The change in the response to stress with position in a solid fraction gradient is shown. Line A is the lower limit of the region where the applied stresses are accommodated viscoelastically. Line B indicates the contour where the interdendritic flow rate is exceeded by the deformation rate.

The eutectic in the band originates from the solute enriched liquid between dendrites where slip occurred. It is proposed that this liquid segregated up the solid fraction gradient towards the die walls due to three mechanisms: First, solidification shrinkage in the wall layer will draw liquid towards the wall; second, the hydrostatic pressure squeezing the viscoelastic ESC plug forces liquid laterally [18]; and third, gaps forming between slipping dendrites draws in liquid. This segregation provides a component of velocity perpendicular to the bulk flow direction, so that interdendritic fluid flow occurs in the manner shown schematically in Figure 15: Eutectic pathways to the segregation band appear similar to this description as shown in Figure 6a.

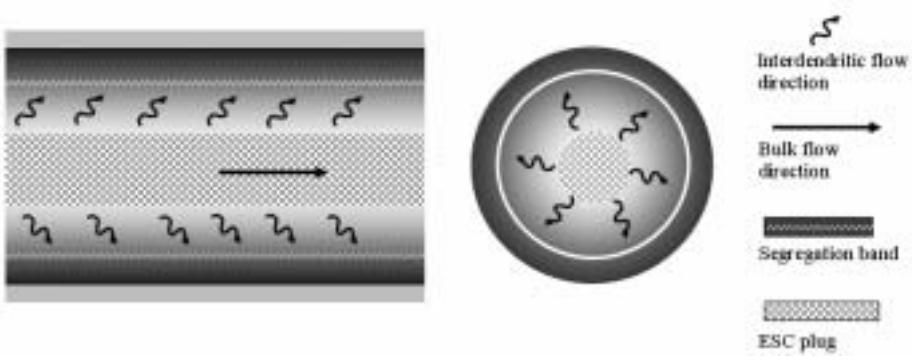

a) b)

Figure 15: Flow occurring after considerable solidification has taken place: Interdendritic flow has a velocity component towards the die wall providing feed liquid to the slipping regions of the band. (a) Section parallel to the bulk flow direction as in Figure 12 and (b) section perpendicular to bulk flow direction (i.e. plane A in Figure 2b). Again, a darker tone indicates a larger fraction solid.

It is probable that the make-up of the band is determined in the final stages of solidification when there is less liquid available to be drawn into the gaps between slipping dendrites. If there is insufficient interdendritic fluid flow to the band, the slip of dendrites past one another will be resisted by the pressure drop due to the interdendritic volume change on sliding. If the applied stress is sufficiently large, the pressure drop could cause pores to form and in extreme cases tearing could occur. The degree of interdendritic fluid flow to the band in the final stages of solidification is strongly dependent on the network structure and permeability, the solidification range, the eutectic volume fraction and the contraction (both thermal and solidification shrinkage) of the alloy used. As these parameters vary widely between alloys, the make-up of bands (whether segregated, porous or torn) is also highly alloy dependent.

Application of the Model

This framework provides a basis to explain the trends observed in this study: Decreasing the die temperature causes a steeper temperature gradient to exist in the metal so that both lines A and B in Figure 14 are moved away from the die wall. Figure 8 shows that the band-position is displaced away from the die wall with decreasing die temperature.

Increasing f_s^{ESC} was observed to significantly reduce the bulk flow rate during filling. This is most likely because the ESC-rich central region becomes broader with increasing initial fraction solid [15]. A broader ESC containing region results in a broader ESC network and also more ESCs that have not formed part of the network, which flows in the liquid region as a suspension. The mostly liquid region will then have a larger viscosity [1], and coupled with the effect of a broader ESC network, this will cause the bulk volumetric flow rate to decrease with increasing f_s^{ESC}.

A smaller bulk volumetric flow rate results in a smaller deformation rate in the solidifying wall layer. The proposed model assumes that flow induced network collapse occurs when the component of interdendritic flow rate in the bulk flow direction is less than the deformation rate. Reducing the deformation rate then allows interdendritic flow to occur through a less permeable dendrite network before collapse or slip occurs. Thus, if a lower deformation rate were applied to a solid fraction gradient, flow induced network collapse would occur at a larger local fraction solid. That is to say, contour B in Figure 14 would move towards the wall with increasing f_s^{ESC}. Figure 10 indeed confirms the band-position moves towards the wall in this manner.

As described above, increasing f_s^{ESC} reduces the deformation rate. Therefore, at a higher f_s^{ESC}, the region of the solid fraction gradient able to resist deformation viscoelastically increases and contour A in Figure 14 moves away from the die wall. Thus, increasing f_s^{ESC} not only moves contour B nearer to the wall, but also moves contour A away from the wall. For a sufficiently high f_s^{ESC}, these two contours would cross and no band could form. It is possible that this occurred in the experiments with f_s>0.25 (Figure 9b). Conversely, at a low f_s^{ESC}, the region where network collapse could occur would be relatively wide. This could be the reason that multiple bands formed at low f_s^{ESC} (Figure 9a). This argument could also explain why the band at higher f_s^{ESC} is more distinct: contours A and B in Figure 14 are closer together and the

region where slip can occur is narrower causing stress concentration and more localized deformation.

Conclusions

Defect bands similar to those found in commercial cold chamber HPDC aluminum and magnesium alloys have been witnessed in laboratory gravity die castings.

In the Al-Si die castings, the band is a region of higher fraction eutectic than the surroundings and consists of a number of interconnected eutectic pathways. The position of the bands has been found to move towards the die wall with increasing die temperature and external fraction solid f_s^{ESC}. The nature of the bands has been found to develop from poorly defined multiple bands to a well-defined single band and to no band at all with increasing external fraction solid.

A mechanism describing the formation of the band has been proposed based on the idea of local slip occurring in the dendrite network as a result of fluid flow past a stagnant solidifying wall layer.

Acknowledgements

The authors would like to acknowledge the support of the Cooperative Research Centre for Cast Metals Manufacturing (CAST). CAST was established under and is supported by the Australian Government's Cooperative Research Centre Program. One of the authors (C.M. Gourlay) gratefully acknowledges the financial support provided by an International Postgraduate Research Scholarship (IPRS).

Professor Lars Arnberg and Professor Otto Lohne from the Department of Materials Technology, NTNU are acknowledged for their comments on the present work.

References

[1] Spencer, D. B.; Mehrabian, R.; Flemings, M. C. *Metall. Trans.*, **1972**, vol. 3, 1925-1932.

[2] Dahle, A. K.; St. John, D. H. *Acta Mater.* **1999**, vol. *47*, 31-41.

[3] Dahle, A. K.; Arnberg, L. *Acta Mater.* **1997**, vol. *45*, 547-559.

[4] Arnberg, L.; Chai, G.; Backerud, L. *Mater. Sci. and Eng. A* **1993**, vol. *173A*, 101-103.

[5] Sumitomo, T.; StJohn, D. H.; Steinberg, T. *Mater. Sci. Eng. A* **2000**, vol. *289A*, 18-29.

[6] Dahle, A. K.; Instone, S.; Sumitomo, T. *Metall. Mater. Trans. A* **2003**, vol. *34A*, 105-113.

[7] Ohnaka, I.; Kang, I., *Solidification Processing 1997- Proceedings of the 4th Decennial International Conference on Solidification Processing*, ed. J. Beech and H. Jones. University of Sheffield, UK, **1997**; 346-349.

[8] Dahle, A. K.; St. John, D. H. *Trans. 20th Int. Die Casting Congress & Exposition,* North American Die Casting Association (NADCA), Rosemont IL **1999**, 203-210 (*T99-062)*.

[9] Dahle, A. K.; Sannes, S.; St. John, D. H.; Westengen, H. *J. Light Metals* **2001**, vol. *1*, no.2, 99-103.

[10] Rodrigo, D.; Murray, M. T.; Mao, H.; Brevick, J.; Mobley, C.; Esdaile, R. *Trans. 20th Int. Die Casting Congress and Exposition*, North American Die Casting Association (NADCA), Cleveland, Ohio, **1999**; 219-225.

[11] Pitsaris, C.; Abbott, T.; Davidson, C. *Proceedings of the 1st Light Metals Technology Conference*, ed. A.K. Dahle, Brisbane, Australia, **2003**, 223-226.

[12] Laukli, H. I.; Lohne, O.; Sannes, S.; Gjestland, H.; Arnberg, L. *Int. J. Cast Met. Res.* **2003**, vol.16, no.6, 515-521.

[13] Laukli, H. I.; Graciotti, A.; Lohne, O.; Gjestland, H.; Sannes, S. *Trans. 2002 Die Casting Congress*. North American Die Casting Association (NADCA), Rosemont, IL. **2002**, T02-035.

[14] Rodrigo, P. D. D.; Ahuja, V. Magnesium 2000, *Proceedings of the 2nd Israeli Conference on Magnesium Science and Technology*, Dead Sea, Israel, **2000**; 97-104.

[15] Laukli, H. I.; Gourlay, C. M.; Dahle, A. K. Segregation of crystals during the filling of semi-solid castings. To be published **2004**.

[16] Flemings, M. C. *Solidification Processing*; McGraw-Hill, New York **1974**. 219-224.

[17] Campbell, J. *Castings*; 2nd ed., Butterworth Heinemann, Oxford. **2003**. 76-87.

[18] Yang, Z.; Zhang, H.; Wang, A.B; Hu, Z. *J. Mater. Sci. Tech.* **2003**, vol. *19*, no. 3, 209-212.

[19] Campbell, J. *AFS Cast Metal Research* **1969**, vol. *5*, 1- .

[20] Metz, S. A.; Flemings, M. C. *AFS Trans.* **1970**, vol. 78, 453- 460.

[21] Dahle, A. K.; Thevik, H. J.; Arnberg, L.; St. John, D. H. *Metall. Mater. Trans. B* **1999**, vol. *30B*, 287-293.

APPENDIX

APPENDIX A

It can be difficult and time consuming to achieve well prepared die cast samples for microstructure investigations. Some useful methods are provided here. The methods require grinding, (120-2400mesh, the last step with soap), and polishing, (3σ and 1σ, with Struers blue and red lubricant, respectively). The applied pressure should be moderate. When looking at porosity, longer polishing times should be emphasized.

Optical microscopy

Alloy	*Grain structure etching*	*Eutectic ecthing*
AM60	50ml CH_2OHCH_2OH	75ml CH_2OHCH_2OH
	17ml Dist. H_2O	1ml HNO_3
	1ml HNO_3	24ml Dist. H_2O
	20ml CH_3COOH	
	3-7s, light stirring	*1-3s*
	Rinse with ethanol	*Rinse with ethanol*
A356	5%HBF_4 solution	(Modified Murakami):
		60ml H_2O
		10gr NaOH
		5gr $K_3Fe(CN)_6$
	Voltage: 20, Time: 60s	*Stir moderately for 10s*
	Rinse with ethanol	*Rinse with water*
	alternatively;	
	Modified Murakami for 60s	

SEM, EPMA, EBSD

Alloy	*Ion milling*
	Tilt: 15^o
	Current: 5mA
	Acceleration voltage: 5kV
AM60	*Time*: 4.5h
A356	*Time*: 2.5h

Although, there are no TEM results presented in this thesis, the following procedure was appropriate in the preparation of AM60 thin foils: On ground samples; dimpling, and then ion milling: 3.5kV, 1mA, 12^o tilt, 16h.

APPENDIX B

Details about the simulation example shown in Figure 7:

MagmaSoft simulation:
Shot sleeve material: H13 steel
Shot sleeve length: 340mm
Shot sleeve inner diameter: 60mm
Shot sleeve outer diameter: 130mm
Initial shot sleeve temperature: 250^{o}C
Plunger material: CuCoBe
Initial plunger temperature: 25^{o}C
Alloy: A356
Superheat on pouring: 60K
Fill fraction: 0.5
Fill time: 1.25seconds
Shot delay time: 2seconds
Geometry resolution, meshing: 455197 elements comprising the casting
Heat transfer coefficients:
h (shot sleeve – A356 alloy): constant 12 kWm^{-2}K^{-1}
h (shot sleeve – plunger): constant 10 Wm^{-2}K^{-1}
h (plunger – A356 alloy): constant 12k Wm^{-2}K^{-1}

APPENDIX C

The process parameters used in the production of die castings in the doctorate work are summarized as follows:

Cold chamber HPDC machine: Bühler Shot Controlled SC42D, 420 ton locking force
Shot sleeve dimensions: Length: 340mm; inner diameter: 60mm; wall thickness: 35mm
Fill fraction: ~0.5
Die temperature: 200^{o}C

Table A-1. Process parameters used in most of the HPDC casting experiments.

Alloy	**Pouring time [s]**	**Shot delay [s]**	**V_p [ms^{-1}] (slow shot)**	**V_p [ms^{-1}] (die fill)**	**P [bar]**	**P time [s]**	**Die open [s]**
A356	2-3	0.5-2	0.15 Ÿ 0.3	3-4	600	6-8	~3
AM60	1.25	-	0.30 Ÿ 1.0	4.5-6.5	600	~6	~3